UNIVERSITY OF CALIFORNIA

Santa Barbara

Upgrading Hydrocarbons and Olefins with Organometallic Catalysis: Reaction, Kinetics, and Mechanism

A dissertation submitted in partial satisfaction of the

requirements for the degree Doctor of Philosophy

in Chemistry

by

Chan Young Park

Committee in charge:

Professor Mahdi M. Abu-Omar, Chair

Professor Steven K. Buratto

Professor Trevor W. Hayton

Professor Gabriel Ménard

March 2020

The dissertation of Chan Young Park is approved.

_____
Steven K. Buratto

_____
Trevor W. Hayton

_____
Gabriel Ménard

_____
Mahdi M. Abu-Omar, Committee Chair

March 2020

Upgrading Hydrocarbons and Olefins with Organometallic Catalysis: Reaction, Kinetics, and Mechanism

by

Chan Young Park

ACKNOWLEDGMENTS

Thank you, God, for your abundant blessings, giving me strengths to complete my studies, and for all the people around me who have helped me along the way.

Pursuing graduate studies at Purdue University and UC Santa Barbara has provided me with exceptional research experience and opportunities to work with amazing, talented people. First, I wish to express my sincere appreciation to my supervisor, Prof. Mahdi Abu-Omar, who has gifted me with an exceptional learning and research experience. He was not only my research advisor, but he was a life mentor and a great friend. So, I decided to follow him to UC Santa Barbara, which was a great decision, especially for its fantastic weather. I am very thankful for his guidance, support, and encouragement throughout my graduate career. I would also like to thank Profs. Steven Buratto, Trevor Hayton, and Gabriel Ménard for serving on my committee during my time at UC Santa Barbara. Thank you for your feedback and comments that made me a better scientist.

I want to thank my collaborators for their supports and diverse perspectives. I am grateful to Prof Jim Caruthers, Dr. Grigori Medvedev, and Dr. Jeffrey Switzer for evaluating and building kinetic modeling of our copolymerization studies. I will miss our weekly meetings with thorough discussions that made me a better chemist with some chemical engineers' perspectives. I express my gratitude to Dr. Orson Sydora for allowing me to work on impactful oligomerization studies and providing me important feedback. Your collaborative works and career advice gave me whole new perspectives in the chemical industry. I also want to thank Dr. Lara Kabalan for the DFT results and discussions.

Special thanks to my mentors and colleagues. My interest and passion for chemistry have developed with the help and guidance of my undergraduate research advisor, Prof. Oleg Ozerov, and my mentor, Dr. Rafael Huacuja, at Texas A&M. Dr. Ram Pichaandi was a great mentor who taught me all basic lab techniques and how to think as a scientist. Your patience and thoughtful discussions were always encouraging. Special thanks to Jun Hee Jang for being the best colleague and friend. I will miss your humor and countless nights in the lab discussing our research and lives. My graduate studies would have been miserable without you.

I would like to thank all of the members of the Abu-Omar group, past and present; Baoyuan Liu for training and troubleshooting pressure reactors and GC, Joshua Speer for your support in collaborative work, Manxi Xiong and Tayyebeh Bakhshi for research discussions, Danny Zeng for his insights in science and politics, Dr. Shou Zhao for his scientific and baby-related discussions, Dr. Thilina "TG" Gunasekara and Dr. Andrew Preston for helping me with the ethylene oligo/poly-merization set-up, Dr. Mike Mazzotta for safety and instrument training, and all group members for their supports and helpful ideas.

I am deeply grateful to my family in both Korea and the US. Thank you for giving me a chance to study here in the states. Moving to the states has allowed me to experience two different cultures and broadened my perspectives. I thank my parents for supporting me with their hard work and for believing in me to complete my studies. I'm very grateful to have loving parents-in-law; thank you for your support and prayer.

I would not have made it this far without my amazing, loving wife, Hannah Lee. Marrying you was the best decision I made in my life. Thank you for supporting and believing in me, even when I did not believe in myself. You postponed your graduate work to support me to achieve my dreams. I appreciate all the sacrifices you made for me. Thank you for letting me sleep through the nights peacefully by taking care of our five-month-old baby son, Daniel. Thank you, my son, for making every day so special.

VITA OF CHAN YOUNG PARK

March 2020

EDUCATION

Bachelor of Science in Chemistry, Texas A&M University, College Station, May 2014

Doctor of Philosophy in Chemistry, University of California, Santa Barbara, March 2020 (expected)

PROFESSIONAL EMPLOYMENT

2011-14: Undergraduate Researcher and REU Participant, Department of Chemistry, Texas A&M University, College Station

2014-16: Teaching and Research Assistant, Department of Chemistry, Purdue University, West Lafayette

2016-20: Teaching and Research Assistant, Department of Chemistry, University of California, Santa Barbara

FIELDS OF STUDY

Major Field: Inorganic Chemistry

Studies in Organometallic catalysis for upgrading hydrocarbons and olefins with Professor Mahdi Abu-Omar

ABSTRACT

Upgrading Hydrocarbons and Olefins with Organometallic Catalysis: Reaction, Kinetics, and Mechanism

by

Chan Young Park

In attempts to develop tandem catalysis of alkane dehydrogenation and polyol deoxydehydration, the reactivity of a (^{tBu}PCP)IrH_2/H_4 (PCP=[κ^3-2,6-C_6H_3($CH_2P^tBu_2$)$_2$]) and methyltrioxorhenium was explored. The resulting bimetallic complex, [(^{tBu}PCP)Ir(ReO_3)(H)], which was stable at low-temperature, quickly turned into [(^{tBu}PCP)Ir(ReO_4)(H)] at room temperature. The reactivity of these highly oxophillic bimetallic complexes was studied. With NMR and DFT studies, the pathway of bimetallic formation was elucidated.

Ethylene/1-hexene copolymerization by a single-site hafnium salan-type catalyst activated by B(C_6F_5)$_3$ produced high 1-hexene-incorporated copolymers. The composition dependence on monomer concentrations and reaction time was explored. Deuterium labeling experiments revealed that primary sites decreased as secondary sites increased over the course of the reaction. The secondary sites showed no reactivity towards the polymerization of ethylene and 1-hexene. High 1-hexene concentration suppressed catalyst deactivation. *In-*

situ NMR demonstrated a positive comonomer effect, where higher k_{obs} of ethylene and 1-hexene were achieved with increased $[1\text{-hexene}]_0$.

New methods (*in-situ* NMR with high-pressure NMR cell and batch reactor with Auto-Sampler) for quantitative kinetic study of selective ethylene tri/tetra-merization by chromium N-phosphinoamidine were developed. The monomer consumption and 1-hexene versus 1-octene product formation in real-time was reported for various catalysts.

TABLE OF CONTENTS

CHAPTER I. Introduction

A. Upgrading Natural Gas

Natural gas is an abundant source of energy with over 187 trillion cubic meters reserved worldwide (2014).[1] Currently, the majority of natural gas (more than 90 %), is burned to make energy such as heating and electrical power.[2-3] This ineffective usage of natural gas clearly indicates a lack of technology developments. Thus, chemical transformations of light aliphatic hydrocarbons from natural gas to produce more valuable chemicals such as functionalized or higher molecular weight hydrocarbon have received much interest in both academia and industry.[2, 4-6] The most well-established processes of methane from natural gas include the Gas-to-Liquids (GTL) conversion process via Fischer–Tropsch catalysis (making liquid fuels)[7], oxidative coupling of methane (making ethylene)[8], and methane oxidation (making methanol)[9]. Other than GTL, the oxidative reaction of methane is not economically attractive due to their low selectivity from the over-oxidation.[10] More recently, oxidation of natural gas with non-oxygen-containing agents have been developed to eliminate over-oxidation and byproducts such as water and carbon oxides.[11-12]

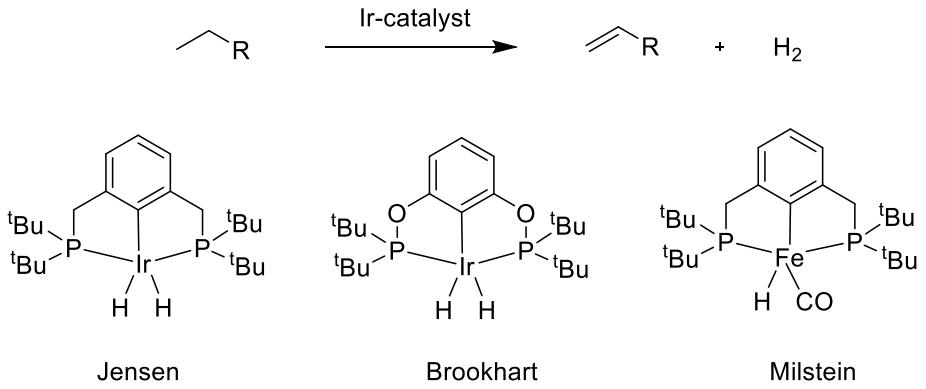

Scheme 1.1. Examples of alkane dehydrogenation by various pincer-iridium catalysts.

In addition to the methane, typically natural gas consists of 1 – 25% of unsaturated aliphatic hydrocarbons, mostly C_2 through C_6.[3] Because these higher alkanes are easier to handle, there have been many studies of dehydrogenation of alkane to make the corresponding alkene by transition-metal complexes.[13] In 1979, the first example of stoichiometric alkane dehydrogenation by $[IrH_2(Me_2\text{-}CO)(PPh_3)_2]^+$ with tert-butylethylene as hydrogen acceptor.[14] Since then, catalytic studies of alkane dehydrogenation by various transition metals including rhenium, iridium, and rhodium were reported.[15-17] In 1999, Jensen reported catalytic alkane dehydrogenation by a highly active iridium complex with PCP pincer ligand[18] (developed by Moulton and Shaw).[17] The novel PCP-Ir catalyst was one of the first examples to dehydrogenate alkane without hydrogen acceptor as well (Scheme 1.1). This initial acceptorless dehydrogenation had much lower turnover frequency (TOF) of 1.41 h^{-1}, which was about 700 times slower than transfer dehydrogenation with hydrogen acceptor. This was partially due to the fact that the build-up of hydrogen pushing the equilibrium to the reactant.[17, 19]

Followed by Jensen's work, alkane dehydrogenation using pincer-iridium has been heavily investigated by Goldman, Brookhart, and Milstein.[20-21] The conditions were optimized and the effect of metal, ligand variation, temperature, hydrogen acceptor, and additives have been studied thoroughly. Goldman and coworkers elucidated the mechanism of dehydrogenation and transfer-dehydrogenation of alkane by pincer-iridium by experimental and DFT studies (Scheme 1.2).[22-23] The study revealed (pincer)IrH_2 is the thermodynamically resting state, and that formation of Ir (I), or removal of hydride from iridium, is the rate-determining step with or without hydrogen acceptor. This study was consistent with the experimental results that catalytic activity was significantly reduced without hydrogen acceptor and that hydrogen build-up inhibited further dehydrogenation of alkane.

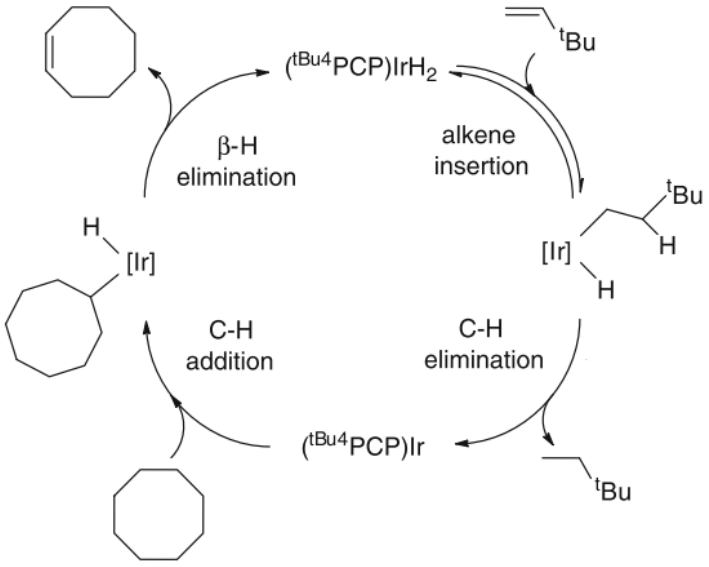

Scheme 1.2. Simplified mechanism of alkane dehydrogenation by pincer-iridium complex with tert-butylethylene as hydrogen-acceptor.

Goldman and Brookhart reported tandem catalysis of alkane dehydrogenation and olefin-metathesis, or metathesis of alkanes to produce ethane and longer n-alkanes (Scheme 1.3).[24] This innovative tandem catalysis eliminated the need for sacrificial additives as the "resting (pincer)IrH_2" was activated by alkene intermediates. Further experimental and mechanistic studies improved the activity by optimizing the conditions and using more thermally stable rhenium metal oxides for olefin metathesis.[25] However, this novel alkane metathesis had no control over product selectivity; the products ranged from C_2 to C_{30} when n-hexane was used as a reactant. In addition, the overall catalytic activity was severely restricted by the operating temperature. At practical conditions for alkane dehydrogenation (around 200 °C), Mo olefin metathesis catalysts were degrading quickly.

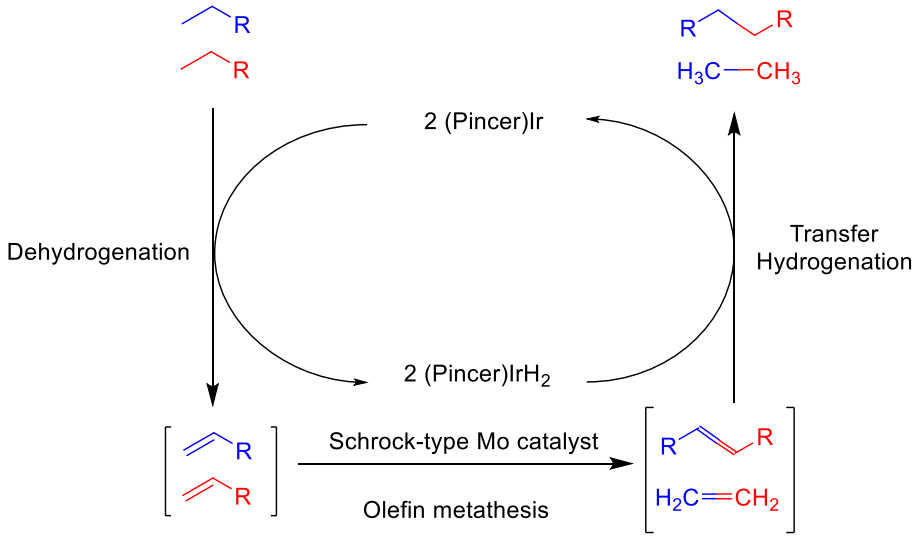

Scheme 1.3. Catalytic cycle of alkane metathesis, tandem catalysis of alkane dehydrogenation and olefin metathesis, catalyzed by pincer iridium and Schrock-type Mo complexes by Goldman and Brookhart.[24]

Goldman and Brookhart reported tandem catalysis of alkane dehydrogenation and olefin-metathesis, or metathesis of alkanes to produce ethane and longer n-alkanes (Scheme 1.3).[24] This innovative tandem catalysis eliminated the need for sacrificial additives as the "resting (pincer)IrH_2" was activated by alkene intermediates. Further experimental and mechanistic studies improved the activity by optimizing the conditions and using more thermally stable rhenium metal oxides for olefin metathesis.[25] However, this novel alkane metathesis had no control over product selectivity; the products ranged from C_2 to C_{30} when n-hexane was used as a reactant. In addition, the overall catalytic activity was severely restricted by the operating temperature. At practical conditions for alkane dehydrogenation (around 200 °C), Mo olefin metathesis catalysts were degrading quickly.

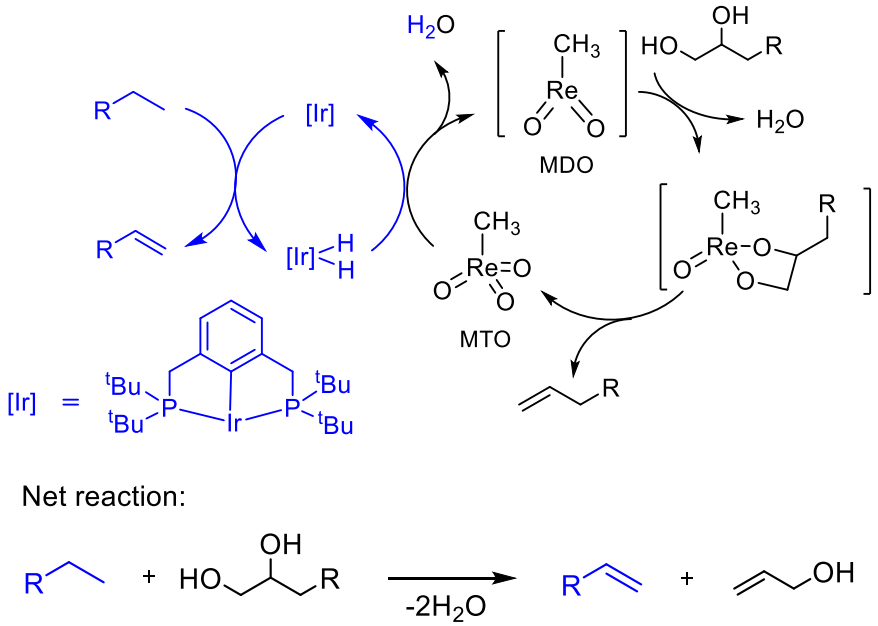

Scheme 1.4. Proposed catalytic cycle of coupled alkane dehydrogenation of light alkane and deoxydehydration of diols from biomass.

Inspired by the successful tandem catalysis.[24-26], we envisioned to couple alkane dehydrogenation with deoxydehydration of oxygen-rich products from biomass conversion (Scheme 1.4). Our group previously studied deoxydehydration of biomass-derived polyols catalyzed by methyltrioxorhenium (MTO) with reductant (alcohol or hydrogen).[27-28] The proposed cycle was proposed to be beneficial for both catalytic cycles: (1) MTO acts as a hydrogen acceptor and (2) (pincer)IrH_2 acts reductant. The only byproduct of the proposed reaction is water, which was shown to not degrade the (PCP)Ir catalyst.[29] An expected obstacle of the proposed cycle is that the two catalyst sites, which are in low concentrations, need to interact during the reaction. We proposed that this issue could be relieved by designing a bimetallic Ir-Re catalyst. Chapter 2 describes the formation of the Ir-Re bimetallic complex from the reaction between (PCP)IrH_2 and MTO. The temperature-sensitive behavior and reactivity of Ir-Re complexes were studied with in-depth NMR and DFT studies.

B. Upgrading Olefins

Global production of plastics has reached around 350 million metric tons in 2018 and has been growing over 10 million metric tons per year since 2005.[30] Out of the entire plastic production, olefin polymerization is the largest plastic industrial process, with over 150 million metric tons per year globally in 2018.[30-33] Most of the polyolefin production consists of polyethylene and polypropylene resins and small fractions of high-value polymers such as block copolymers.[34]

In the early 1950s, Ziegler-Natta and Phillips chromium catalysis technology completely reformed the existing non-catalyzed polyethylene and polypropylene resins process.[34] Since then, in-depth research optimized the technology by increasing productivity and removing purification steps.[35] Since the 1990s, the development of metallocene single-site catalysts allowed the chemical industry to produce polymers with better control of composition distributions and branching.[35-36] More recently, post-metallocene single site catalysts with tunable organometallic ligands enabled precise control polyolefin regio-/stereoselectivity,[34, 37-38] development of olefin block copolymers via chain shuttling polymerization,[39-40] and high-temperature reactions (above 120 °C) while maintaining high activities and polymer properties with constrained geometry catalysts.[40-41] Kol and coworkers also introduced post-metallocene salan-like ligands with an extra donor pendant arm.[42-44] With group IV transition metals, their catalysts showed high activity towards 1-hexene polymerization.

In many applications, polyolefin resins contain a small fraction of comonomers (e.g. α-olefin). The addition of a comonomer to olefin polymerization yields copolymers with tunable mechanical and thermal properties. Most importantly, incorporation of α-olefin in ethylene polymerization yields semicrystalline linear ethylene copolymers with a low density, linear low-density polyethylene (LLDPE).[45] With its unique rheological properties due to significant numbers of short branches and lack of long branching, LLDPE has been widely used for films and packaging. The production of LLDPE accounts for roughly 37% market share of all polyethylene resins manufactured in the United States in 2012.[45]

Today, the production of LLDPE resins is heavily dictated by Ziegler-Natta catalysts, Phillips catalysts, and metallocene catalysts.[46] However, the development of

copolymerization based on single-site catalysts that yield uniform compositions and tunable properties has attracted much attention in both academia and industry.[34, 37, 40-41, 45] Our group reported multi-response kinetic data as well as kinetic modeling of 1-hexene polymerization based on single-site Zr, Hf–amine bis(phenolate) catalysts, M[tBu-ON^{X}O]Bn$_2$ (where X = THF, pyridine, NMe$_2$, furan, SMe), activated by B(C$_6$F$_5$)$_3$.[47-50] The kinetic modeling of 1-hexene polymerization of these systems yielded rate constants for the key elementary reaction steps. The success of these kinetic modeling exercises has motivated us to explore the uncharted area of copolymerization of ethylene and α-olefin, in this case, the commercially relevant 1-hexene. Chapter 3 describes ethylene/1-hexene copolymerization by hafnium salan-type catalyst. The effects of monomer concentration, reaction time, and catalyst concentration on reactivity and copolymer composition have been studied. The catalyst deactivation behavior and comonomer effects are explained.

With the rapidly growing production of LLDPE, the demand for α-olefin also has been increasing. Traditionally, about 40% of the entire LLDPE resins worldwide was manufactured with 1-butene due to its low price and availability from the distillation of refinery streams.[45] However, ethylene copolymers with higher α-olefin such as 1-hexene and 1-octene have been increasing because of the superior mechanical properties compared to copolymers with 1-butene.[45] Recently developed by Chevron Phillips Chemicals and Sasol, chromium catalysts with organometallic ligands are extremely active towards selective 1-hexene/1-octene productions.[51] Our group studied the kinetics of ethylene trimerization catalyzed by a highly active chromium N-phosphinoamidine catalyst, provided by Chevron Phillips Chemical Company,[52] using *in-situ* high-pressure NMR techniques.[53] Our kinetic

study with quantitative kinetic modeling enabled us to propose a simple metallacyclic mechanism with established rate constants. The success of these kinetic studies via high-pressure operando NMR techniques has motivated us to explore a more complex tri-/tetramerization of ethylene to give 1-hexen and 1-octene. Chapter 4 describes development of new methods to study the kinetics of ethylene consumption and 1-hexene/1-octene formation. We report preliminary results from the developed methods and describe the limitation and areas in need of improvements.

C. References

1. Faramawy, S.; Zaki, T.; Sakr, A. A. E., Natural gas origin, composition, and processing: A review. *Journal of Natural Gas Science and Engineering* **2016,** *34*, 34-54.
2. McFarland, E., Chemistry. Unconventional chemistry for unconventional natural gas. *Science* **2012,** *338* (6105), 340-2.
3. Paunovic, V.; Zichittella, G.; Moser, M.; Amrute, A. P.; Perez-Ramirez, J., Catalyst design for natural-gas upgrading through oxybromination chemistry. *Nat Chem* **2016,** *8* (8), 803-9.
4. Sousa-Aguiar, E. F.; Noronha, F. B.; Faro, J. A., The main catalytic challenges in GTL (gas-to-liquids) processes. *Catalysis Science & Technology* **2011,** *1* (5).
5. Podkolzin, S. G.; Stangland, E. E.; Jones, M. E.; Peringer, E.; Lercher, J. A., Methyl chloride production from methane over lanthanum-based catalysts. *Journal of the American Chemical Society* **2007,** *129* (9), 2569-2576.
6. Parkyns, N. D.; Warburton, C. I.; Wilson, J. D., Natural gas conversion to liquid fuels and chemicals: Where does it stand? *Catalysis Today* **1993,** *18* (4), 385-442.

7. Lange, J. P.; Tijm, P. J. A., Processes for converting methane to liquid fuels: Economic screening through energy management. *Chemical Engineering Science* **1996,** *51* (10), 2379-2387.

8. Lunsford, J. H., The Catalytic Oxidative Coupling of Methane. *Angewandte Chemie-International Edition in English* **1995,** *34* (9), 970-980.

9. Gélin, P.; Primet, M., Complete oxidation of methane at low temperature over noble metal based catalysts: a review. *Applied Catalysis B: Environmental* **2002,** *39* (1), 1-37.

10. Keil, F. J., Methane activation: Oxidation goes soft. *Nat Chem* **2013,** *5* (2), 91-2.

11. Periana, R. A.; Taube, D. J.; Gamble, S.; Taube, H.; Satoh, T.; Fujii, H., Platinum catalysts for the high-yield oxidation of methane to a methanol derivative. *Science* **1998,** *280* (5363), 560-564.

12. Lorkovic, I. M.; Yilmaz, A.; Yilmaz, G. A.; Zhou, X.-P.; Laverman, L. E.; Sun, S.; Schaefer, D. J.; Weiss, M.; Noy, M. L.; Cutler, C. I.; Sherman, J. H.; McFarland, E. W.; Stucky, G. D.; Ford, P. C., A novel integrated process for the functionalization of methane and ethane: bromine as mediator. *Catalysis Today* **2004,** *98* (1-2), 317-322.

13. Crabtree, R. H., Organometallic alkane CH activation. *Journal of Organometallic Chemistry* **2004,** *689* (24), 4083-4091.

14. Burk, M. J.; Crabtree, R. H., Selective Catalytic Dehydrogenation of Alkanes to Alkenes. *Journal of the American Chemical Society* **1987,** *109* (26), 8025-8032.

15. Baudry, D.; Ephritikhine, M.; Felkin, H.; Holmessmith, R., The Selective Catalytic Conversion of Cycloalkanes into Cycloalkenes Using a Soluble Rhenium Polyhydride System. *Journal of the Chemical Society-Chemical Communications* **1983,** (14), 788-789.

16. Shih, K. C.; Goldman, A. S., Alkane Dehydrogenation Catalyzed by Rhodium(I) Phosphine Complexes - Observation of the Stoichiometric Alkane-to-Rhodium Hydrogen-Transfer Step. *Organometallics* **1993,** *12* (9), 3390-3392.

17. Jensen, C. M., Iridium PCP pincer complexes: highly active and robust catalysts for novel homogeneous aliphatic dehydrogenations. *Chemical Communications* **1999,** *3* (24), 2443-2449.

18. Moulton, B. C. J.; Shaw, B. L., Transition Metal-Carbon Bonds. Part XLII. Complexes of Nickel, Palladium, Platinum, Rhodium and Iridium with the Tridentate Ligand 2,6- Bis[(di-t-butylphosphino)methyl]pheny. *J. Chem. Soc. Dalton Trans.* **1975,** (1020), 1020-1024.

19. Xu, W. W.; Rosini, G. P.; Gupta, M.; Jensen, C. M.; Kaska, W. C.; KroghJespersen, K.; Goldman, A. S., Thermochemical alkane dehydrogenation catalyzed in solution without the use of a hydrogen acceptor. *Chemical Communications* **1997,** (23), 2273-2274.

20. Zell, T.; Milstein, D., Hydrogenation and dehydrogenation iron pincer catalysts capable of metal-ligand cooperation by aromatization/dearomatization. *Acc Chem Res* **2015,** *48* (7), 1979-94.

21. Choi, J.; MacArthur, A. H.; Brookhart, M.; Goldman, A. S., Dehydrogenation and related reactions catalyzed by iridium pincer complexes. *Chem Rev* **2011,** *111* (3), 1761-79.

22. Zhu, K.; Achord, P. D.; Zhang, X.; Krogh-Jespersen, K.; Goldman, A. S., Highly effective pincer-ligated iridium catalysts for alkane dehydrogenation. DFT calculations of relevant thermodynamic, kinetic, and spectroscopic properties. *J Am Chem Soc* **2004,** *126* (40), 13044-53.

23. Renkema, K. B.; Kissin, Y. V.; Goldman, A. S., Mechanism of alkane transfer-dehydrogenation catalyzed by a pincer-ligated iridium complex. *J Am Chem Soc* **2003,** *125* (26), 7770-1.

24. Goldman, A. S.; Roy, A. H.; Huang, Z.; Ahuja, R.; Schinski, W.; Brookhart, M., Catalytic alkane metathesis by tandem alkane dehydrogenation-olefin metathesis. *Science* **2006,** *312* (5771), 257-61.

25. Haibach, M. C.; Kundu, S.; Brookhart, M.; Goldman, A. S., Alkane metathesis by tandem alkane-dehydrogenation-olefin-metathesis catalysis and related chemistry. *Acc Chem Res* **2012,** *45* (6), 947-58.

26. Leitch, D. C.; Lam, Y. C.; Labinger, J. A.; Bercaw, J. E., Upgrading light hydrocarbons via tandem catalysis: a dual homogeneous Ta/Ir system for alkane/alkene coupling. *J Am Chem Soc* **2013,** *135* (28), 10302-5.

27. Yi, J.; Miller, J. T.; Zemlyanov, D. Y.; Zhang, R.; Dietrich, P. J.; Ribeiro, F. H.; Suslov, S.; Abu-Omar, M. M., A reusable unsupported rhenium nanocrystalline catalyst for acceptorless dehydrogenation of alcohols through gamma-C-H activation. *Angew Chem Int Ed Engl* **2014,** *53* (3), 833-6.

28. Liu, S.; Senocak, A.; Smeltz, J. L.; Yang, L. N.; Wegenhart, B.; Yi, J.; Kenttamaa, H. I.; Ison, E. A.; Abu-Omar, M. M., Mechanism of MTO-Catalyzed Deoxydehydration of Diols to Alkenes Using Sacrificial Alcohols. *Organometallics* **2013,** *32* (11), 3210-3219.

29. Morales-Morales, D.; Lee, D. W.; Wang, Z.; Jensen, C. M., Oxidative Addition of Water by an Iridium PCP Pincer Complex: Catalytic Dehydrogenation of Alkanes by IrH(OH){C6H3-2,6-(CH2PBut2)2}. *Organometallics* **2001,** *20* (6), 1144-1147.

30. Plastics - the Facts 2019. **2019**.

31. Sita, L. R., Ex uno plures ("out of one, many"): new paradigms for expanding the range of polyolefins through reversible group transfers. *Angew Chem Int Ed Engl* **2009,** *48* (14), 2464-72.

32. Global plastic production from 1950 to 2018 (in million metric tons) | Statista.

33. Polypropylene Market To Reach USD 155.57 Billion By 2026 | Reports And Data.

34. Qiao, J. L.; Guo, M. F.; Wang, L. S.; Liu, D. B.; Zhang, X. F.; Yu, L. Q.; Song, W. B.; Liu, Y. Q., Recent advances in polyolefin technology. *Polymer Chemistry* **2011,** *2* (8), 1611-1623.

35. Galli, P.; Vecellio, G., Technology: driving force behind innovation and growth of polyolefins. *Progress in Polymer Science* **2001,** *26* (8), 1287-1336.

36. Galli, P.; Vecellio, G., Polyolefins: The most promising large-volume materials for the 21st century. *Journal of Polymer Science Part a-Polymer Chemistry* **2004,** *42* (3), 396-415.

37. Coates, G. W., Precise control of polyolefin stereochemistry using single-site metal catalysts. *Chem Rev* **2000,** *100* (4), 1223-52.

38. McKnight, A. L.; Waymouth, R. M., Group 4 ansa-Cyclopentadienyl-Amido Catalysts for Olefin Polymerization. *Chem Rev* **1998,** *98* (7), 2587-2598.

39. Arriola, D. J.; Carnahan, E. M.; Hustad, P. D.; Kuhlman, R. L.; Wenzel, T. T., Catalytic production of olefin block copolymers via chain shuttling polymerization. *Science* **2006,** *312* (5774), 714-9.

40. Chum, P. S.; Swogger, K. W., Olefin polymer technologies-History and recent progress at The Dow Chemical Company. *Progress in Polymer Science* **2008,** *33* (8), 797-819.

41. Klosin, J.; Fontaine, P. P.; Figueroa, R., Development of group IV molecular catalysts for high temperature ethylene-alpha-olefin copolymerization reactions. *Acc Chem Res* **2015,** *48* (7), 2004-16.

42. Tshuva, E. Y.; Groysman, S.; Goldberg, I.; Kol, M.; Goldschmidt, Z., [ONXO]-type amine bis(phenolate) zirconium and hafnium complexes as extremely active 1-hexene polymerization catalysts. *Organometallics* **2002,** *21* (4), 662-670.

43. Tshuva, E. Y.; Goldberg, I.; Kol, M.; Goldschmidt, Z., Zirconium complexes of amine-bis(phenolate) ligands as catalysts for 1-hexene polymerization: Peripheral structural parameters strongly affect reactivity. *Organometallics* **2001,** *20* (14), 3017-3028.

44. Tshuva, E. Y.; Goldberg, I.; Kol, M., Isospecific Living Polymerization of 1-Hexene by a Readily Available NonmetalloceneC2-Symmetrical Zirconium Catalyst. *Journal of the American Chemical Society* **2000,** *122* (43), 10706-10707.

45. Kissin, Y. V., Polyethylene, Linear Low Density. *Kirk-Othmer Encyclopedia of Chemical Technology* **2015**, 1-33.

46. Kissin, Y. V.; Mink, R. I.; Nowlin, T. E., Ethylene polymerization reactions with Ziegler-Natta catalysts. I. Ethylene polymerization kinetics and kinetic mechanism. *Journal of Polymer Science Part a-Polymer Chemistry* **1999,** *37* (23), 4255-4272.

47. Pletcher, P. D.; Switzer, J. M.; Steelman, D. K.; Medvedev, G. A.; Delgass, W. N.; Caruthers, J. M.; Abu-Omar, M. M., Quantitative Comparative Kinetics of 1-Hexene Polymerization across Group IV Bis-Phenolate Catalysts. *Acs Catalysis* **2016,** *6* (8), 5138-5145.

48. Steelman, D. K.; Pletcher, P. D.; Switzer, J. M.; Xiong, S. L.; Medvedev, G. A.; Delgass, W. N.; Caruthers, J. M.; Abu-Omar, M. M., Comparison of Selected Zirconium and Hafnium Amine Bis(phenolate) Catalysts for 1-Hexene Polymerization. *Organometallics* **2013,** *32* (17), 4862-4867.

49. Steelman, D. K.; Xiong, S.; Pletcher, P. D.; Smith, E.; Switzer, J. M.; Medvedev, G. A.; Delgass, W. N.; Caruthers, J. M.; Abu-Omar, M. M., Effects of pendant ligand binding

affinity on chain transfer for 1-hexene polymerization catalyzed by single-site zirconium amine bis-phenolate complexes. *J Am Chem Soc* **2013,** *135* (16), 6280-8.

50. Switzer, J. M.; Travia, N. E.; Steelman, D. K.; Medvedev, G. A.; Thomson, K. T.; Delgass, W. N.; Abu-Omar, M. M.; Caruthers, J. M., Kinetic Modeling of 1-Hexene Polymerization Catalyzed by Zr(tBu-ONNMe2O)Bn2/B(C6F5)3. *Macromolecules* **2012,** *45* (12), 4978-4988.

51. Sydora, O. L., Selective Ethylene Oligomerization. *Organometallics* **2019,** *38* (5), 997-1010.

52. Sydora, O. L.; Jones, T. C.; Small, B. L.; Nett, A. J.; Fischer, A. A.; Carney, M. J., Selective Ethylene Tri-/Tetramerization Catalysts. *Acs Catalysis* **2012,** *2* (12), 2452-2455.

53. Gunasekara, T.; Kim, J.; Preston, A.; Steelman, D. K.; Medvedev, G. A.; Delgass, W. N.; Sydora, O. L.; Caruthers, J. M.; Abu-Omar, M. M., Mechanistic Insights into Chromium-Catalyzed Ethylene Trimerization. *Acs Catalysis* **2018,** *8* (8), 6810-6819.

CHAPTER II. Formation and Reactivity of Ir-Re Bimetallic Complexes from the Reaction of Methyltrioxorhenium and PCP-Iridium hydride

A. Introduction

Heterobimetallic complexes have shown interesting reactivity because of a polar metal-metal bond and unique two reactive sites.[1-3] In biology, Ni-Fe bond is used in hydrogenase enzymes.[4-5] Various inorganic Ta-Ir[6-7] and Zr-Ir[8-9] complexes studied by Bergman have shown dinuclear oxidative addition and substrate coordination reactions based on the large electronegativity difference between the two metal sites. More recently, catalysis involving two active sites such as Zr-Co for hydrosilylation[10-11] and Pd-Ti for allylic substitution[12] have been reported. Cooperation of unique metal sites to benefits the overall catalysis.

Due to the oxygen-richness in bio-derived molecules, removing oxygen is crucial to make valuable chemicals from biomass.[13] Our group and others have shown that rhenium based catalysts are effective at deoxydehydration (DODH) of diols and polyols in the presence of a reductant such as alcohol or H_2.[14-18] Utilizing readily available and cheap chemical reductants is attractive. Upgrading light hydrocarbons, which are abundant from natural gas, have been studied extensively. Our idea is to couple DODH of diols and polyols and alkane dehydrogenation of light alkane (Scheme 2.1).

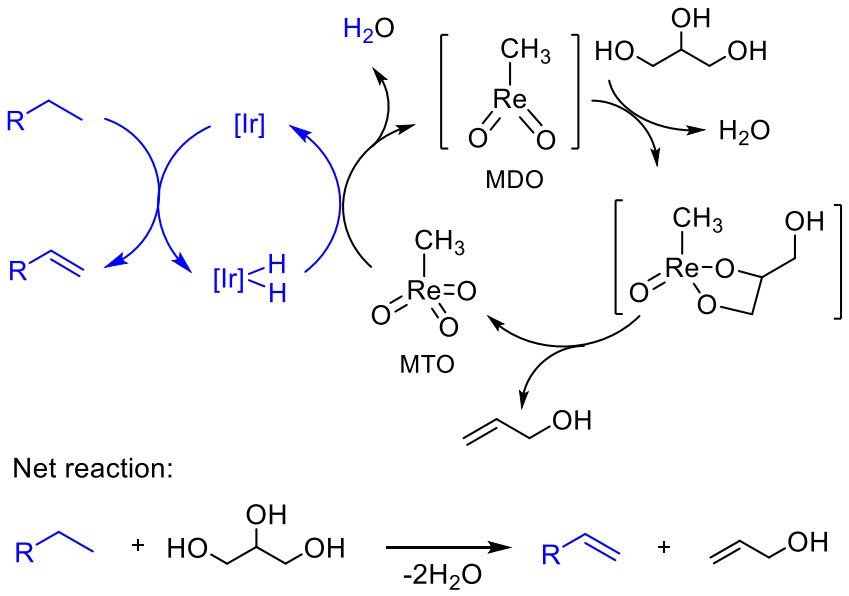

Scheme 2.1. Proposed conversion of light hydrocarbons with biomass-derived glycerol using a bimetallic Ir-Re system.

The concept of tandem catalysis of alkane dehydrogenation has been demonstrated in the literature.[19-21] As shown in Scheme 2.1, the hydride of pincer-based Ir catalysts would reduce MTO to methyldioxorhenium (MDO). The latter has been shown to regenerate MTO from diols and activated Ir to dehydrogenate hydrocarbons.[16, 22] Thorough mechanistic and DFT studies have shown that release of hydride from iridium is the turn-over limiting step, and we hypothesized that MTO can act as hydrogen acceptor.[23-26] Before investigating the tandem catalysis, we wanted to understand the fundamental chemistry and reactivity of iridium pincer complexes and MTO.

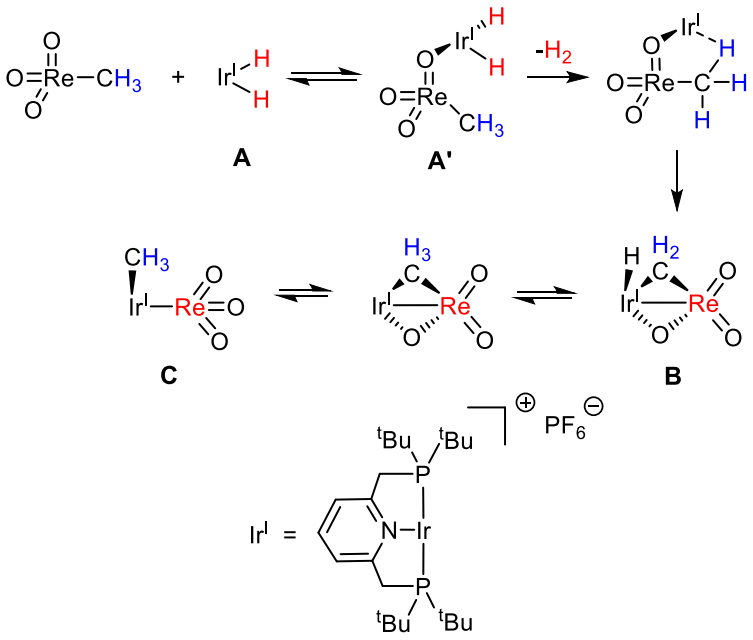

Scheme 2.2. The reaction of (PNP)IrH_2 complex with MTO

In this regard, we have recently reported that the reaction of (PNP)IrH_2 (**A**) with methyltrioxorhenium (MTO) gave the bimetallic complex [(PNP)(H)Ir-μ(CH_2)-μ(O)-$Re(O)_2$][PF_6] (**B**) with the liberation of H_2 (Scheme 2.2).[27] We proposed that the reaction initiates with the oxo coordination of MTO to iridium. Loss of dihydrogen followed by the C-H activation by iridium give complex **B** as the final product.[27] Our DFT investigation combined with experimental kinetics revealed that the structural isomer [(PNP)(Me)Ir-ReO_3][PF_6] (**C**) can be in equilibrium with **B** upon switching the solvent from methylene chloride to acetonitrile via methyl bridged Ir-Re center. While compounds **B** and **C** were isolated and characterized by NMR and X-ray techniques, others were proposed structures from DFT calculations. Herein, we report the reaction of MTO with (PCP)IrH_2 (**1a**) to give a different iridium-rhenium bimetallic complex (PCP)Ir(ReO_3)(H) (**2a**) with a loss of methane. The reaction chemistry of **2a** either via disproportionation or with another equivalent of

MTO leads to (PCP)Ir(H)(-μ(O)ReO_3)] (**4**), which was characterized structurally. The reaction pathways of **1a** with MTO were studied via DFT calculations providing insights into the mechanism.

B. Results and Discussion

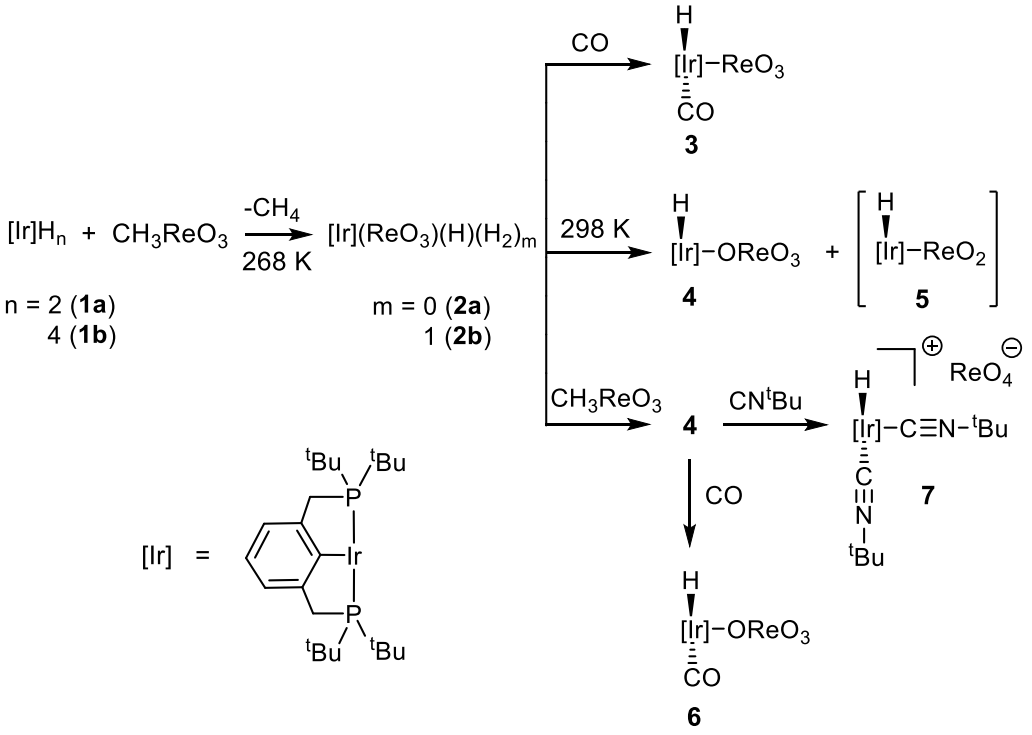

Scheme 2.3. Reaction chemistry of (PCP)IrH_2 complex **1** with MTO

Synthesis of complex **1** resulted in a mixture of two complexes (PCP)IrH_2 (**1a**) and (PCP)IrH_4 (**1b**) as reported in the literature.[28] Pure **1a** and **1b** were obtained from the mixture by applying vacuum or bubbling hydrogen, respectively.[29] Mixing one equivalent of MTO with the mixture of **1a** and **1b** at 273 K for 4 hours resulted in formation of the bimetallic complexes (PCP)Ir(ReO_3)(H) **2a** and (PCP)Ir(ReO_3)(H)(H_2) **2b** and methane,

which were observed by low-temperature ^{1}H and $^{31}P\{^{1}H\}$ NMR (Scheme 2.3). The mixture of **1a** and **1b** with MTO at 233 K only results in **2a** with the loss of methane observed by ^{1}H NMR at δ 0.22. As the temperature increased to 273 K, formation of **2b** and additional methane was observed in the duration of 4 hours. Elucidating the structures of **2a** and **2b** was not straightforward because they were unstable above 273 K and attempts to obtain single crystals of **2a** and **2b** were not successful. We adopted a combination of NMR and reaction chemistry in tandem with DFT calculations to propose the structures of **2a** and **2b**.

The formation of methane was confirmed by deuterium labeling experiments. The reaction of (PCP)IrD_2 (**1a-D_2**) and MTO formed CH_3D, which was observed at δ 0.21 with triplet from H-D coupling of J = 1.9 Hz in ^{1}H NMR. Furthermore, the reaction between **1a** and deuterated MTO (CD_3ReO_3) resulted in CHD_3, and the ^{1}H NMR showed a distinct signal at δ 0.18 with heptet (J = 1.5 Hz) splitting pattern. The labeling studies confirmed that methane formed from the CH_3 of MTO and one of the hydrides from (PCP)$Ir(H)_n$ (n = 2 or 4).

Bubbling CO gas into the reaction solution of **2a** at 273 K over 2 h resulted in clean formation of (PCP)Ir(H)(ReO_3)(CO) (**3**) having CO trans to the hydride. The structure of complex **3** was confirmed unambiguously by IR, NMR, and single crystal X-ray crystallography, thereby confirming the elemental composition of complex **2a**. Interestingly, the reaction of **2b** and CO gas also resulted in **3** cleanly, suggesting that dihydrogen ligand of **2b** is weakly coordinated to the Ir center.

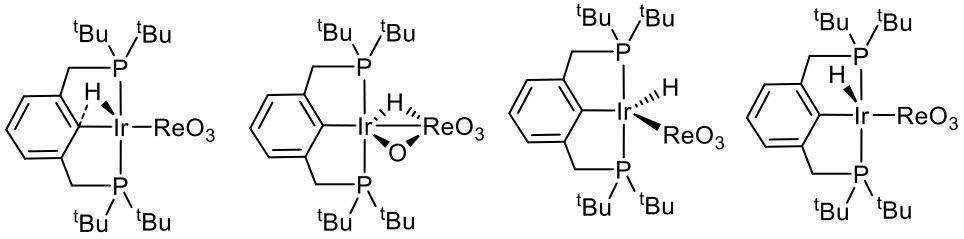

Chart 2.1. Possible structures for complex **2a**.

Based on the release of methane as well as the formation of CO adduct **3**, possible structures of complex **2a** are shown in **Chart 2.1**. We used variable temperature-NMR for further elucidating the structure. At 233 K, the ^{1}H NMR signal for the Ir-H appeared at δ -36.2 as a broad singlet. Previously reported PCP complexes of Rh, Co, and Pd with η^2-C_{arene}-H agostic bond showed distinctively more deshielded hydride signal near 4 ppm[30-33] and thereby eliminated the possibility of structure **2a-1**. Upon enriching **2a** with ^{17}O by using ^{17}O enriched MTO, ^{17}O{^{1}H} NMR spectrum (at 230 K) showed a single peak at 773 ppm, which can be assigned to Re oxo functionality. This eliminated the possibility of structure **2a-2** as we observed ^{17}O NMR signal of previously reported oxo bridged (^{tBu}PNP)Ir-*O*-Re complex appeared at 565 ppm.[27] In addition, no significant broadening of the 773 ppm signal was observed at variable temperature from 230 K to 273 K; broadening is characteristic for ^{17}O signals attributed to μ-oxo ligands.[27] The distinct upfield hydride signal of **2a** is characteristic of a hydride ligand trans to a vacant site in contrast to a hydride trans to ligands (**2a-3**), which are shifted downfield. Thus, **2a-4** with the hydride trans to a vacant site must be the structure of **2a**.

Analogously (PCP)Ir(ReO_3)(D_2)(D) (**2b-D**) was formed by the reaction of MTO and deuterium-labeled **1b** (**1b-D$_4$**), (synthesized by bubbling D_2 into the solution of **1a**. In the

^{1}H-NMR of **2b-D**, the broad Ir-dihydride ligand signal at δ -3.0 became triplet resulting from H-D splitting (J = 1.8 Hz) as shown in Figure 2.1. No effect on the signal at -3.0 ppm by ^{1}H{^{31}P} NMR by phosphorous nuclei indicated that the triplet of Ir(H_2)is from H-D coupling and Ir-D must be coupled to Ir(H_2). On the other hand, the triplet splitting of the Ir-H signal disappeared in ^{1}H{^{31}P} NMR.

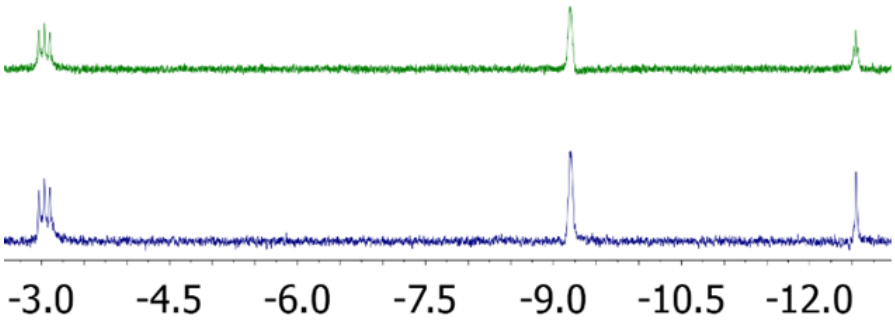

Figure 2.1. Top to bottom: ^{1}H-NMR of **1b-D** and (PCP)Ir(ReO_3)(D)(H_2) (**2b-D**), ^{1}H{^{31}P}-NMR of **1b-D$_n$** and (**2b-D**) at 233K.

The structure of **2b** was also investigated by variable temperature ^{1}H and ^{31}P{^{1}H} NMR. At 233 K, two types of ^{1}H NMR signals corresponding to Ir-H of **2b** at δ -3.0 (broad singlet) and δ -12.6 (broad triplet) with a 2:1 ratio. These two signals showed a strong correlation in the COSY NMR experiment at 233 K, consistent with the structure of **2b** with iridium having both dihydrogen as well as hydride ligands (Figure 2.2). Interestingly **2b** also exhibited temperature-dependent fluxional behavior. As the temperature was raised to 260 K, the hydride signal at δ -12.6 became sharper but the dihydrogen signal was not affected. Furthermore, ^{1}H{^{31}P} NMR experiment resulted in a broad singlet for the hydride. The overall broadness of the hydride signal can be attributed to the fast exchanges of structural isomers or different conformers. Thus we propose that the structure of **2a** is appropriate to be

2D with a square pyramidal around the metal center and the hydride on axial position and structure of the **2b** has dihydrogen ligand trans to Ir-H (Figure 2.2).

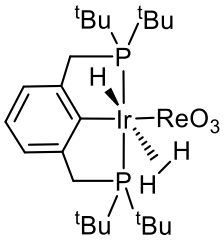

Figure 2.2. Structure of complex **2b**.

Both complexes **2a** and **2b** were stable at 273 K. However, at 298 K, they underwent a disproportionation reaction (over 2 days) to form (PCP)Ir(H)(ReO_4) (**4**) (isolated yield = 35%) and (PCP)Ir(H)(ReO_2) (**5**). Complex **5** was only observed by NMR and attempts to isolate it was not successful and lead to intractable compounds. The formation of a black precipitate during the course of this reaction indicated that complex **5** was not stable. Analogous Re(III) complexes with vacant sites were reported to be reactive and form polymers analogous to methyldioxorhenium (MDO).[34] In ^{1}H NMR, complexes **4** and **5** showed signals at -40 and -45 ppm, respectively, and were consistent with their hydride structure with no ligand trans to the hydride. By contrast, adding another equivalent of MTO to complex **2** at 273 K resulted in complex **4** with an isolated yield of 73% and black precipitate with no formation of complex **5**.[34] Introduction of CO gas into the toluene solution of isolated **4** at room temperature gave the CO adduct **6** cleanly. On the other-hand introduction of tert-butyl isocyanide resulted in the formation of complex **7** with perrhenate

as the anion and breaking of the Ir-Re bond in complex **4**. Both complexes **6** and **7** were unambiguously characterized by multinuclear NMR and single-crystal X-ray crystallography.

Because the reduction of MTO to MDO requires strong reducing agents like trimethylphosphine, utilization of the oxophilicity of **2** in catalysis was warranted.[35] Stable bimetallic complexes are useful in catalysis. In that context in order to check the utility of **2** in catalytic applications, stable Ir-Re bond in complex **2** is a necessity. So the addition of a bridging ligand such as bis(dimethylphosphino)methane (dmpm) could be helpful in maintaining the Ir-Re bond. Adding dmpm to the toluene solution of **2** at 195 K resulted in adduct **8**, which was confirmed by NMR and X-ray crystallography (Scheme 2.4).

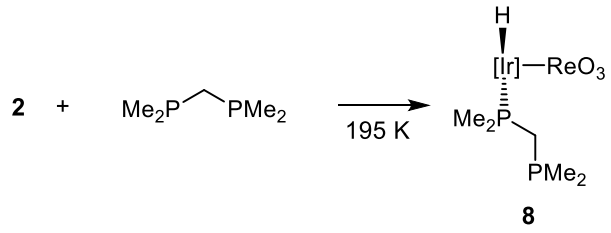

Scheme 2.4. Reaction of complex **2** with bis(dimethylphosphino)methane (dmpm) at 195 K

In ^{1}H NMR observation of a doublet of triplet of doublet at δ –12.5 (J_{H-P} = 130, 18, 5 Hz) for the hydride ligand was consistent with the structure of **8**. In addition to the triplet (J_{H-P} = 13 Hz) by PCP ligand and large doublet (J_{H-P} = 130 Hz) by phosphine trans to the Ir-H, there is a doublet with a weak coupling (J_{H-P} = 5 Hz) by the uncoordinated phosphorus. The ^{31}P{^{1}H} of **8** exhibited broad singlet at δ 50, –55, and –61 (roughly 2:1:1 ratio), which was unusual because ^{31}P{^{1}H} of the phosphines coordinated to iridium usually show up relatively downfield like 50 ppm. The selective ^{1}H{^{31}P} NMR experiment at δ –55 of **8** removed the large doublet and resulted in a triplet of doublet at δ –12.2 (J_{H-P} = 18, 5 Hz),

suggesting that the unusual shift is from the weakly coordinated dmpm. Furthermore, the other two phosphorus signals were assigned by the selective $^{1}H\{^{31}P\}$ NMR experiments. The introduction of trimethylphosphine to **8** at room temperature rapidly afforded **9**, which could be independently synthesized by adding PMe_3 to a solution of **2** at 268 K (Scheme 2.5). The replacement of dmpm with PMe_3 confirmed the weak coordination between (PCP)Ir and dmpm of **8**.

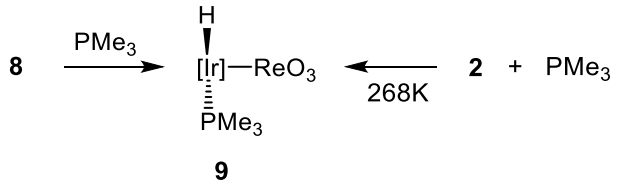

Scheme 2.5. The reaction of complex **8** with PMe_3

Complexes **3**, **6**, **7**, and **8** have iridium with octahedral geometry whereas **4** has square pyramidal geometry around the iridium atom leaving a vacant site trans to the H atom (Figure 2.3, Table 2.1). The bond angles around Ir showed that the structures were not significantly distorted. The iridium-rhenium bond length in **3** is 2.608(2) Å and longer than the bond length reported for **B** (2.4915(5) Å), suggesting a weaker Ir-Re bond in **3**.[27] Furthermore, terminal Re-O bonds lengths of **3** were slightly longer (~0.06 Å) than those of complexes with ReO_4 (**4**, **6**, **7**). The iridium-phosphorus of dmpm bond lengths of **8** (2.43(1) Å) was slightly longer than PCP-iridium bond lengths (2.37(1) Å).

Table 2.1. Comparison of bond lengths, bond angles and dihedral angle of complexes 3, 4, 6, 7, and 8.

Bond length and bond angles	3	4	6	7	8
C(ipso)-Ir	2.11 (3)	2.031(9)	2.05(1)	2.10(2)	2.10(5)
Ir-O		2.09(1)	2.192(8)		
Re-O (bridged)		1.80(1)	1.748 (8)		
Re-O (terminal)	1.76(3), 1.79(3), 1.78(3)	1.698(9), 1.73(1), 1.68(1)	1.695(9), 1.69(1), 1.72(1)	1.69(2), 1.72(3), 1.67(2), 1.70(3)	1.72(4), 1.71(4), 1.70(5)
Ir-*C*O	1.90(4)		1.95(1)	2.01(1), 2.02(2)	
Ir-H	1.64(3)		1.81 (1)	1.60(1)	1.53(5)
Ir-Re	2.602(2)	3.8569(6)	3.798		2.5564 (5)
Ir-(*P*C*P*)	2.363(9), 2.365(8)	2.321(2), 2.315(2)	2.356(3), 2.362(3)	2.353(8), 2.317(8)	2.37(1), 2.37(1)
Ir-P_3					2.43(1)
C(ipso)Ir-Re	173.9(9)	177.4(2)	169.75		177.68
H-Ir-C(O)	172(2)		170(4)	169.0(9), 90.6(9)	
C(ipso)-Ir-P-Re	-173.85	179.5(2)	170.5(3)		

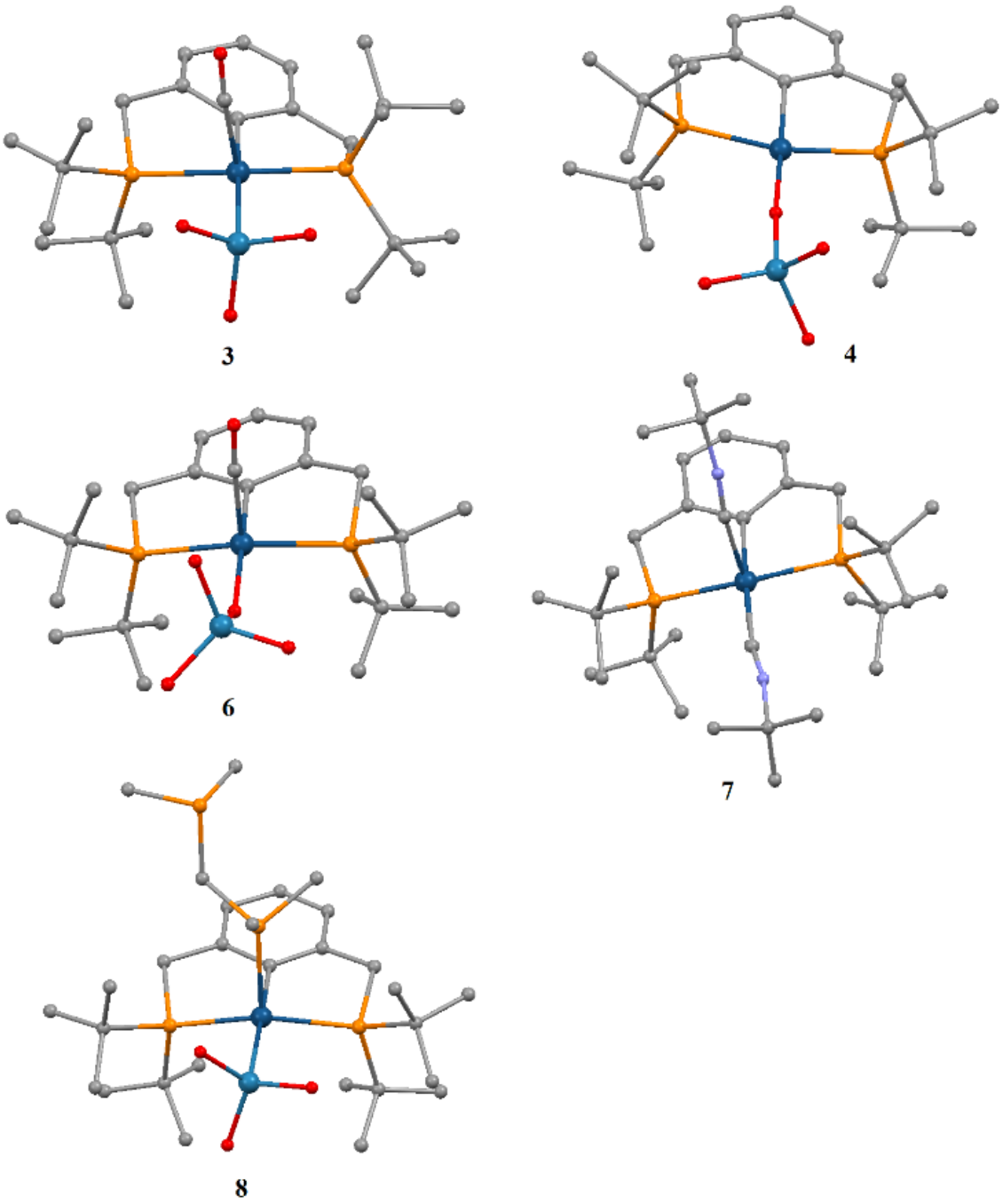

Figure 2.3. X-ray structure of complexes **3**, **4**, **6**, **7**, **8**. Hydrogen atoms and counter ions are omitted for clarity. Carbons are in gray, iridium in darker blue, rhenium in light blue, phosphorus in yellow, oxygen in red, nitrogen in purple.

The reactivity of complexes **1** with MTO when compared to previously studied complex **A** revealed completely different chemistry. We propose that complex **1** reacts with MTO as a simple Lewis acid-base reaction to release methane and form **2** whereas **A** initiates with oxo coordination of MTO to iridium. To study the reaction mechanism, the reaction between **1** and MTO was monitored by ^{1}H and ^{31}P NMR at 268 K. For **A**, we observed the broadening of the Ir-H signal as it reacted with MTO, which showed a fast equilibrium between **A** and intermediate A' (Scheme 2.2). However, no significant change in the Ir-H peak of **1** was observed as the reaction proceeded.

We also investigated the reaction of MTO with complex **1a** by DFT to get a better understanding of the reaction pathway leading to the formation of complex **2a** with the release of methane. Four possible scenarios for MTO's interaction with complex **1a** were considered and discussed below (Figure 2.4).

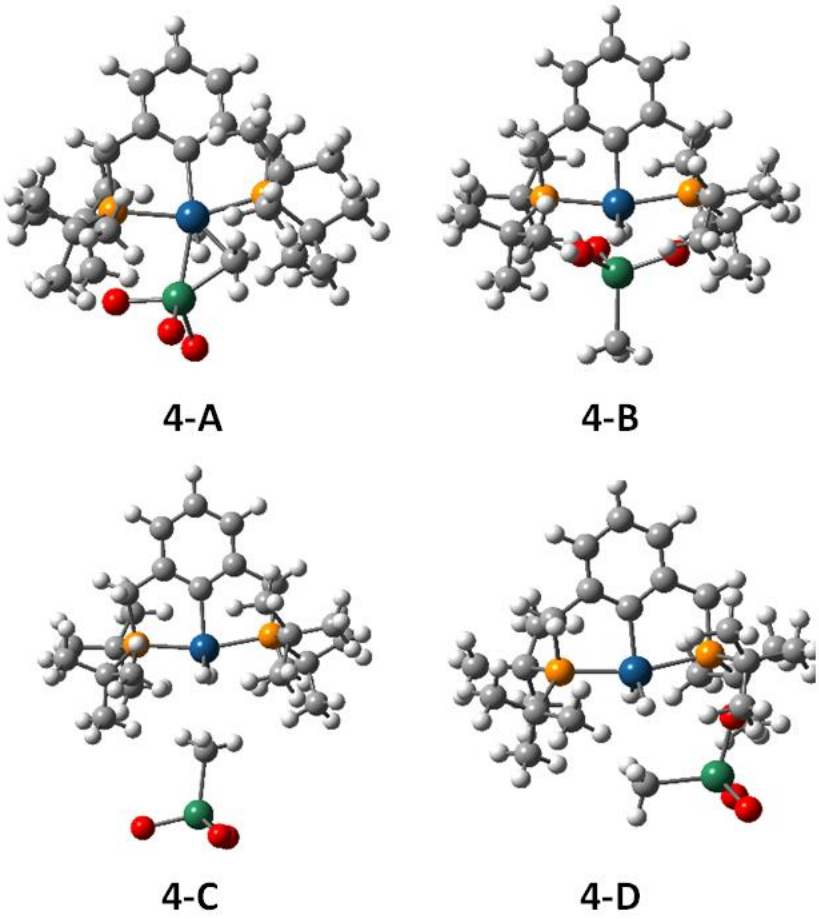

Figure 2.4. Possible attacks of MTO. Carbons are in gray, iridium in light blue, rhenium in green, phosphorus in yellow, nitrogen in dark blue, and hydrogen in white.

(4-A) Formation of methyl bridged complex of MTO, resulting in Ir-Re analogous to the structure reported earlier[27], (4-B) Lewis-acid base complex between Ir and MTO, (4-C) Interaction of methyl group in MTO to Ir metal center of **1a**, (4-D) η^2-coordination of the C-H bond in MTO to Ir metal center in **1a**. Out of four possibilities, the elimination of CH_4 occurred only from 4-A. In all other scenarios, the dissociation of the complexes resulted in no reaction and thereby these approaches were ignored. The pathway from 4-A leading to form **2a** is shown with the potential energy diagram in Figure 2.5.

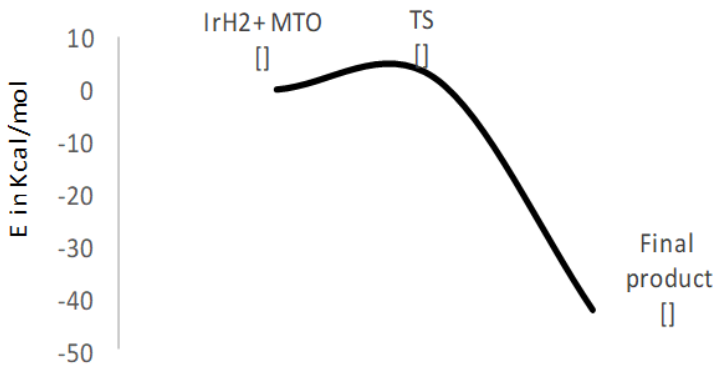

Figure 2.5. Potential energy diagram of the reaction between **1a** and MTO to form **2a**.

We have located one transition state at 2.22 kcal/mol from the initial structure 4-A in Figure 2.4 which is consistent with the experimental observation. The structure of this transition state is shown in Figure 2.6. That TS happens as a first step just before structure 5a. Ir-CH3 distance is equal to 2.77 Å while Re-CH3 is at 2.21Å.

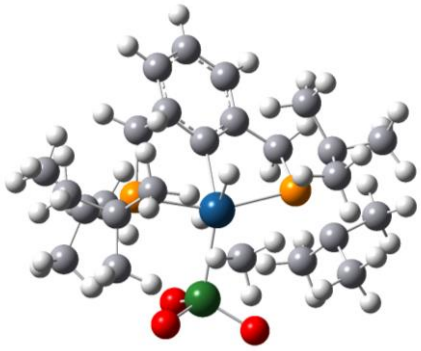

Figure 2.6. The transition state found for the reaction.

With the DFT study, the pathway for the formation of **2a** from MTO and **1a** is described in Figure 2.7. To start with, CH_3, Re and Ir share one of the H from IrH_2 (7-A) followed by elongation of Ir-Re bond (7-B). Subsequent stages are the elongation of the Ir-CH_3 bond (7-C) followed by CH_3 coming closer to ReO_3 (7-D) and H closer to CH_3 eventually breaking the Ir-H bond. The next step is the formation of methane (7-E). The final step is the tightening of the Re-Ir bond with the simultaneous movement of CH_4 away from Ir and Re (7-F).

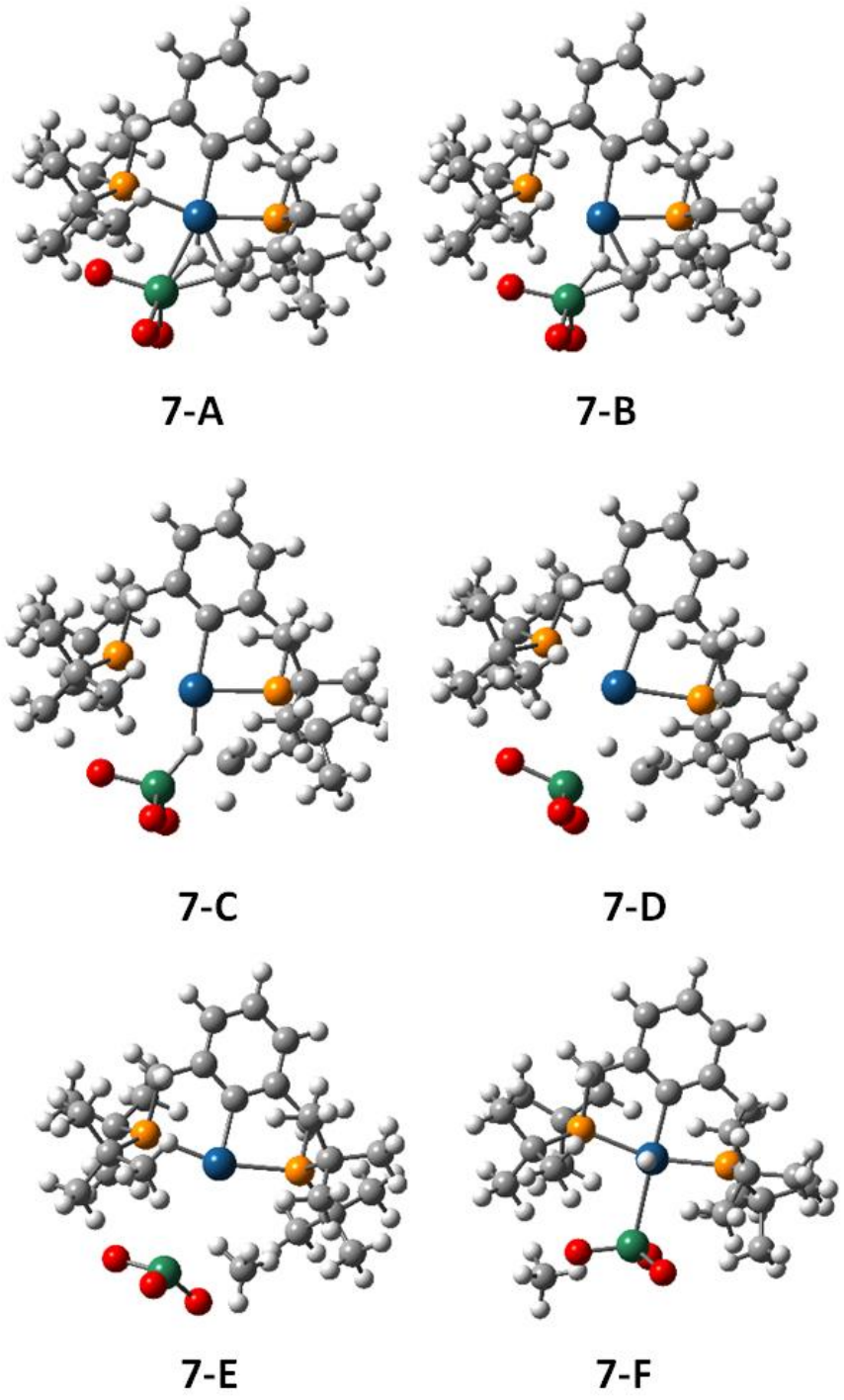

Figure 2.7. Reaction sequence of scenario d from the MTO attack on complex **1**. Carbons are in gray, iridium in light blue, rhenium in green, phosphorus in yellow, nitrogen in dark blue, and hydrogen in white.

C. Conclusion

The reaction between [(PCP)IrH_2] (1a) and methyltrioxorhenium (MTO) at 273 K formed [(PCP)Ir(ReO_3)(H)] (**2a**) with the concurrent release of methane. The formation of methane was confirmed by deuterium labeling study. The addition of CO into a solution of **2a** resulted in the formation of a stable bimetallic complex [(PCP)Ir(ReO_3)(CO)(H)] (**3**) at 273 K, confirming the elemental composition of **2a**. At room temperature, **2a** underwent a disproportionation reaction to form [(PCP)Ir(ReO_4)(H)] (**4**), which was also formed by adding excess MTO to the solution of **2a.** Addition of a bridging phosphine ligand, 1,2-bis(dimethylphosphino)methane (dmpm), to a solution of **2a** formed (PCP)Ir(ReO_3)(dmpm)(H) **8** with one phosphorus bound to Ir. DFT results on the mechanism and reaction pathway of formation of **2a** are reported.

D. Experimental Procedure

1. General Considerations

All reactions were performed in an argon-filled glove box or using standard Schlenk techniques under argon unless otherwise specified. Solvents were degassed, purified with a solvent purification system (Pure Process Technology INC), and stored over activated molecular sieves prior to use. Benzene-d_6 and toluene-d_8 were dried with CaH_2, distilled under argon, and stored over molecular sieves. All other reagents were purchased from commercial vendors (Fischer Scientific and Sigma) and used without further purification.

[(^{tBu}PCP)Ir(H)$_4$][36] (**1**), CDReO$_3$[37], CH$_3$ReO$_3$ (^{17}O-enriched)[38] were prepared according to the published procedure.

One-dimensional and two-dimensional NMR spectra were recorded on a Bruker DRX500-1 NMR spectrometer equipped with a 5mm TXI Z-gradient cryoprobe or a Bruker DRX-500-2 NMR spectrometer equipped with a 5 mm broadband (BBFO) probe and. Bruker TopSpin software (version 1.3) was used for data acquisition and MestReNova (version 9.0) was used for processing of spectra. All spectra obtained were referenced to residual solvent peaks accordingly. Infrared spectra were recorded on a Thermo-Nicolet Nexus FT-IR spectrometer, operated in transmission mode using KBr Pellets. ^{17}O{^{1}H} NMR was referenced to D_2O. All electrospray ionization analyses were carried out on a Waters Micromass ZQ (Waters Corp, Milford, MA) mass spectrometer system. The cone voltage was set to 20 V for all mass spectral analyses. Typical background source pressure was 1.2 x 10-5 torr as read by an ion gauge. The sample flow rate was approximately 60 μL/min. The drying gas was nitrogen. The LCQ is typically scanned to 2000 amu.

2. Reactions

2.1 Reaction of complex 1 with MTO. Formation of [(^{tBu}PCP)Ir(ReO$_3$)(H)] (2)

In a typical reaction, a toluene-d_8 solution (0.2 mL) of [(^{tBu}PCP)Ir(H)$_4$] (**1**) (20 mg, 0.040 mmol) was placed in a capped NMR tube equipped with a septum. A toluene-d_8 solution (0.3 mL) of MTO (8.5 mg, 0.040 mmol) was placed in a capped vial equipped with a septum. After both solutions were cooled to –78 °C using a dry ice/acetone bath, the MTO solution was added to the NMR tube containing **1** via syringe. After the addition, the reaction mixture was placed in an ice bath for 2 hours where the color change was observed

from orange to dark brown. ^{1}H NMR (225K, 500 MHz, toluene-d_8): 7.07 (t, 1H, J_{HH} = 7.7 Hz, Aryl-*H*), 6.97 (d, 2H, J_{HH} = 7.4 Hz, Aryl-*H*), 2.94 (br vt, 4H, -C*H*$_2$), 1.14 (br, 36H, ^{t}Bu), –12.55 (br t, 1H, J_{PH}= 12.6 Hz, Ir-*H*). ^{31}P{^{1}H} NMR (225K, 500 MHz, toluene-d_8): 59.4 (s). The ^{17}O enriched complex **2** was prepared following the same procedure with ^{17}O enriched MTO. ^{1}H NMR (225K, 500 MHz, toluene-d_8): 7.07 (t, 1H, J_{HH} = 7.7 Hz, Aryl-*H*), 6.97 (d, 2H, J_{HH} = 7.4 Hz, Aryl-*H*), 2.91 (br vt, 4H, -C*H*$_2$), 1.13 (br, 36H, ^{t}Bu), –12.49 (br t, 1H, J_{PH}= 12.6 Hz, Ir-*H*). ^{31}P{^{1}H} NMR (225K, 500 MHz, toluene-d_8): 60.4 (s). ^{17}O{^{1}H} NMR (225K, 500 MHz, toluene-d_8): 773.1.

2.3. Reaction of complex 2 with CO. Formation of [(^{tBu}PCP)Ir(ReO_3)(CO)(H)] (3)

To the crude product in a capped NMR tube obtained from the formation of [(^{tBu}PCP)Ir(ReO_3)(H)] **(2)** described above (0.040 mmol) in an ice bath, CO was injected via syringe, resulting in a slow color change from dark brown to dark yellow. After 2 hours in a chiller at 0 °C, the solvent was dried, and the yellow residue was washed with pentane. ^{1}H NMR (500 MHz, C_6D_6): 7.03 (t, 1H, J_{HH} = 7.4 Hz, Aryl-*H*), 6.97 (d, 2H, J_{HH} = 7.1 Hz, Aryl-*H*), 2.97 (q of vt, J_{PH} = 3.3 Hz, 4H, -C*H*$_2$), 1.34 (vt, 18H, *J* = 7.2 Hz, ^{t}Bu), 1.19 v(t, 18H, *J* = 7.2 Hz, ^{t}Bu), –9.41 (t, 1H, J_{PH}=15.6 Hz, Ir-*H*). ^{13}C{^{1}H} NMR (500 MHz, toluene-d_8): 181.3 (CO), 151.0 (i-Ar), 147.7 (o-Ar), 125.4 (m-Ar), 121.3 (p-Ar), 43.82 (-*C*H$_2$), 38.1 (*C*(CH$_3$)$_2$), 29.8 (C(*C*H$_3$)$_2$). ^{31}P{^{1}H} NMR (500 MHz, toluene-d_8): 56.8 (s).

2.4. The disproportionation of complex 2. Formation of [(^{tBu}PCP)Ir(ReO_4)(H)] (4) and [(^{tBu}PCP)Ir($O)_2$(H)] (5)

A toluene-d_8 solution (0.5 mL) of [(^{tBu}PCP)Ir(H)$_4$] (**1**) (20 mg, 0.040 mmol) was placed in a capped vial equipped with septum. A toluene-d_8 solution (0.5 mL) of MTO (8.5 mg,

0.040 mmol) was placed in a capped vial equipped with a septum. After both solutions were cooled to –78 °C using a dry ice/acetone bath, the MTO solution was added to the vial containing **1** via syringe. After the addition, the reaction mixture was placed in an ice bath for 2 hours where the color change was observed from orange to dark brown. The vial was then left at room temperature for 2 days. The ^{1}H and ^{31}P NMR shows complex **4** and unidentified complex in 1:1 ratio. [(^{tBu}PCP)Ir(ReO_4)(H)] (4): ^{1}H NMR (500 MHz, toluene-d_8): 6.85 (d, 2H, J_{HH} = 7.5 Hz, Aryl-*H*), 6.77 (t, 1H, J_{HH} = 7.0 Hz, Aryl-*H*), 2.97 (q of vt, 4H, -C*H*$_2$), 1.09 (m, 36H, ^{t}Bu), –43.78 (br, 1H, Ir-*H*). ^{31}P{^{1}H} NMR (500 MHz, toluene-d_8): 72.8 (s). [(^{tBu}PCP)Ir($O)_2$(H)] (5): ^{1}H NMR (225K, 500 MHz, C_6D_6): 7.27 (d, 2H, J_{HH} = 7.3 Hz, Aryl-*H*), 7.17 (t, 1H, J_{HH} = 7.5 Hz, Aryl-*H*), 3.50 (br vt, 4H, -C*H*$_2$), 1.14 (br, 36H, ^{t}Bu), –36.21 (br t, 1H, J_{PH}= 10.0 Hz, Ir-*H*). ^{31}P{^{1}H} NMR (500 MHz, toluene-d_8): 66.8 (s).

2.5. The reaction of complex 2 with MTO. Formation of [(^{tBu}PCP)Ir(ReO_4)(H)] (4)

To the crude product in a capped vial obtained from the formation of [(^{tBu}PCP)Ir(ReO_3)(H)] **(2)** described above (0.040 mmol) in an ice bath, MTO (8.5 mg, 0.040 mmol) in toluene-d_8 was injected, resulting in formation of bubbles and black precipitates. After 6 hours in a chiller at –0 °C, the dark solution was filtered through celite and dried thoroughly. The maroon residue was washed with pentane to remove excess MTO.

2.6. Alternative route to synthesize [(^{tBu}PCP)Ir(ReO_4)(H)] (4)

In a 15-mL Schlenk flask, [(^{tBu}PCP)Ir$(H)_4$] (**1**) (50 mg, 0.085 mmol) and MTO (42 mg, 0.085 mmol) were dissolved in toluene (5 mL), resulting formation of bubbles and black precipitates. After stirred for 1 day, the dark solution was filtered through celite and dried thoroughly. The maroon residue was washed with pentane to remove excess MTO.

2.7. The reaction of complex 4 with CO. Formation of [(^{tBu}PCP)Ir(ReO_4)(CO)(H)] (6)

In a 15-mL Schlenk flask, [(^{tBu}PCP)Ir(ReO_4)(H)] **(4)** (15 mg, 0.021 mmol) was dissolved in toluene-d_8 (0.8 mL). The solution was stirred under CO atmosphere for 2 hours where the color change was observed from maroon to colorless. ^{1}H NMR (500 MHz, THF-d_8): 6.80 (d, 2H, J_{HH} = 7.5 Hz, Aryl-*H*), 6.71 (t, 1H, J_{HH} = 7.3 Hz, Aryl-*H*), 3.39 (q of vt, J_{PH} = 4.3 Hz, 4H, -C*H*$_2$), 1.54 (t, 18H, *J* = 7.3 Hz, ^{t}Bu), 1.35 (vt, 18H, *J* = 7.2 Hz, ^{t}Bu), –5.41 (vt, 1H, J_{PH}= 14.6 Hz, Ir-*H*). ^{13}C{^{1}H} NMR (500 MHz, THF-d_8): 184.9 (CO), 146.3, 126.6, 125.0, 122.5, 37.0, 36.7, 35.7, 30.0, 29.0. ^{31}P{^{1}H} NMR (500 MHz, THF-d_8): 62.8 (s).

2.8. The reaction of complex 4 with t-butyl isocyanide. Formation of [(^{tBu}PCP)Ir($CN^tBu)_2$(H)]$^-$[ReO4]$^-$ (7)

To the toluene solution (5 mL) of [(^{tBu}PCP)Ir(ReO_4)(H)] **(4)** (15 mg, 0.021 mmol), t-butyl isocyanide (0.07 mL, 0.619 mmol) was added. After stirred for 2 hours, the maroon solution became pale yellow. The solution was washed with pentane to remove excess t-butyl isocyanide. ^{1}H NMR (500 MHz, toluene-d_8): 6.95 (d, 2H, J_{HH} = 7.4 Hz, Aryl-*H*), 6.81 (t, 1H, J_{HH} = 7.5 Hz, Aryl-*H*), 3.47 (q of vt, J_{PH} = 4.5 Hz, 4H, -C*H*$_2$), 1.47 (s, 9H, CN^t*Bu*), 1.39 (vt, 18H, 7.1 Hz, ^{t}Bu), 1.23 (s, 9H, CN^t*Bu*), 1.20 (vt, 18H, 6.9 Hz, ^{t}Bu), –12.60 (vt, 1H, J_{PH}= 14.6 Hz, Ir-*H*).

E. References

1. Wheatley, N.; Kalck, P., Structure and Reactivity of Earlyminus signLate Heterobimetallic Complexes. *Chem Rev* **1999,** *99* (12), 3379-3420.

2. Gade, L. H., Highly polar metal - Metal bonds in "early-late" heterodimetallic complexes. *Angewandte Chemie-International Edition* **2000,** *39* (15), 2658-2678.

3. Powers, I. G.; Uyeda, C., Metal-Metal Bonds in Catalysis. *Acs Catalysis* **2017,** *7* (2), 936-958.

4. Kubas, G. J., Fundamentals of H2 binding and reactivity on transition metals underlying hydrogenase function and H2 production and storage. *Chem Rev* **2007,** *107* (10), 4152-205.

5. Nicolet, Y.; de Lacey, A. L.; Vernede, X.; Fernandez, V. M.; Hatchikian, E. C.; Fontecilla-Camps, J. C., Crystallographic and FTIR spectroscopic evidence of changes in Fe coordination upon reduction of the active site of the Fe-only hydrogenase from Desulfovibrio desulfuricans. *J Am Chem Soc* **2001,** *123* (8), 1596-601.

6. Hostetler, M. J.; Bergman, R. G., Synthesis and reactivity of Cp2Ta(CH2)2Ir(CO)2: an early-late heterobimetallic complex that catalytically hydrogenates, isomerizes and hydrosilates alkenes. *Journal of the American Chemical Society* **1990,** *112* (23), 8621-8623.

7. Hostetler, M. J.; Butts, M. D.; Bergman, R. G., Rate and equilibrium study of the reversible oxidative addition of silanes to the iridium center in Cp2Ta(.mu.-CH2)2Ir(CO)2 and of alkene hydrosilylation/isomerization catalyzed by this system. *Organometallics* **1993,** *12* (1), 65-75.

8. Hanna, T. A.; Baranger, A. M.; Bergman, R. G., Reaction of Carbon-Dioxide and Heterocumulenes with an Unsymmetrical Metal-Metal Bond - Direct Addition of Carbon-Dioxide across a Zirconium-Iridium Bond and Stoichiometric Reduction of Carbon-Dioxide to Formate. *Journal of the American Chemical Society* **1995,** *117* (45), 11363-11364.

9. Baranger, A. M.; Bergman, R. G., Cooperative Reactivity in the Interactions of X-H Bonds with a Zirconium-Iridium Bridging Imido Complex. *Journal of the American Chemical Society* **1994,** *116* (9), 3822-3835.

10. Greenwood, B. P.; Rowe, G. T.; Chen, C. H.; Foxman, B. M.; Thomas, C. M., Metal-metal multiple bonds in early/late heterobimetallics support unusual trigonal monopyramidal geometries at both Zr and Co. *J Am Chem Soc* **2010,** *132* (1), 44-5.

11. Thomas, C. M.; Napoline, J. W.; Rowe, G. T.; Foxman, B. M., Oxidative addition across Zr/Co multiple bonds in early/late heterobimetallic complexes. *Chem Commun (Camb)* **2010,** *46* (31), 5790-2.

12. Tsutsumi, H.; Sunada, Y.; Shiota, Y.; Yoshizawa, K.; Nagashima, H., Nickel(II), Palladium(II), and Platinum(II) η3-Allyl Complexes Bearing a Bidentate Titanium(IV) Phosphinoamide Ligand: A Ti←M2Dative Bond Enhances the Electrophilicity of the π-Allyl Moiety. *Organometallics* **2009,** *28* (7), 1988-1991.

13. Serrano-Ruiz, J. C.; Luque, R.; Sepulveda-Escribano, A., Transformations of biomass-derived platform molecules: from high added-value chemicals to fuels via aqueous-phase processing. *Chem Soc Rev* **2011,** *40* (11), 5266-81.

14. Shiramizu, M.; Toste, F. D., Deoxygenation of biomass-derived feedstocks: oxorhenium-catalyzed deoxydehydration of sugars and sugar alcohols. *Angew Chem Int Ed Engl* **2012,** *51* (32), 8082-6.

15. Raju, S.; Moret, M.-E.; Klein Gebbink, R. J. M., Rhenium-Catalyzed Dehydration and Deoxydehydration of Alcohols and Polyols: Opportunities for the Formation of Olefins from Biomass. *ACS Catalysis* **2014,** *5* (1), 281-300.

16. Yi, J.; Liu, S.; Abu-Omar, M. M., Rhenium-catalyzed transfer hydrogenation and deoxygenation of biomass-derived polyols to small and useful organics. *ChemSusChem* **2012,** *5* (8), 1401-4.

17. Boucher-Jacobs, C.; Nicholas, K. M., Oxo-Rhenium-Catalyzed Deoxydehydration of Polyols with Hydroaromatic Reductants. *Organometallics* **2015,** *34* (10), 1985-1990.

18. Liu, S.; Senocak, A.; Smeltz, J. L.; Yang, L. N.; Wegenhart, B.; Yi, J.; Kenttamaa, H. I.; Ison, E. A.; Abu-Omar, M. M., Mechanism of MTO-Catalyzed Deoxydehydration of Diols to Alkenes Using Sacrificial Alcohols. *Organometallics* **2013,** *32* (11), 3210-3219.

19. Goldman, A. S.; Roy, A. H.; Huang, Z.; Ahuja, R.; Schinski, W.; Brookhart, M., Catalytic alkane metathesis by tandem alkane dehydrogenation-olefin metathesis. *Science* **2006,** *312* (5771), 257-61.

20. Findlater, M.; Choi, J.; Goldman, A. S.; Brookhart, M., Alkane Dehydrogenation.

21. Leitch, D. C.; Lam, Y. C.; Labinger, J. A.; Bercaw, J. E., Upgrading light hydrocarbons via tandem catalysis: a dual homogeneous Ta/Ir system for alkane/alkene coupling. *J Am Chem Soc* **2013,** *135* (28), 10302-5.

22. Renkema, K. B.; Kissin, Y. V.; Goldman, A. S., Mechanism of alkane transfer-dehydrogenation catalyzed by a pincer-ligated iridium complex. *J Am Chem Soc* **2003,** *125* (26), 7770-1.

23. Xu, W. W.; Rosini, G. P.; Gupta, M.; Jensen, C. M.; Kaska, W. C.; KroghJespersen, K.; Goldman, A. S., Thermochemical alkane dehydrogenation catalyzed in solution without the use of a hydrogen acceptor. *Chemical Communications* **1997,** (23), 2273-2274.

24. Krogh-Jespersen, K.; Czerw, M.; Goldman, A. S., Computational and experimental studies of the mechanism of (PCP)Ir-catalyzed acceptorless dehydrogenation of alkanes. *Journal of Molecular Catalysis A: Chemical* **2002,** *189* (1), 95-110.

25. Krogh-Jespersen, K.; Czerw, M.; Kanzelberger, M.; Goldman, A. S., DFT/ECP study of C-H activation by (PCP)Ir and (PCP)Ir(H)2(PCP=eta3-1,3-C6H3(CH2PR2)2). Enthalpies and free energies of associative and dissociative pathways. *J Chem Inf Comput Sci* **2001,** *41* (1), 56-63.

26. Karunananda, M. K.; Mankad, N. P., Heterobimetallic H-2 Addition and Alkene/Alkane Elimination Reactions Related to the Mechanism of E-Selective Alkyne Semihydrogenation. *Organometallics* **2017,** *36* (1), 220-227.

27. Pichaandi, K. R.; Fanwick, P. E.; Abu-Omar, M. M., C-H Activation of Methyltrioxorhenium by Pincer Iridium Hydride To Give Agile Ir-Re Bimetallic Compounds. *Organometallics* **2014,** *33* (19), 5089-5092.

28. Reactions, G.; Stavropoulos, P.; Kiani, S.; Tapper, A.; Pinnapareddy, D.; Paraskevopoulou, P.; Examples, F., *C – H Transformation at Unfunctionalized Alkanes*. 2005.

29. Lee, D. W.; Kaska, W. C.; Jensen, C. M., Mechanistic Features of Iridium Pincer Complex Catalyzed Hydrocarbon Dehydrogenation Reactions: Inhibition upon Formation of a μ-Dinitrogen Complex. *Organometallics* **1998,** *17* (1), 1-3.

30. Vigalok, A.; Uzan, O.; Shimon, L. J. W.; Ben-David, Y.; Martin, J. M. L.; Milstein, D., Formation of η2C−H Agostic Rhodium Arene Complexes and Their Relevance to Electrophilic Bond Activation. *Journal of the American Chemical Society* **1998,** *120* (48), 12539-12544.

31. Montag, M.; Efremenko, I.; Cohen, R.; Shimon, L. J.; Leitus, G.; Diskin-Posner, Y.; Ben-David, Y.; Salem, H.; Martin, J. M.; Milstein, D., Effect of CO on the oxidative addition of arene C-H bonds by cationic rhodium complexes. *Chemistry* **2010,** *16* (1), 328-53.

32. Murugesan, S.; Stoger, B.; Pittenauer, E.; Allmaier, G.; Veiros, L. F.; Kirchner, K., A Cobalt(I) Pincer Complex with an eta(2) -C(aryl)-H Agostic Bond: Facile C-H Bond Cleavage through Deprotonation, Radical Abstraction, and Oxidative Addition. *Angew Chem Int Ed Engl* **2016,** *55* (9), 3045-8.

33. Connelly, S. J.; Chanez, A. G.; Kaminsky, W.; Heinekey, D. M., Characterization of a palladium dihydrogen complex. *Angew Chem Int Ed Engl* **2015,** *54* (20), 5915-8.

34. Abu-Omar, M. M.; Appelman, E. H.; Espenson, J. H., Oxygen-Transfer Reactions of Methylrhenium Oxides. *Inorganic Chemistry* **1996,** *35* (26), 7751-7757.

35. Holm, R. H.; Donahue, J. P., A Thermodynamic Scale for Oxygen Atom Transfer-Reactions. *Polyhedron* **1993,** *12* (6), 571-589.

36. Moulton, B. C. J.; Shaw, B. L., Transition Metal-Carbon Bonds. Part XLII. Complexes of Nickel, Palladium, Platinum, Rhodium and Iridium with the Tridentate Ligand 2,6- Bis[(di-t-butylphosphino)methyl]pheny. *J. Chem. Soc. Dalton Trans.* **1975,** (1020), 1020-1024.

37. Herrmann, W. A.; Kuhn, F. E.; Fischer, R. W.; Thiel, W. R.; Romao, C. C., Simple and Efficient Synthesis of Methyltrioxorhenium (Vii) - a General-Method. *Inorganic Chemistry* **1992,** *31* (21), 4431-4432.

38. Herrmann, W. a.; Kiihnj, F. E.; Rauch, M. U.; Correia, J. D. G.; Technischen, A.-c. I. D.; Miinchen, U., Multiple Bonds between Transition Metals and Main-Group Elements. 142.l Lewis-Base Adducts of Organorhenium(VI1) Oxides: Structures and Dynamic Behavior in Solution. *J. Organomet. Chem* **1995**, 2914-2920.

CHAPTER III. Ethylene/1-Hexene Copolymerization by Single-Site Hafnium Amine Bis-(Phenolate) Catalyst: Insights into Deactivation Pathways

A. Introduction

Previously, our group studied 1-hexene polymerization by single-site Ti, Zr, Hf–amine bis(phenolate) catalysts activated by $B(C_6F_5)_3$.[1-4] The studies demonstrated that complex fundamental steps of the olefin polymerization can be studied with the multi-response kinetic data including 1-hexene consumption profiles, active-site quantifications, end-group concentrations, and the change of molecular weight distribution of the polymer. The quantitative kinetic model was built with the experimental kinetic results and enabled us to obtain rate constants for the elementary reaction steps. With the successful studies of mechanistic and kinetic investigations, we were motivated to explore the uncharted area of copolymerization of ethylene and α-olefin. The objective of this study is to understand elementary kinetic steps and mechanisms of ethylene/1-Hexene copolymerization with multi-response data, including the ones mentioned above and the evolution of the copolymer's E/H compositions (Scheme 3.1).

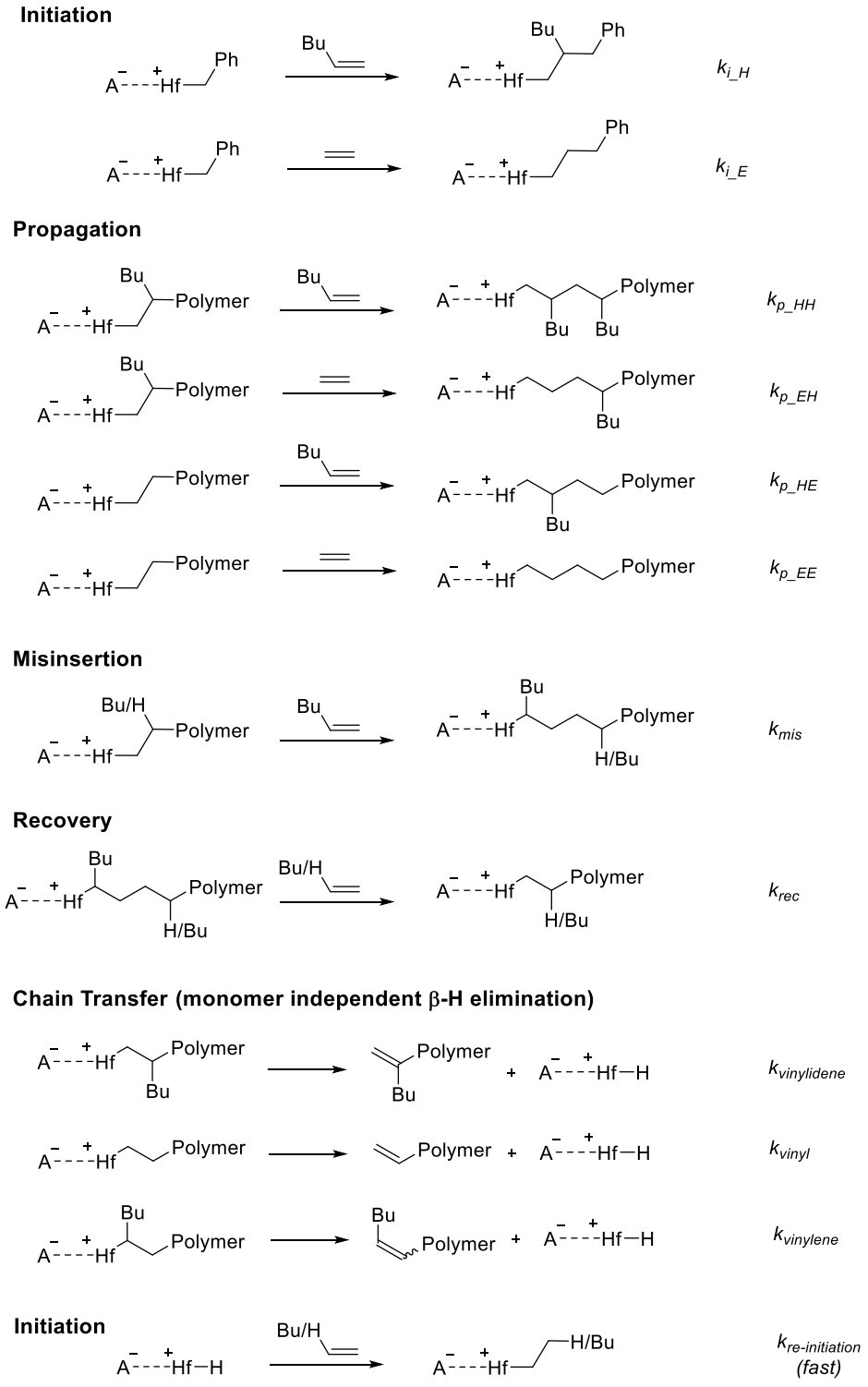

Scheme 3.1. Elementary kinetic steps used in kinetic modeling for copolymerization of ethylene/1-hexene by Hf/B(C_5F_6)$_3$ system

Herein, we report kinetic analysis of ethylene/1-hexene copolymerization catalyzed by hafnium salan-type catalyst. We developed an ethylene/1-hexene copolymerization system with Hf[tBu-ON^{THF}O]Bn_2 activated by $B(C_6F_5)_3$, yielding high 1-hexene-incorporated copolymers. Triads composition of the resulting copolymer studied by ^{13}C NMR and its dependence on monomer concentrations and reaction time was explored. The GPC analysis showed the resulting copolymers have dispersity (Đ) lower than 2.0, suggesting that the catalyst behaves as a single-site catalyst in copolymerization. Deactivation of the Hf catalyst during copolymerization was observed, and over the course of the reaction, primary active-sites decreased as secondary sites increased. Catalyst deactivation was found to be sensitive to the initial concentration of monomers. *In-situ* NMR experiments of ethylene/1-hexene copolymerization demonstrated a positive comonomer effect – both k_{obs} of ethylene and 1-hexene increase with increased $[1\text{-hexene}]_0$.

B. Catalyst Selection

The salan-type ligand was prepared as previously reported. Hf[*t*-Bu-ON^{THF}O]Bn_2 was prepared by reacting the ligand in toluene with $HfBn_4$. Previously, we studied 1-hexene homopolymerization using various Hf, Zr, Ti catalysts with salan-type ligands with different pendant arms.[3] We chose Hf[*t*-Bu-ON^{THF}O]Bn_2 as it showed a good activity with the slow misinsertion rate for 1-hexene polymerization.

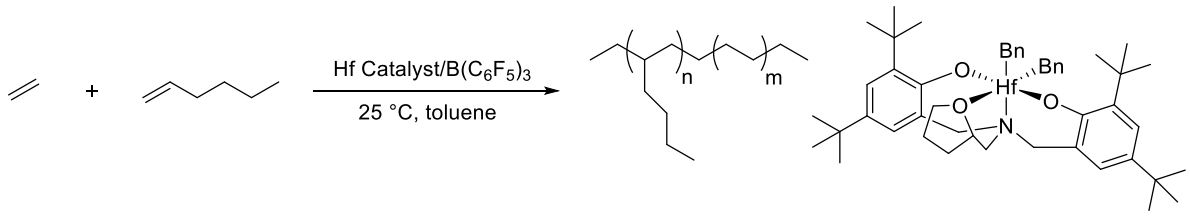

Scheme 3.2. Ethylene/1-hexene copolymerization by Hf[*t*-Bu-ON^{THF}O]Bn$_2$/B(C$_5$F$_6$)$_3$ system at 25 °C

C. Batch Ethylene/1-Hexene Copolymerization

Batch ethylene/1-hexene copolymerizations were studied in a 25 mL Schlenk flask in a 1-hexene/toluene solution under a constant feed of 1 bar of ethylene atmosphere at 25 °C (Figure SI 3.1). Precatalyst, Hf[*t*-Bu-ON^{THF}O]Bn$_2$, was activated by B(C$_6$F$_5$)$_3$ in ethylene saturated 1-hexene/toluene solution to initiate the polymerization reaction. The activated catalyst [Hf[*t*-Bu-ON^{THF}O]Bn][B(C$_6$F$_5$)$_3$Bn] is excellent for α-olefin, 1-hexene, insertions over a wide range of ethylene incorporation (Scheme 3.2, Table 3.1).

Ethylene/1-hexene triads composition and ethylene incorporation calculated from quantitative ^{13}C NMR using the method of Seger and Maciel are summarized in Table 3.1 (Figure SI 3.2).[5] With the increase in [1-hexene]$_0$ from 0.10 to 1.5 M, EEE, EEH, and EHE decreased while HHH increased (Table 3.1, runs 1-4). In our system, HEH and EHH triads showed no dependence on [1-hexene]$_0$ or reaction time. With the [1-hexene]$_0$ is higher than 0.5 M, the resulting copolymers did not have any EEE blocks and favored HHH. Over the reaction, the triads were not significantly affected, especially when [1-hexene]$_0$ was above 1.5 M, which is attributed to the large excess of the remaining [1-hexene] compared to [ethylene] (Table 3.1 runs 4, 6, and 8). At lower [1-hexene]$_0$ of 0.5 M, slight increases in EEH and EHE and decrease in HHH were observed (Table 3.1 runs 3, 5, and 7).

Table 3.1. ^{13}C Characterization of Ethylene/1-Hexene Copolymers

Run[a]	Time (min)	$[H]_0$ (M)[b]	% E[c]	EEE	EEH	EHE	HEH	EHH	HHH
1	30	0.1	75	39	30	15	6	12	0
2	30	0.25	55	10	31	16	13	26	4
3	30	0.5	26	1	9	5	16	31	39
4	30	1.5	13	2	4	3	14	27	51
5	10	0.5	22	0	7	4	17	32	41
6	10	1.5	16	0	4	2	12	24	58
7	90	0.5	32	1	14	8	17	32	27
8	90	1.5	19	0	7	3	14	27	50

[a]Conditions: [cat.] = 3.00 mM; solvent = added desired amount of 1-hexene and diluted with toluene to 10 mL; $[B(C_5F_6)_3]$ = 1.1 eq; ethylene pressure = 1 bar; temp = 25 °C. [b][cat.] = 5.00 mM [c]Percent ethylene in the copolymer was determined by ^{13}C NMR. [d]Triads calculated by ^{13}C NMR.

Copolymerizations were done at a variety of 1-hexene concentrations to study copolymers with a wide range of ethylene incorporation (Table 3.2). The M_w/M_n remains low (below 2.0) even at high conversions, indicating that the Hf/$B(C_6F_5)_3$ behaves as a single-site catalyst. The ethylene incorporation varied from 75 % to 15% as $[1\text{-hexene}]_0$ increased from 0.10 M to 2.5 M (Table 3.2, runs 1-9). At $[1\text{-hexene}]_0$ = 0.5 M, ethylene incorporation increased as 1- hexene was consumed over time; however, at higher $[1\text{-hexene}]_0$ of 1.5 M, increase in ethylene incorporation was not observed (Table 3.2, runs 6-8). A significant decrease in productivity over the reaction and relatively low conversions of 1-hexene suggested catalyst deactivation over time. The catalyst lost its activity at a higher catalyst loading of 6.0 mM as well, and 1-hexene conversion and the polymer yield reached its plateau after 30 min (Table 3.2, runs 10-12). The deactivation at higher catalyst concentration confirms that catalyst death is not due to a fixed impurity in reagents. Interestingly, higher $[1\text{-hexene}]_0$ resulted in higher 1-hexene conversion and increased productivity. Our results of $[1\text{-hexene}]_0$ dependence on conversion are in agreement with literature results on the positive comonomer effect, where the addition of comonomer increases the productivity of overall polymerization, in both homogeneous and heterogeneous copolymerization.[6-9]

Table 2. Ethylene/1-Hexene copolymerization with Hf[*t*-Bu-ON^{THF}O]Bn$_2$/B(C_5F_6)$_3$ at 25 °C

Run[a]	Time (min)	$[H]_0$ (M)[b]	Δ [H] (M)[c]	Δ[H] (%)[c]	yield (g)	prod[d]	% E[e]
1	30	0.1	0.038	39.2	0.081	5.4	75
2	30	0.25	0.111	43.4	0.143	9.5	54
3	10	0.5	0.123	25.2	0.202	40.4	22
4	30	0.5	0.206	40.4	0.264	17.6	26
5	90	0.5	0.281	57.2	0.313	6.9	32
6	10	1.5	0.488	33.5	0.184	36.8	16
7	30	1.5	0.680	46.8	0.675	45.0	13
8	90	1.5	1.118	75.8	1.075	23.9	19
9	90	2.5	2.017	82.2	1.869	41.6	15
10[f]	10	0.5	0.284	58.0	0.313	33.4	17
11[f]	30	0.5	0.439	87.3	0.390	16.8	47
12[f]	90	0.5	0.448	89.2	0.395	5.7	46

[a]Conditions: [cat.] = 3.00 mM; solvent = added desired amount of 1-hexene and diluted with toluene to 10 mL; [B(C_5F_6)$_3$] = 1.1 eq; ethylene pressure = 1 bar; temp = 25 °C. [b][cat.] = 5.00 mM [c][H] was determined by ^{1}H NMR. [d] Productivity = (g polymer)/(mmol h) [e]Percent ethylene in the copolymer was determined by ^{13}C NMR. [f][cat.] = 6.00 mM.

To understand the catalyst deactivation behavior and the comonomer effect, the active-sties during copolymerization were quantified following Landis's deuterium-labeling method.[10] There are three possible active-sites during ethylene/1-hexene copolymerization (Scheme 3.3). At the end of each batch reaction, MeOD was added to quench the polymerization and label the resulting copolymer with deuterium, which was quantified in

^{2}H NMR. We observed two types of active sites at δ 0.83 (DH_2C−Polymer; **primary**) and 1.22 (DH(Bu)C−Polymer; **secondary**) in ^{2}H NMR. The primary active sites result from a 1,2-insertion of 1-hexene and that of ethylene were not distinguishable by ^{2}H NMR.

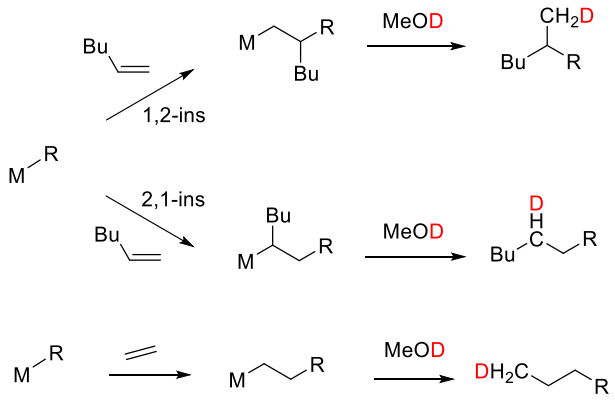

Scheme 3.3. Possible Active-sites Prepared by Adding MeOD during the Copolymerization of Ethylene/1-Hexene.

The active-site counting results with varying reaction time, initial concentration of 1-hexene, and catalyst loading are shown in Figures 3.1–3.3. Copolymerization with $[1\text{-hexene}]_0$ = 0.50 M at 10 min showed only 35 % of the precatalyst as primary sites, which decreased to 5 % over 90 min (Figure 3.1). On the other hand, the secondary active sites increased to 15 % over 90 min. No increase in the weight of copolymer after 90 min suggested that the secondary sites are not active for polymerization of ethylene or 1-hexene in our system. The decrease in productivity due to dormant behavior of secondary sites in olefin polymerizations has been observed in a wide range of catalysts[11] while some studies showed active secondary sites.[12] There are proposed mechanisms of its inactive nature such as the high steric hindrance at the active center.[11] The inactive secondary sites can be

activated by undergoing chain transfer (β-H elimination or β-H transfer) or recovery (1,2-insertion of a monomer). In our study of 1-hexene homopolymerization, a small percentage of secondary sites were observed and the increase in sites over the course of reaction was not observed.[3] However, we observed polymer with vinylene end-group, which is a chain-transfer product from 2,1-insertion of 1-hexene. With kinetic modeling, we established that $k_{recovery}$ is ~7 times faster than $k_{mis\text{-}insertion}$ in 1-hexene homopolymerization. Our copolymerization results suggest that the presence of ethylene increases secondary sites and inhibits the recovery of those secondary sites.

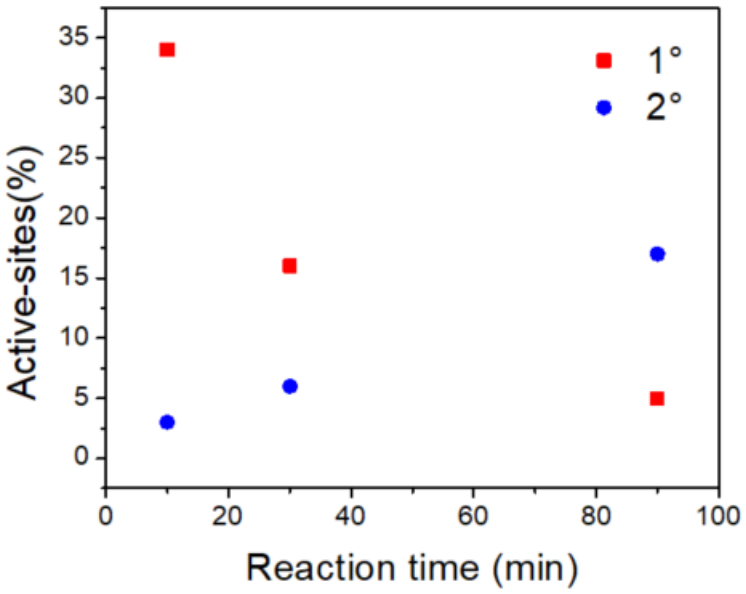

Figure 3.1. Active-sites at different reaction time, quantified by deuterium labeling. [cat.] = 3.00 mM; ethylene pressure = 1 bar; $[H]_0$ = 0.5 M; ethylene pressure = 1 bar; red is % 1° site; blue is % 2° site.

Next, the active-sites of a range of $[1\text{-hexene}]_0$ were quantified after 90 min of reaction (Figure 3.2). With higher $[1\text{-hexene}]_0$, both primary and secondary active sites can be observed even at the end of the reaction. Having more 1-hexene somehow preserved the catalyst by suppressing deactivation. At a higher [cat.] at 6 mM, we observed a significant increase in primary sites (83%) during the early part of the reaction (Figure 3.3). At 90 min, the primary sites were below 15% regardless of [cat.]. With higher [cat.], the conversion of 1-hexene was ~2 times higher at 30 min (Table 3.1, run 4,11); it is possible that the higher catalyst loading benefited less from the commoner effect after 30 min. It is worthy to note that the secondary sites were growing at the same rate for both catalyst loading.

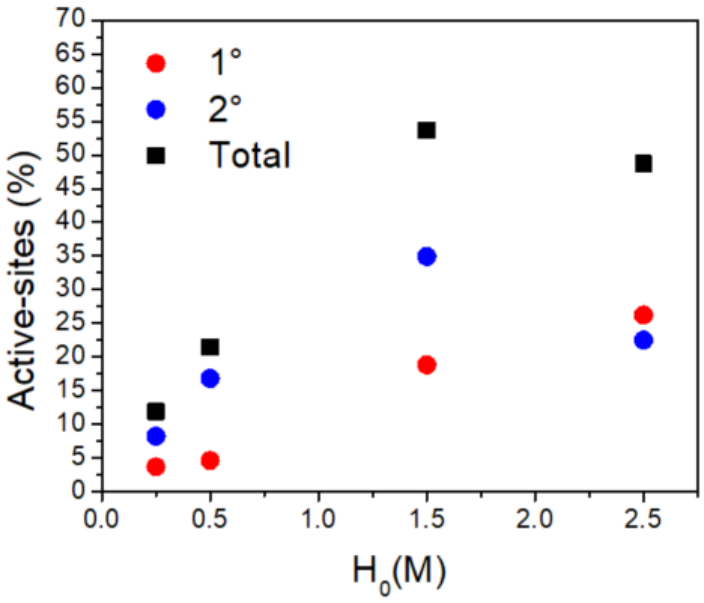

Figure 3.2. Active-sites at different $[H]_0$, quantified by deuterium labeling. [cat.] = 3.00 mM; ethylene pressure = 1 bar; reaction time = 90 min; ethylene pressure = 1 bar; red is % 1° site; blue is % 2° site; black is a total % site.

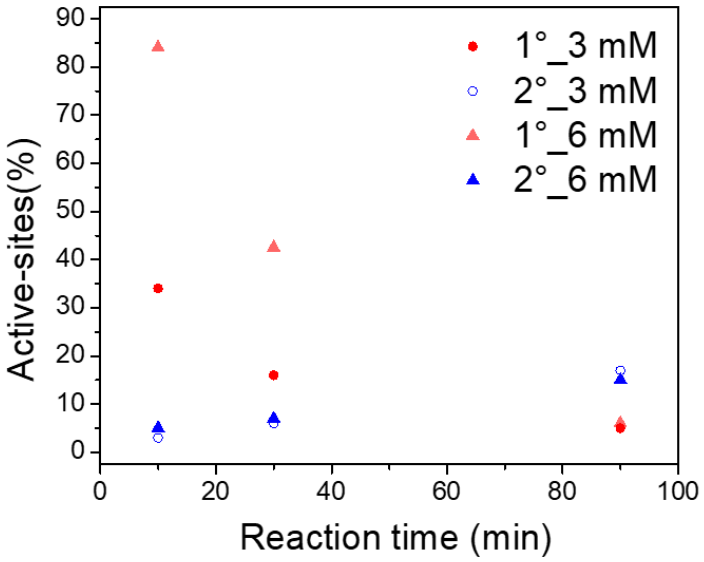

Figure 3.3. Active-sites at different reaction time with different catalyst loadings. ethylene pressure = 1 bar; $[H]_0$ = 0.5 M; [cat.] = 3mM (circle); [cat.] = 6 mM (triangle). red is % 1° site; blue is % 2° site; black is a total % site.

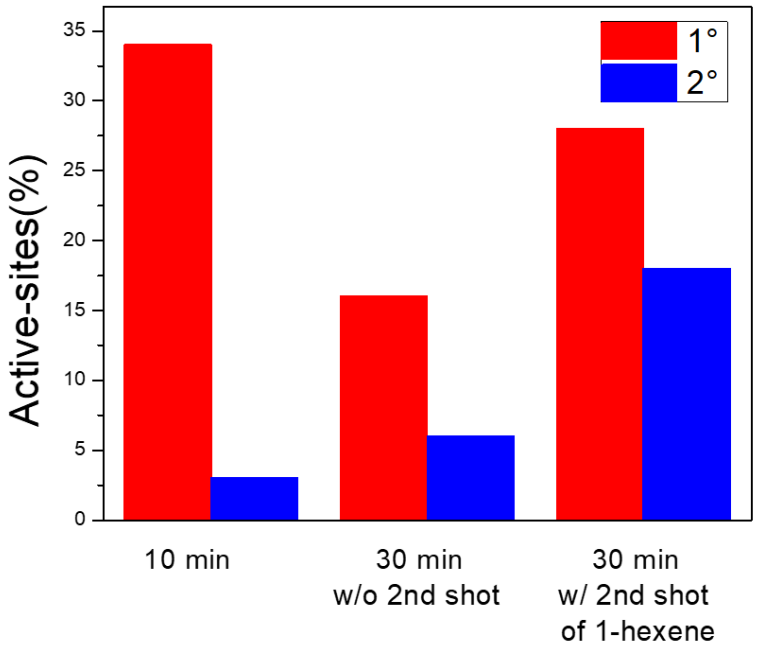

Figure 3.4. Effect of additional 1-hexene on active-sites. $[H]_0$ = 0.5 M; [cat.] = 3mM. For the second-shot experiment, at 10 min of reaction, 1.0 M of 1-hexene was added. red is % 1° sites; blue is % 2° sites.

To understand the $[1\text{-hexene}]_0$ effect on catalyst deactivation, a second-shot of 1-hexene was added to a running copolymerization reaction at 10 min and quenched at 30 min. The active site count was compared to the reaction without the additional second-shot of 1-hexene (Figure 3.4). With the second-shot of 1-hexene, the decrease in the primary site was suppressed by a factor of 3, confirming that high [1-hexene] prevents catalyst deactivation. The large increase in secondary site showed that it has no dependence on $[1\text{-hexene}]_0$.

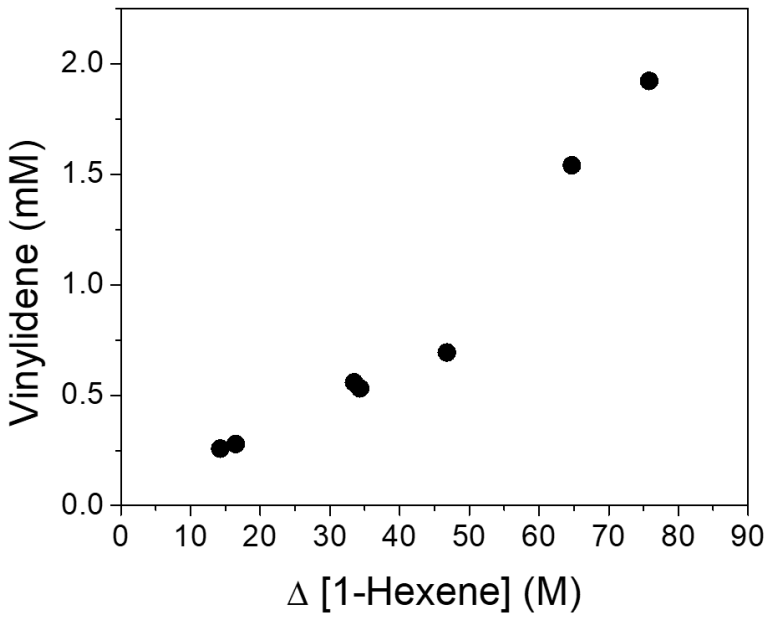

Figure 3.5. End-group analysis of the batch copolymerization of ethylene/1-hexene. $[H]_0$ = 1.5 M

Next, chain transfer reactions were investigated via quantifying vinyl end groups of the resulting copolymer. There are two possible mechanisms of chain transfer: monomer dependent and monomer independent pathways. In our copolymerization study, we only observed β-H elimination, as the formation of vinylidene had no dependence on monomer concentration (Figure 3.5). In the copolymerization of ethylene/1-hexene, there are three possible end groups: vinylidene, vinyl, and vinylene (Scheme 3.1). In our study, we only observed the formation of vinylidene. Vinyls and vinylenes were not observed. However, we observed secondary active-sites from 2,1-insertion of 1-hexene (Scheme 3.3). It is evident that the secondary sites, which are inactive for polymerization, do not undergo chain-transfer. Additionally, the rate of recovery of the misinsertion products must be much slower than the rate of misinsertion.

D. In-situ NMR Ethylene/1-Hexene Copolymerization

In-situ NMR ethylene/1-hexene copolymerization was prepared in an NMR tube with a septa-cap filled with precatalyst in ethylene saturated toluene, 1-hexene, and internal standard. The reaction was started by adding $B(C_6F_5)_3$ solution in toluene and the consumptions of both monomers ethylene and 1-hexene were monitored by ^1H NMR at 25 °C. Both consumptions of ethylene and 1-hexene displayed first-order behavior and k_{obs} are summarized in Table 3.3. Interestingly, k_{obs} of ethylene/1-hexene in copolymerization were much faster than k_{obs} of ethylene homopolymerization. The k_{obs} of ethylene increased by a factor of 2 when as little as 0.3 equivalent of 1-hexene was added. The NMR scale copolymerization demonstrated a positive comonomer effect as well. In NMR studies, the active sites could not be quantified due to the small scale. However, the NMR studies demonstrated that large excess of $[1\text{-hexene}]_0$ results in higher productivity. The same phenomena are observed in batch copolymerization. Additionally, k_{obs} for both 1-hexene and ethylene were constant throughout the reaction and no catalyst deactivation was observed in the NMR scale. It further confirms that the catalyst death is not due to an impurity in the reagents.

Table 3.3. NMR ethylene/1-hexene copolymerization by Hf[tBu-ON^{THF}O]Bn_2 /$B(C_6F_5)_3$ at 25 °C

Run[a]	X_H/X_E[c]	k_{obs}_H (10^{-4} s^{-1})[d]	k_{obs}_E (10^{-4} s^{-1})[d]
1[c]	0	-[c]	5.8
2	0.3	3.0	7.9
3	0.8	4.0	11.7
4	3.7	8.3	25.5
5	17.0	11.4	44.9

[a]Conditions: solvent = added desired amount of 1-hexene and diluted with toluene to 2.0 mL; reaction volume = 2.75 mL; [cat.] = 5.00 mM; [act.] = 1.1 eq; temp = 25 °C. [b]1-hexene was not added [c]concentration was monitored by ^{1}H NMR. [d\]Fitted to 1st order.

The catalyst deactivation is only observed in a batch reactor with a constant feed of ethylene. Thus, the deactivation in a batch copolymerization could be attributed to (1) a large excess of ethylene and (2) building up of secondary sites, which is not dependent on [1-hexene]$_0$. The active-site counting and second-shot results demonstrate that increasing [1-hexene], or with lower relatively lower [ethylene], preserves primary active sites.

E. Conclusion

Copolymerization of ethylene and 1-hexene by a single-site catalyst, Hf[*t*-Bu-ON^{THF}O]Bn_2, activated by $B(C_6F_5)_3$ yielded copolymers with high 1-hexene incorporation. The ^{13}C NMR-based triad analysis showed that the E/H incorporation ratio is dependent on [1-hexene]. Catalyst deactivation was observed during the copolymerization. Deuterium labeling experiments showed the primary sites decreased and secondary sites (inactive)

increased over the course of the reaction. Excess of 1-hexene preserved the catalyst activity for longer, suggesting that the deactivation is dependent on [ethylene]. The positive comonomer effect of 1-hexene was observed by i*n-situ* NMR experiments.

F. Supporting Information

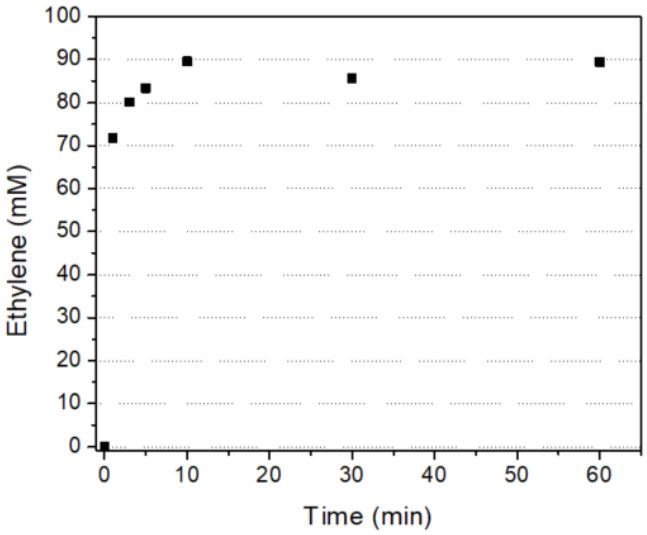

Figure SI 3.1. Ethylene saturation experiment. 1-hexene of 1.5 M in 10 mL toluene solution at 1 bar ethylene.

For the kinetic modeling study, we examined the rate of ethylene saturation in 1-hexene/toluene mixture in batch reactions. Typical reaction solution with toluene and 1-hexene was degassed and saturated with ethylene by stirring vigorously. At a predetermined time, an aliquot was collected, and ethylene was quantified by ^{1}H NMR. Figure SI 3.1 shows that 72 mM of ethylene (78 % to maximum saturation) was dissolved within the first 1 minute of saturation. We established that the replenishment of ethylene is fast compared to

the reaction rate; thus, the ethylene concentration was assumed to be constant in a batch reaction.

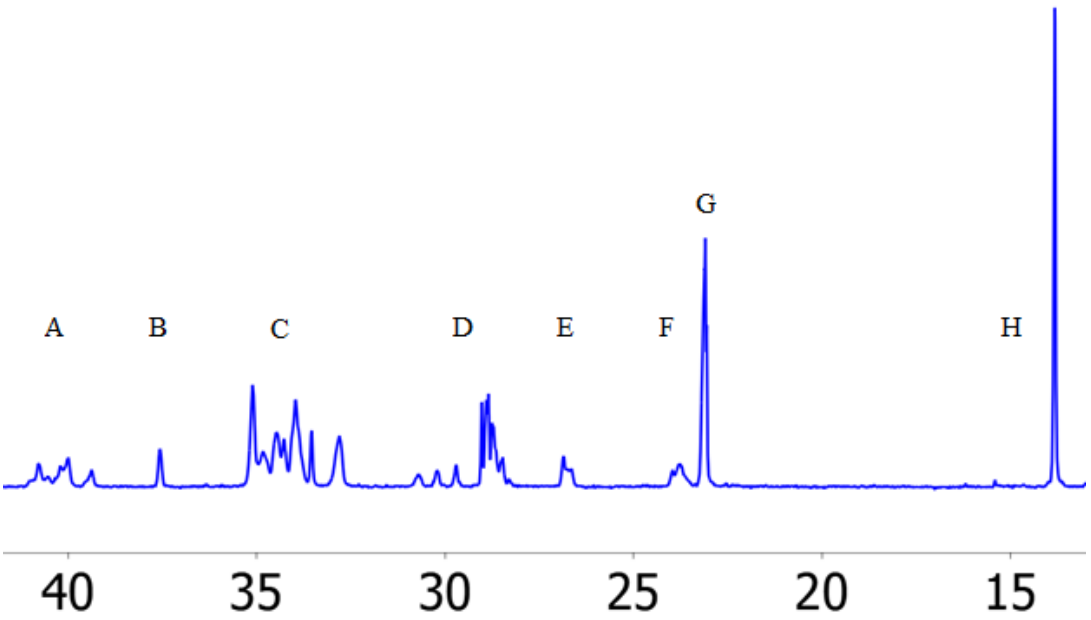

Figure SI 3.2. ^{13}C NMR spectrum of the ethylene/1-hexene copolymer prepared. %E = 39

G. Experimental Procedure

1. General Consideration

All reactions were performed in an argon-filled glove box or using standard Schlenk techniques under argon unless otherwise specified. Ethylene (99.999%), purchased from Praxair, was filtered through Oxiclear purifier (RGP-R1-500) for polymerization. Solvents were degassed, purified with a solvent purification system (Pure Process Technology INC), and stored over activated molecular sieves before use. Benzene-d_6, 1-hexene, and toluene-d_8 were dried with CaH_2 and stored over activated molecular sieves. $B(C_6F_5)_3$ was purchased from Strem and purified by sublimation. $HfBn_4$ was purchased from Strem and used as

received. All other reagents were purchased from commercial vendors (Fischer Scientific and Sigma) and used without further purification. 6,6′-((((Tetrahydrofuran-2-yl)methyl)-azanediyl)bis(methylene))bis(2,4-di-tert-butylphenol), *t*-Bu-ON^{THF}O ligand, and Hf[*t*-Bu-ON^{THF}O]Bn$_2$ were prepared following literature procedures.[1, 13-14] All ^{1}H, ^{2}H, and array NMR experiments were done on a Varian Unity Inova AS600 600MHz with Varian triple resonance ^{1}H/^{13}C/^{15}N probe with PFG, 5mm at 25 °C unless otherwise specified. Quantitative ^{13}C NMR was collected on Agilent 400-MR spectrometer using 5mm One NMR Probe with PFG operating at 70 °C with an inverse gated decoupled pulse sequence with NOE turned off, a relaxation delay of 4.0 s, and acquisition time of 1.8 s.

2. NMR scale copolymerization of ethylene and 1-hexene

The procedure for NMR scale copolymerization was adopted and modified from literature.[2, 4] In a typical experiment, a vacuum storage flask inside a glovebox was charged with 2.5 mL of 50:50 (v/v) toluene/toluene-d_8 and a stir bar. The toluene solution was degassed by freeze-pump-thaw and placed under 1.5 bar of ethylene while stirring vigorously at room temperature for 30 minutes before taking into the inert atmosphere glovebox. To a 2 mL volumetric flask, Hf[tBu-ON^{THF}O]Bn$_2$ (0.01233 g, 0.0138 mmol), diphenylmethane (0.02062 g, 0.123 mmol) and 1-hexene (0.1041 g, 1.237 mmol) were added and diluted with the ethylene saturated toluene. The catalyst solution was transferred to a capped NMR tube and sealed with a screw-cap septum. B(C_6F_5)$_3$ (0.00774 g, 0.0151 mmol) was dissolved in 0.75 mL of the ethylene saturated toluene and sealed in a vial with a screw-cap septum. The vial containing the activator solution was pierced with a 1 mL syringe and placed in an Ar-filled bag and equilibrated to 25 °C. The NMR tube was placed

in the spectrometer and allowed to equilibrate to 25 °C with a VT controller. A spectrum was collected to quantify the initial monomer concentrations relative to diphenylmethane. The NMR tube was removed, and the activator solution was added to the solution by piercing the NMR tube's septum while the syringe remained in the Ar bag. After shaking the reaction mixture for approximately 30 s, it was placed back in the spectrometer. Spectra were acquired at regular time intervals until the reaction reached at least 90% completion.

3. Batch copolymerization of ethylene and 1-hexene

The procedure for batch scale copolymerization was adopted and modified from literature.[1] The method of Manual Quench is based on literature.[10] For a typical copolymerization, $B(C_6F_5)_3$ (0.02414 g, 0.0472 mmol) was added to a 3 mL volumetric flask and diluted with toluene. The activator solution was transferred to a 5 mL vial with a screw-cap septum. The vial containing the activator solution was pierced with a 5 mL syringe and placed in an Ar-filled bag and equilibrated to 25 °C. To a 10 mL volumetric flask, 1-hexene (1.894 g, 22.50 mmol) was added and diluted with toluene. Using a 3 mL volumetric flask, 3.0 mL of the solution was transferred to a vial with diphenylmethane to quantify the initial 1-hexene concentration by ^{1}H NMR analysis. To a 25 mL Schlenk flask, Hf[tBu-ON^{THF}O]Bn_2 (0.0269 g, 0.0300 mmol), a 7.0 mL aliquot of the 1-hexene solution, and a stir bar were added. The flask was sealed and moved from the glovebox to a Schlenk line under an ethylene atmosphere. Ethylene was bubbled into the solution at −78 °C for 5 minutes. The solution remained under 1 bar of ethylene for an additional 30 minutes while the temperature slowly equilibrated to 25 °C in a temperature-regulated water bath. The reaction started by adding the activator solution into the flask while the syringe remained in the Ar bag. After a

predetermined time, the reaction was quenched by injecting 1.0 mL of methanol-d_4. To quantify 1-hexene consumption, a 1.0 mL aliquot from the quenched solution was removed and added to a vial with diphenylmethane for ^{1}H NMR analysis. The remaining solution was dried under vacuum before dissolving in toluene and filtered through a silica plug to remove the quenched catalyst. Evaporation of the solvent under mild heat yielded colorless poly(ethylene-co-1-hexene), and the weight of the polymer was measured.

4. Copolymer Characterization

For ^{13}C NMR analysis, samples were prepared by dissolving ca. 200 mg of the copolymer in 0.7 mL benzene-d_6 containing ca. 4 mg of chromium(III) acetylacetonate as a spin relaxation agent.[43] All quantitative ^{13}C NMR measurements were taken on an Agilent 400 at 70 °C with an inverse gated decoupled pulse sequence with NOE turned off, a relaxation delay of 4.0 s, and acquisition time of 1.8 s.

For ^{2}H analysis, samples were prepared by dissolving ca. 100 mg of the copolymer in 0.7 mL benzene. Diluted $CDCl_3$ in benzene (0.625 μL, 7.78 μmol) as used as an internal standard for the quantification of active sites. All active site measurements were taken on a Varian AS600 spectrometer at 25 °C with lock off and shimmed on benzene.

For vinyl end group analysis, samples were prepared by dissolving ca. 100 mg of the copolymer in 0.7 mL benzene-d_6 and diphenylmethane was used as an internal standard for the quantification of end groups. All vinyl measurements were taken on a Varian AS600 spectrometer at 25 °C.

For GPC analysis, poly(ethylene-co-1-hexene) samples dissolved in chloroform with 0.25% triethylamine. The solutions were passed through a 0.2 μm filter. GPC analysis was

done on a Waters Alliance HPLC System, 2690 Separation Module, samples were injected through a 40 μL injection loop and passed through Agilent, PLgel, 5 μm MiniMIX-D, 250 x 4.6 mm and guard (MW linear range 200 - 400,000 g/mol) at a flow rate of 0.35 mL/min. The analysis made using Waters 2410 Differential Refractometer and Waters 2998 Photodiode Array Detector. Molecular weights were assigned by way of a universal calibration curve created with polystyrene standards ranging from 580 g/mol to 3,114,000 g/mol.

5. Ethylene saturation experiment

To a 10 mL volumetric flask, 1-hexene (1.894 g, 22.50 mmol) was added and diluted with toluene. The 10 mL solution was transferred to a 25 mL Schlenk flask. The flask was sealed and moved from the glovebox to a Schlenk line under an argon atmosphere. The solution was degassed by freeze-pump-thaw and the temperature was equilibrated to 25 °C in a temperature-regulated water bath. The flask was placed under 1 bar of ethylene atmosphere while stirring vigorously. A 0.5 mL aliquot of the solution was removed with a syringe at the desired time and was added to a capped NMR tube filled with the 1 mL diphenylmethane and toluene-d_8 solution. Ethylene saturation was quantified using a Varian AS600 spectrometer at 25 °C.

6. Second-shot of 1-hexene experiment

To a 10 mL volumetric flask, 1-hexene (1.894 g, 22.50 mmol) was added and diluted with toluene. The 10 mL solution was transferred to a 25 mL Schlenk flask. The flask was sealed and moved from the glovebox to a Schlenk line under an argon atmosphere. The

solution was degassed by freeze-pump-thaw and the temperature was equilibrated to 25 °C in a temperature-regulated water bath. The flask was placed under 1 bar of ethylene atmosphere while stirring vigorously. A 0.5 mL aliquot of the solution was removed with a syringe at the desired time and was added to a capped NMR tube filled with the 1 mL diphenylmethane and toluene-d_8 solution. Ethylene saturation was quantified using a Varian AS600 spectrometer at 25 °C.

I. References

1. Steelman, D. K.; Xiong, S.; Pletcher, P. D.; Smith, E.; Switzer, J. M.; Medvedev, G. A.; Delgass, W. N.; Caruthers, J. M.; Abu-Omar, M. M., Effects of pendant ligand binding affinity on chain transfer for 1-hexene polymerization catalyzed by single-site zirconium amine bis-phenolate complexes. *J Am Chem Soc* **2013,** *135* (16), 6280-8.

2. Switzer, J. M.; Travia, N. E.; Steelman, D. K.; Medvedev, G. A.; Thomson, K. T.; Delgass, W. N.; Abu-Omar, M. M.; Caruthers, J. M., Kinetic Modeling of 1-Hexene Polymerization Catalyzed by Zr(tBu-ONNMe2O)Bn2/B(C6F5)3. *Macromolecules* **2012,** *45* (12), 4978-4988.

3. Pletcher, P. D.; Switzer, J. M.; Steelman, D. K.; Medvedev, G. A.; Delgass, W. N.; Caruthers, J. M.; Abu-Omar, M. M., Quantitative Comparative Kinetics of 1-Hexene Polymerization across Group IV Bis-Phenolate Catalysts. *Acs Catalysis* **2016,** *6* (8), 5138-5145.

4. Steelman, D. K.; Pletcher, P. D.; Switzer, J. M.; Xiong, S. L.; Medvedev, G. A.; Delgass, W. N.; Caruthers, J. M.; Abu-Omar, M. M., Comparison of Selected Zirconium and Hafnium Amine Bis(phenolate) Catalysts for 1-Hexene Polymerization. *Organometallics* **2013,** *32* (17), 4862-4867.

5. Seger, M. R.; Maciel, G. E., Quantitative 13C NMR analysis of sequence distributions in poly(ethylene-co-1-hexene). *Anal Chem* **2004,** *76* (19), 5734-47.

6. Chien, J. C. W.; Nozaki, T., Ethylene Hexene Copolymerization by Heterogeneous and Homogeneous Ziegler-Natta Catalysts and the Comonomer Effect. *Journal of Polymer Science Part a-Polymer Chemistry* **1993,** *31* (1), 227-237.

7. Yang, H. R.; Zhang, L. T.; Fu, Z. S.; Fan, Z. Q., Comonomer Effects in Copolymerization of Ethylene and 1-Hexene with MgCl2-Supported Ziegler-Natta Catalysts: New Evidences from Active Center Concentration and Molecular Weight Distribution. *Journal of Applied Polymer Science* **2015,** *132* (2), 1-9.

8. Li, L.; Metz, M. V.; Li, H.; Chen, M. C.; Marks, T. J.; Liable-Sands, L.; Rheingold, A. L., Catalyst/cocatalyst nuclearity effects in single-site polymerization. Enhanced polyethylene branching and alpha-olefin comonomer enchainment in polymerizations mediated by binuclear catalysts and cocatalysts via a new enchainment pathway. *J Am Chem Soc* **2002,** *124* (43), 12725-41.

9. Awudza, J.; Tait, P., The ‘‘Comonomer Effect’’ in Ethylene/a-Olefin Copolymerization Using Homogeneous and Silica-Supported Cp2ZrCl2/MAO Catalyst Systems: Some Insights from the Kinetics of Polymerization, Active Center Studies, and Polymerization Temperature. *Journal of Polymer Science: Part A: Polymer Chemistry* **2008,** *26*, 267-277.

10. Liu, Z.; Somsook, E.; Landis, C. R., A (2)H-labeling scheme for active-site counts in metallocene-catalyzed alkene polymerization. *J Am Chem Soc* **2001,** *123* (12), 2915-6.

11. Busico, V.; Cipullo, R.; Ronca, S., Propene/Ethene-[1-13C] Copolymerization as a Tool for Investigating Catalyst Regioselectivity. 1. Theory and Calibration. *Macromolecules* **2002,** *35* (5), 1537-1542.

12. Landis, C. R.; Sillars, D. R.; Batterton, J. M., Reactivity of secondary metallocene alkyls and the question of dormant sites in catalytic alkene polymerization. *J Am Chem Soc* **2004,** *126* (29), 8890-1.

13. Tshuva, E. Y.; Goldberg, I.; Kol, M.; Goldschmidt, Z., Zirconium complexes of amine-bis(phenolate) ligands as catalysts for 1-hexene polymerization: Peripheral structural parameters strongly affect reactivity. *Organometallics* **2001,** *20* (14), 3017-3028.

14. Tshuva, E. Y.; Groysman, S.; Goldberg, I.; Kol, M.; Goldschmidt, Z., [ONXO]-type amine bis(phenolate) zirconium and hafnium complexes as extremely active 1-hexene polymerization catalysts. *Organometallics* **2002,** *21* (4), 662-670.

CHAPTER IV. Kinetic Studies of Selective Ethylene Tri-/Tetramerization by Chromium N-phosphinoamidine Catalysts

A. Introduction

With the rapidly growing production of high-quality polyethylene copolymer resins (HDPE, LLDPE, and VLDPE), the demand for α-olefin has been increasing.[1-2] Historically, many industrial processes involved non-selective ethylene oligomerization systems including alkylaluminums (pioneered by Karl Ziegler)[3] and nickel catalysts by Shell (Shell Higher Olefin Process, SHOP)[4]. The non-selective ethylene oligomerization via the Cossee-type mechanism yielded C_4 to C_{20} products, which required further distillation process. Thus, the development of selective oligomerization process with well understood catalytic sites has been explored.[1] Recent progress of selective ethylene oligomerization process by Chevron Phillips Chemical Company[1, 5] and Sasol[6-8] yielded more than 90% selectivity for 1-hexene and/or 1-octene with high productivity. These two systems produced highly selective products because of the metallacyclic mechanism. In spite of the increased interest in metallacyclic mechanism since early 2000, unanswered questions still exist such as oxidation states of the intermediates, the elementary steps, and kinetic dependence on ethylene.[9-11] The detailed kinetic study based on direct measurements of ethylene consumption and/or product formations has been challenging because these ethylene oligomerization studies were often studied in batch reactors that can withstand the high pressure of gas (above 50 bar).

Recently, our group studied the kinetics of ethylene trimerization catalyzed by a highly active chromium N-phosphinoamidine (Cr-(P,N)) catalyst, provided by Chevron Phillips Chemical Company[5], using *in-situ* high-pressure NMR techniques.[12] Our kinetic study with quantitative kinetic modeling supported a metallacyclic mechanism and established rate constants. We reported that at least one of the first two ethylene coordination steps to the active-site must be reversible in order to fit key features of the kinetic results. In addition, we also established a Cossee-type step that led to an undesired polymerization of ethylene. The success of these kinetic studies via high-pressure operando NMR techniques has motivated us to explore a more complex tri-/tetramerization of ethylene. Herein, we demonstrate two possible methods to study the kinetics of ethylene tri-/tetramerization by chromium N-phosphinoamidine pre-catalyst activated by modified methylaluminoxane (MMAO): (1) i*n-situ* ^{1}H NMR using high-pressure NMR cell and (2) high-pressure reactor connected to an auto-sampler. We report preliminary results from the developed methods and describe the limitation and areas to improve.

In our studies, the pre-catalysts **1** – **4** (provided by Chevron Phillips Chemical Company) were studied for selective ethylene oligomerization (Scheme 4.1).[5] The expected selectivity of 1-hexene to 1-octene produced at 70 °C (25 °C for catalyst 1) based on reported results are shown in Scheme 4.1.[5]

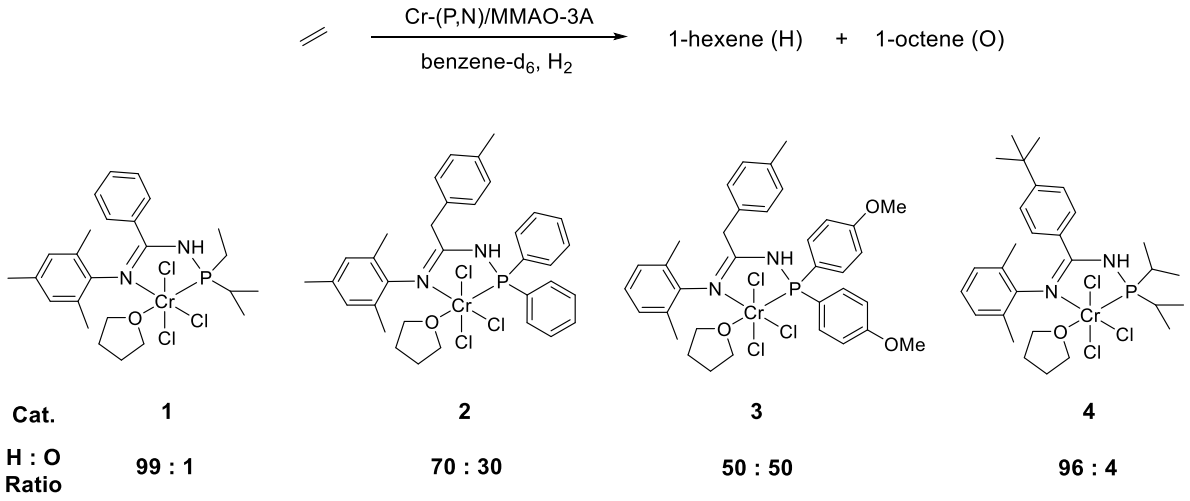

Scheme 4.1. Selective ethylene tri/tetra-merization catalyzed by N-phosphinoamidine-chromium catalysts activated with modified methylaluminoxane-3A (MMAO-3A)

B. Development of In-situ ^{1}H NMR Using High-pressure NMR Cell

Recently, we reported a high-pressure NMR method to collect reliable and reproducible kinetic data including concentrations of monomer and product in ethylene trimerization.[12] We adopted and modified the method from our recent study. The high-pressure NMR cell and its set-up are shown in Figure 4.1. This system with a zirconia tube can withstand up to 1000 bar of pressure and 125 °C in temperature, which allowed us to study reaction kinetics at a condition comparable to the industrial process.[1] In a typical experiment, pre-catalyst, activator, solvent, and an internal standard are mixed in a glovebox filled with argon and loaded into the NMR tube. Then the tube is sealed and connected to our pressure system as shown in Figure 4.1. Because of the air-sensitivity of these oligomerization catalysts, we cycled the gas lines using a connected vacuum pump and charged the tube with hydrogen and ethylene.

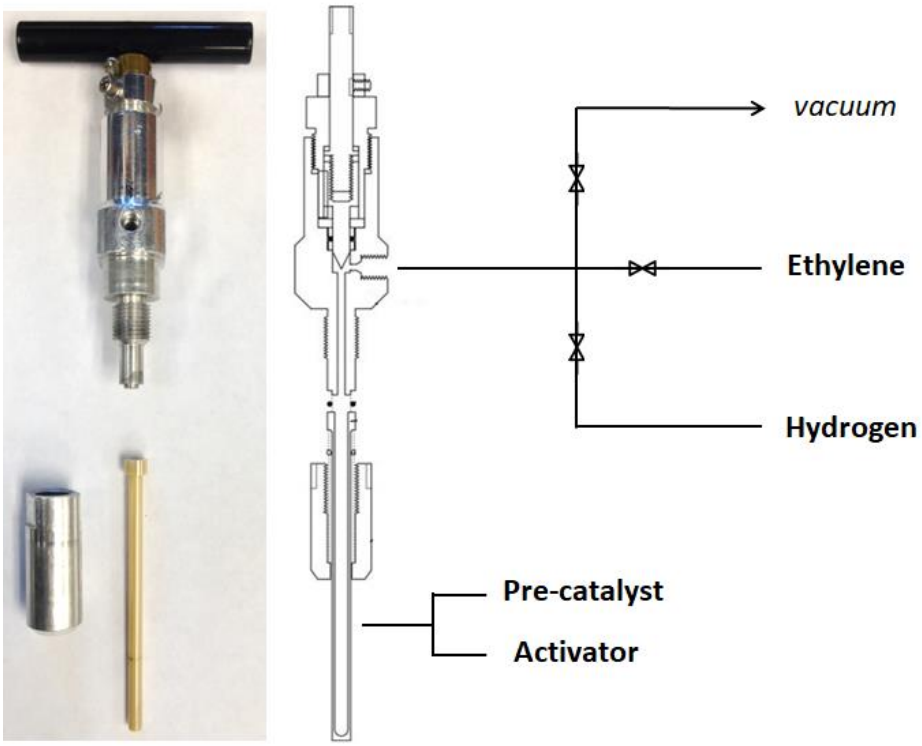

Figure 4.1. High-pressure NMR cell (left) and the set-up

In our previous study, we showed that the reaction does not start due to slow ethylene diffusion in cyclohexane through the small surface area in the NMR tube without mixing.[12] The diffusion rates of ethylene and hydrogen in aromatic solvents (benzene-d_6 and toluene-d_8), which needed to use, were also much slower than a typical reaction time as well. As shown in Figure 4.2, there is no ethylene or hydrogen dissolved in a benzene-d_6 solution before shaking the NMR cell. This slow diffusion of ethylene was an attractive feature to us, as no reaction is expected during the gas addition and NMR instrument preparation including loading, lock, shim, tune, and elevating/stabilizing the temperature. The slow diffusion of ethylene enabled us to monitor most of the oligomerization progress by a highly

active catalyst via mixing the solution (by vigorously shaking the NMR cell) at the spectrometer.

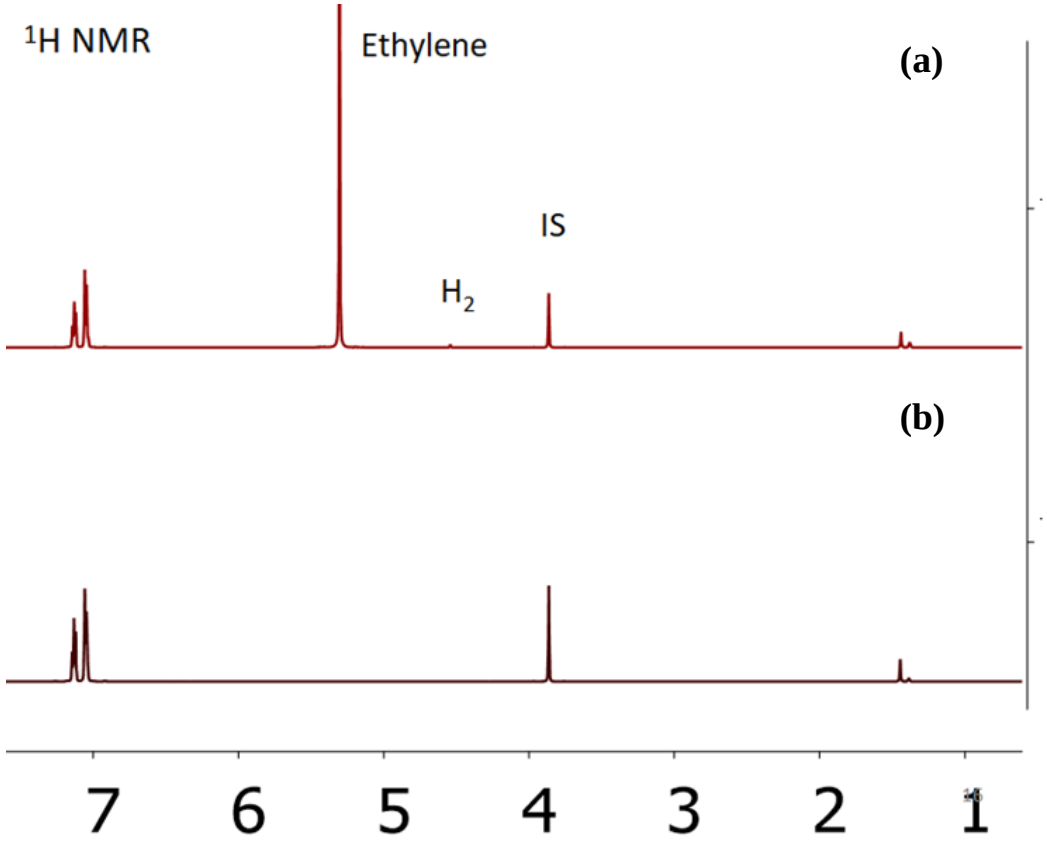

Figure 4.2. ^{1}H NMR of a typical oligomerization reaction (a) after shaking and (b) before shaking the NMR tube cell. 600 MHz, ethylene = 52 bar, H_2 = 5 bar, solvent = toluene-d_8, IS = internal standard (diphenylmethane)

C. Detection of 1-Hexene and 1-Octene in Real-Time.

Next, we examined if ethylene and the products from tri/tetra-merization could be distinguishable by high-field ^{1}H NMR. In our initial ^{1}H NMR analysis of 1-hexene and 1-octene in cyclohexane-d_{12}, all signals including the characteristic olefinic signals as well as CH_2 and CH_3 overlapped completely. With aromatic solvents like benzene-d_6 and toluene-d_8, however, the CH_3 signal of 1-hexene and 1-octene were distinguishable by ^{1}H NMR

(Figure 4.3). Our control experiments, with a different FID processing method (sin bell), demonstrated that the CH_3 signals were well-resolved to quantify the products by ^1H NMR (Figure SI 4.1).

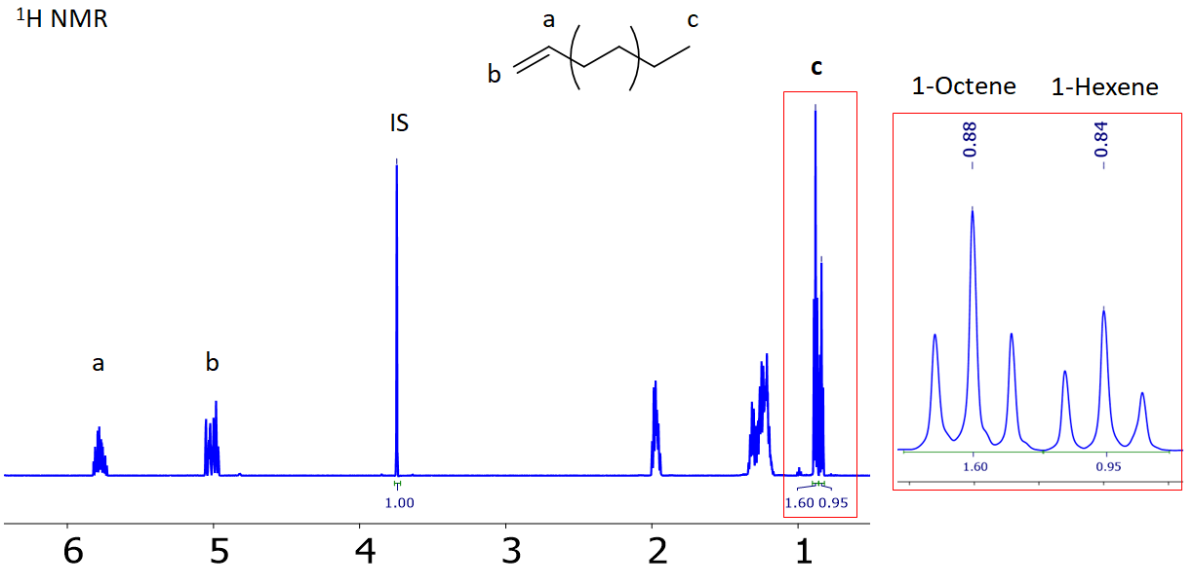

Figure 4.3. ^1H NMR of a 1-hexene and 1-octene mixture in benzene-d_6.600 MHz, IS = internal standard (diphenylmethane), used sine bell apodization at ~15°.

In our initial studies, we observed that the oligomerization results were sensitive to different batches of the activator solutions. To eliminate this inconsistent activator issue, we used the MMAO-3A in heptane solution (AkzoNobel) that our collaborator (Dr. Orson Sydora from Chevron Phillips Chemical) provided. Heptane had to be removed completely from the activator solution in order to differentiate the alkene products based on the CH_3 regions in ^1H NMR. Before drying the solvent, the CH_3 regions were crowded with heptane and other volatile solvents in the activator solution (Figure 4.4a). After removing the solvent

under vacuum for 10 min and dissolving MMAO-3A residues in benzene-d_6, 1-hexene and 1-octene were well-separated (Figure 4.4b). Modification of the activator solution reduced the catalytic activity slightly while preserving the selectivity, which could be due to the loss of alkylaluminum that was present in MMAO.[13]

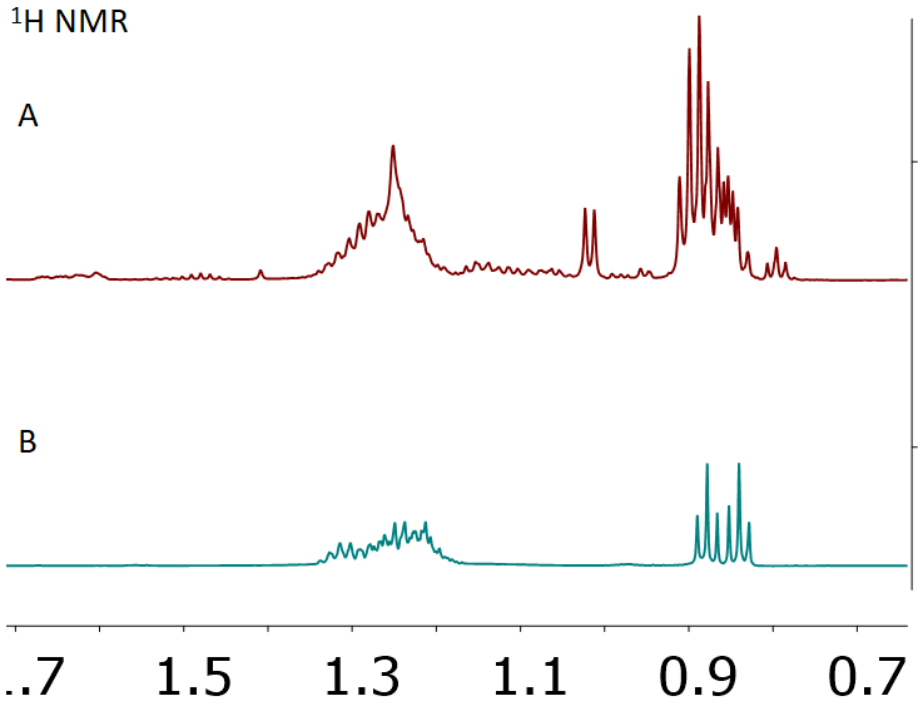

Figure 4.4. ^{1}H NMR of a mixture of 1-hexene, 1-octene, and MMAO-3A (a) as received; (b) after drying the MMAO-3A under vacuum for 10 min. 600 MHz, solvent: benzene-d_6

D. Catalyst Activation and Reaction Conditions

Activation of pre-catalyst with an aluminum-based activator such as AlR_3 and methyl methylaluminoxane (MAO) derivatives is a crucial step for selective oligomerization of ethylene. Many examples of the chromium-based pre-catalyst have halide ligands that are

alkylated by the activator in order to make vacant coordination sites.[1, 6-8, 14-15] After the alkylation, the active center is left with three vacant sites for the metallacycloalkane intermediate and one ethylene. Hagen and co-workers demonstrated that this activation is a slow process and incomplete alkylation intermediate could be the cause of undesired polymerization sites.[16] In addition, excess of MAO, unlike alkylaluminum, acts as a scavenger for impurity and increases productivity. Thus, a large excess of activator (above 300 equiv), and a long premix time (10-120 min) for alkylation are required before introducing ethylene.

The N-phosphinoamidine chromium pre-catalysts have distinctive sky-blue color, which turns into amber (dark yellow) color after activation by MMAO-3A.[5] After excessive drying MMAO-3A under vacuum, we observed significant negative effects. MMAO-3A dried under vacuum for over 2 hours resulted in slow polymerization of ethylene instead of oligomerization. Drying MAO derivatives is known to slowly remove alkylaluminum, which is important for the reactivity and stability of the activator, and change the structure of MMAO.[8, 13] After 12 hours of drying, MMAO-3A did not activate the (Cr-(P,N)) pre-catalyst. Addition of different concentrations various AlR_3 ($AlMe_3$, $AlEt_3$, $AlBu^i_3$) did not restore its activity unlike published works by Gambarotta and Duchateau.[13, 15] Thus, for *in-situ* NMR studies, we dried MMAO-3A/heptane for less than 10 min, which affected the reactivity slightly.

A typical array ^1H NMR spectrum is shown in Figure 4.5. The concentrations of ethylene, 1-hexene, and 1-octene were quantified referenced to an added internal standard. During the reaction, we observed all the signals were broadened due to dissolved gas.

Additional control experiments confirmed that a small amount of unknown signals appeared in the CH_3 region after activation of Cr pre-catalyst with dried MMAO-3A in the absence of ethylene (Figure SI 4.2). However, we concluded that we could get reliable kinetic data with an addition of GC analysis.

The N-phosphinoamidine chromium pre-catalysts have distinctive sky-blue color, which turns into amber, dark yellow, color after activated by MMAO-3A.[5] After excessive drying MMAO-3A under vacuum, we observed significant negative effects. MMAO-3A dried under vacuum for over 2 hours resulted in slow polymerization of ethylene instead of oligomerization. Drying MAO derivatives is known to slowly remove alkylaluminum, which is important for the reactivity and stability of the activator, and change the structure of MMAO.[13, 15] After 12 hours of drying, MMAO-3A did not activate the (Cr-(P,N)) pre-catalyst. Addition of different concentrations various AlR_3 ($AlMe_3$, $AlEt_3$, $AlBu^i_3$) did not restore its activity unlike published works by Gambarotta and Duchateau.[13, 15] Thus, for *in-situ* NMR studies, we dried MMAO-3A/heptane for less than 10 min, which was affected the reactivity slightly.

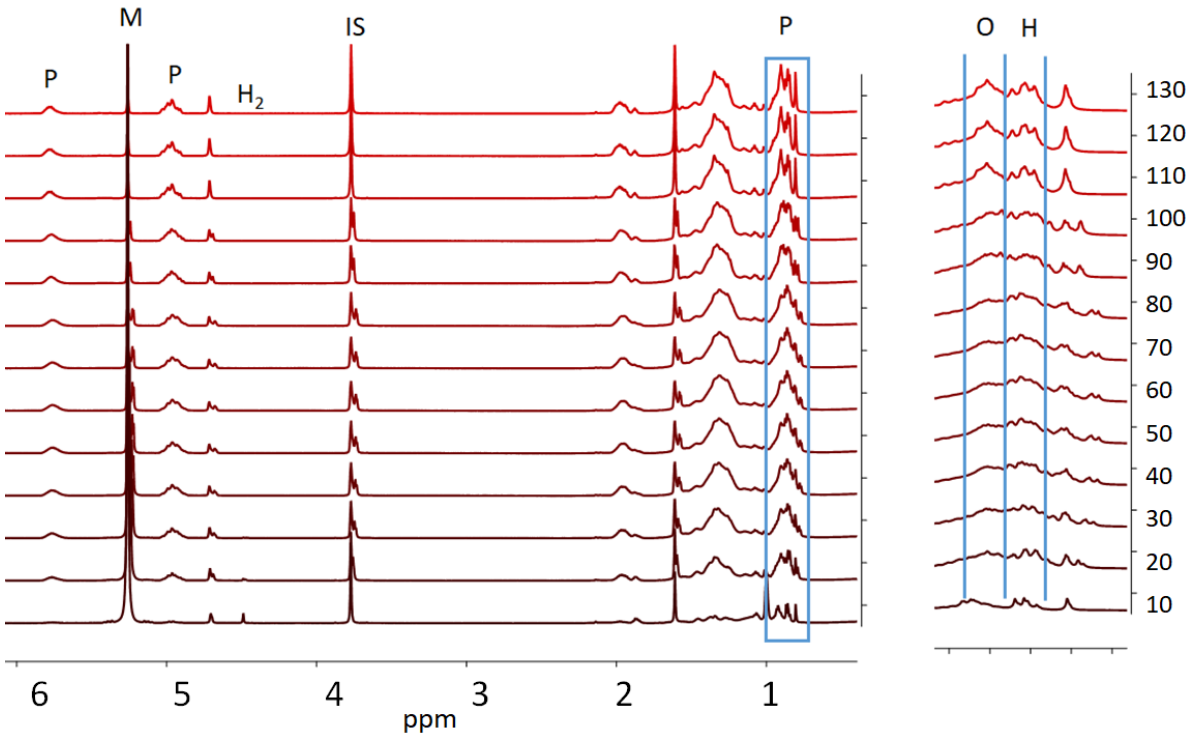

Figure 4.5. An array of ^{1}H NMR collected for a typical ethylene tri-/tetramerization reaction. 600 MHz, temp = 70 °C, solvent = benzene-d_6, M = monomer (ethylene), P = products (signals of 1-hexene and 1-octene), IS = internal standard (diphenylmethane), O = CH_3 peak of 1-octene, H = CH_3 peak of 1-hexene, y-axis = time (min), ^{1}H NMR collected every 10 min.

A typical array ^{1}H NMR spectrum is shown in Figure 4.5. The concentrations of ethylene, 1-hexene, and 1-octene were quantified referenced to an added internal standard. During the reaction, we observed all the signals were broadened due to dissolved gas. Additional control experiments confirmed that a small amount of unknown signals appeared in the CH_3 region after activation of Cr pre-catalyst with dried MMAO-3A in the absence of ethylene (Figure SI 4.2). However, we concluded that we could get reliable kinetic data with an addition of GC analysis.

E. In-situ ^{1}H NMR Experiments Using High-pressure NMR Cell

The pre-catalysts[7] were activated by stirring in a d-MMAO, which is dried MMAO-3A under vacuum for 10 min (Scheme 4.1), solution in benzene-d_6 for 30 – 120 min. Then the solution was charged ethylene (40 – 55 bar) and hydrogen (5 bar). The addition of hydrogen in selective oligomerization increased the catalyst activity possibly due to hydrogen facilitating chain transfer of any undesired polymer sites and, therefore, reducing the polyethylene byproducts.

First, selective trimerization of ethylene was studied with catalyst **1** that makes more than 99% of 1-hexene at 25 °C. As shown in Figure 4.6 a, the ethylene consumption and 1-hexene production time profiles were monitored by ^{1}H NMR. The reactivity and rate of monomer consumption were comparable to our recent ethylene trimerization study using high-pressure NMR.[2] MMAO-3A was dried under vacuum for 10 min and the drying effect on reactivity was investigated under the same condition (Figure 4.6). Catalyst **1** activated with d-MMAO resulted in a decrease in 1-hexene yield by 10% (0.05 M) and no significant effect on the rate of the reaction. As reported by Bercaw and coworkers, the decrease in 1-hexene yield could be attributed to the cotrimerization of 1-hexene with ethylene or formation of polyethylene.[17]

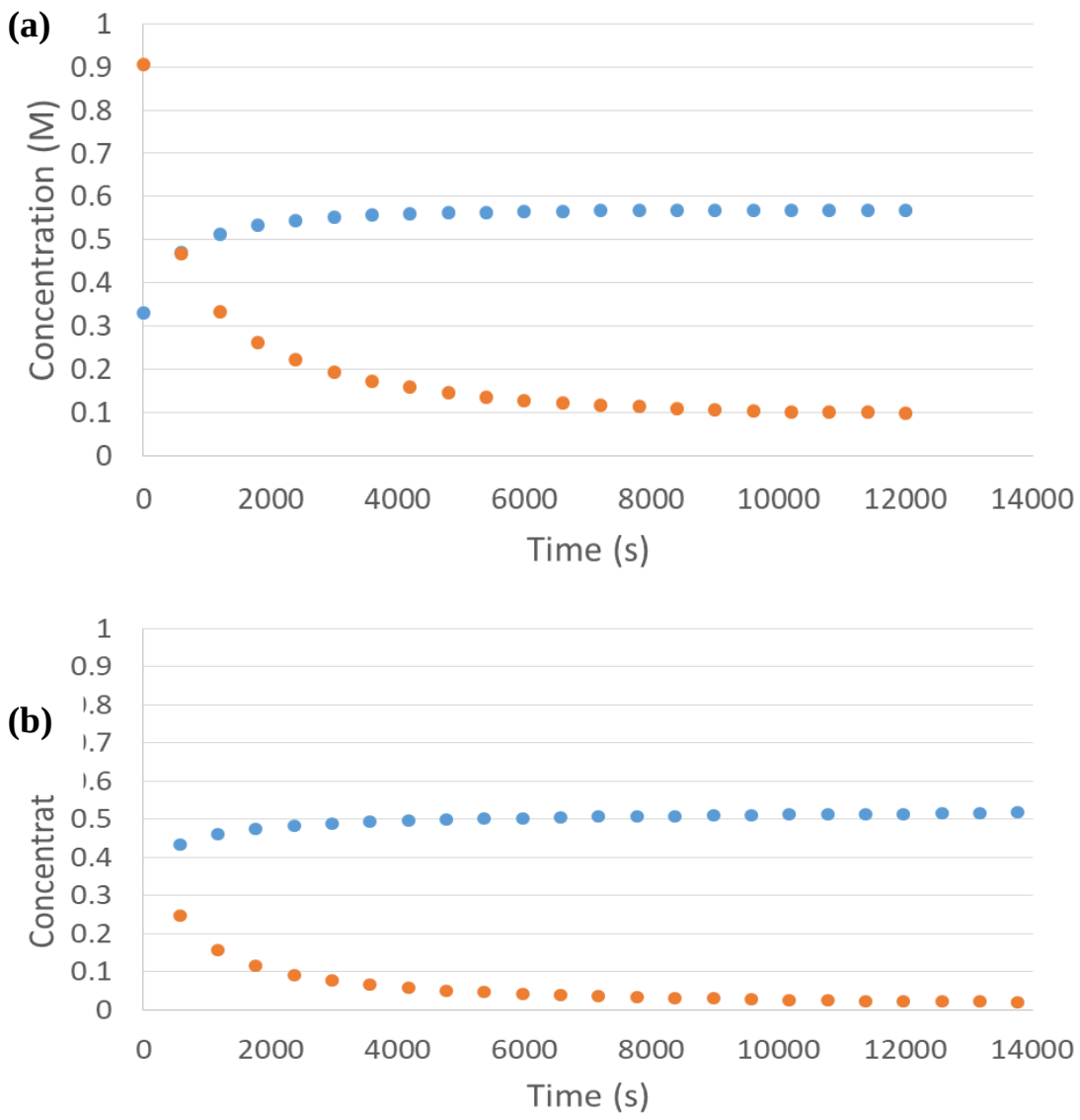

Figure 4.6. Ethylene consumption (orange) and 1-hexene production (blue) time profile for ethylene trimerization with catalyst **1** activated by (a) untreated MMAO-3A and (b) dried-MMAO-3A. [catalyst] = 1.0 mM, 600 equiv of MMAO-3A, [ethylene] = 1.63 M, $P_{hydrogen}$ = 5 bar, temp = 25 °C, solvent = benzene-d_6

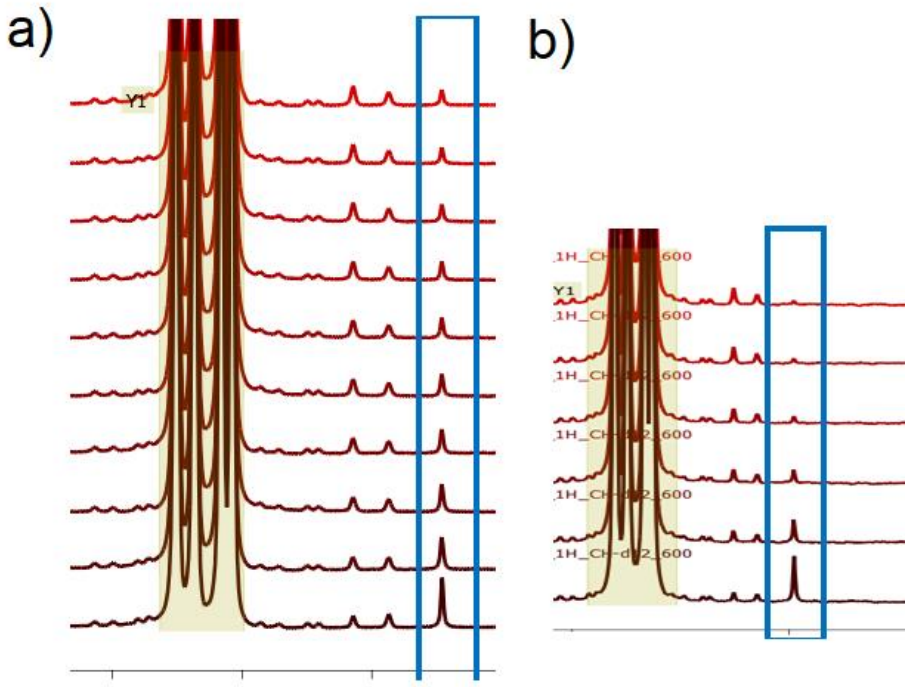

Figure 4.7. Consumption of hydrogen during ethylene trimerization with catalyst **1** activated by (a) untreated MMAO-3A and (b) dried-MMAO-3A shown by an array ^{1}H NMR. [catalyst] = 1.0 mM, 600 equiv of MMAO-3A, [ethylene] = 1.63 M, $P_{hydrogen}$ = 5 bar, temp = 25 °C, solvent = benzene-d_6

The hydrogen consumption during the ethylene trimerization with catalyst **1** activated by (a) untreated MMAO and (b) d-MMAO are shown in Figure 4.7. Hydrogen was observed to be used slowly without affecting the reactivity in our previous study.[12] In addition to the polyethylene formation, the rapid depletion in hydrogen is another feature of the catalytic system with d-MMAO in our studies.

Time profiles of ethylene tri/tetra-merization by catalyst **2**/d-MMAO-3A are shown in Figure 4.8 and 4.9. In Figure 4.8, the production of alkene was calculated according to the vinyl signals in ^{1}H NMR. Figure 4.9 showed that each product was increasing spontaneously and 1-hexene is not an intermediate for 1-octene formation. At the end of the reaction, the

[alkene]$_{final}$ was 0.4 M. However, based on the CH_3 signals, the sum of [1-hexene]$_{final}$ and [1-octene]$_{final}$ was above 0.65 M (Figure 4.9 a). This is due to the fact that the CH_3 signals of 1-hexene and 1-octene are overlapped with other proton signals, including leached alkylaluminum, in the solution (Figure 4.5). To resolve the issue, we calibrated the concentration of each product by referencing the first data point as zero (Figure 4.9 b). After calibration, the ratio between 1-hexene and 1-octene was 63%, which showed the relative ratio was accurate. To evaluate that the calibration, concentration of each product at the end of the reaction was collected and quantified by GC. The product concentration based on GC, [1-hexene] = 0.17 M and [1-octene] = 0.12 M, near-identical to the values obtained from ^{1}H NMR after calibration (Figure 4.8 c).

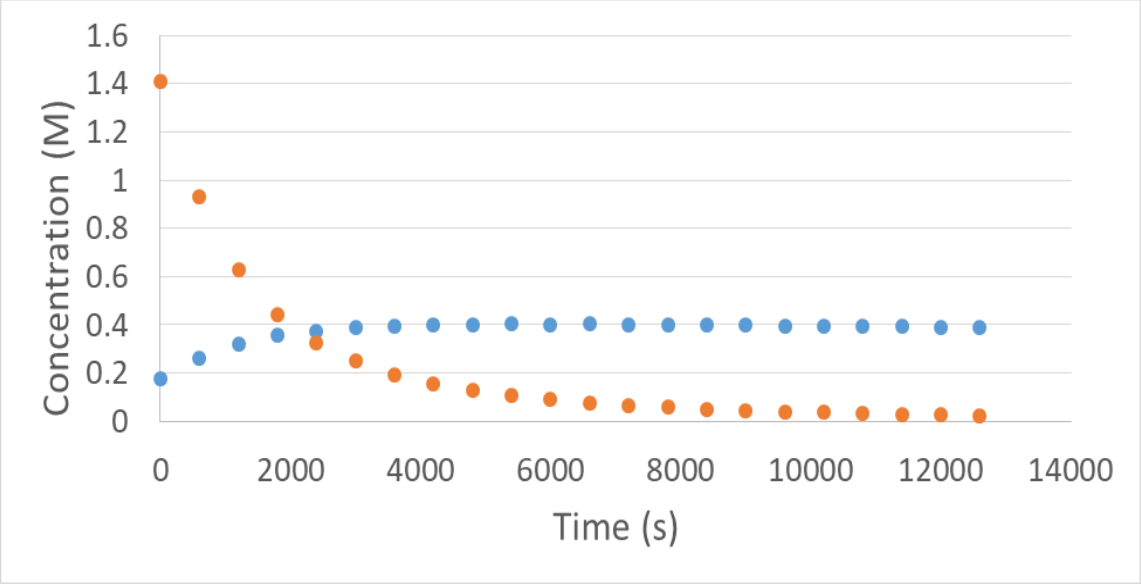

Figure 4.8. Ethylene consumption and alkene formation time profile for ethylene oligomerization with catalyst **2** activated by d-MMAO-3A. orange: ethylene consumption, blue: alkene formation, [catalyst] = 1.0 mM, 700 equiv of MMAO-3A, [ethylene] = 2.03 M, $P_{hydrogen}$ = 5 bar, temp = 70 °C, solvent = benzene-d_6

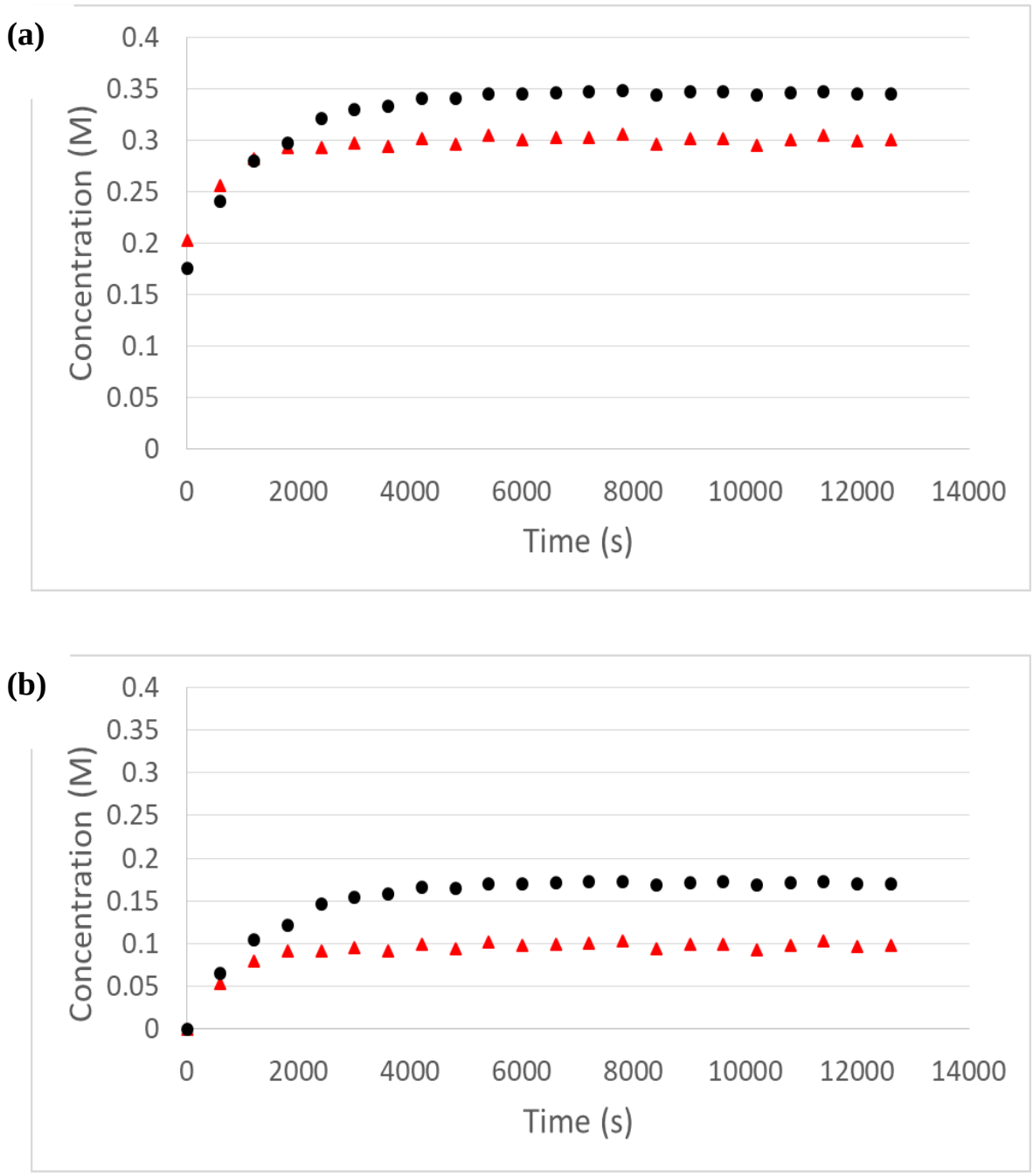

Figure 4.9. Ethylene consumption and 1-hexene/1-octene formation time profile for ethylene oligomerization with catalyst **2** activated by d-MMAO-3A. (a) black: 1-hexene, red: 1-octene, (b) black: 1-hexene, red: 1-octene, referenced. [catalyst] = 1.0 mM, 700 equiv of MMAO-3A, [ethylene] = 2.03 M, $P_{hydrogen}$ = 5 bar, temp = 70 °C, solvent = benzene-d_6

Next, ethylene oligomerization of catalyst **3** with d-MMAO-3A was studied by ^{1}H NMR and each alkene production was confirmed by GC (Figure 4.10). Similar to the system with catalyst **2**, the concentration of 1-hexene and 1-octene gradually increased to roughly 0.25 M.

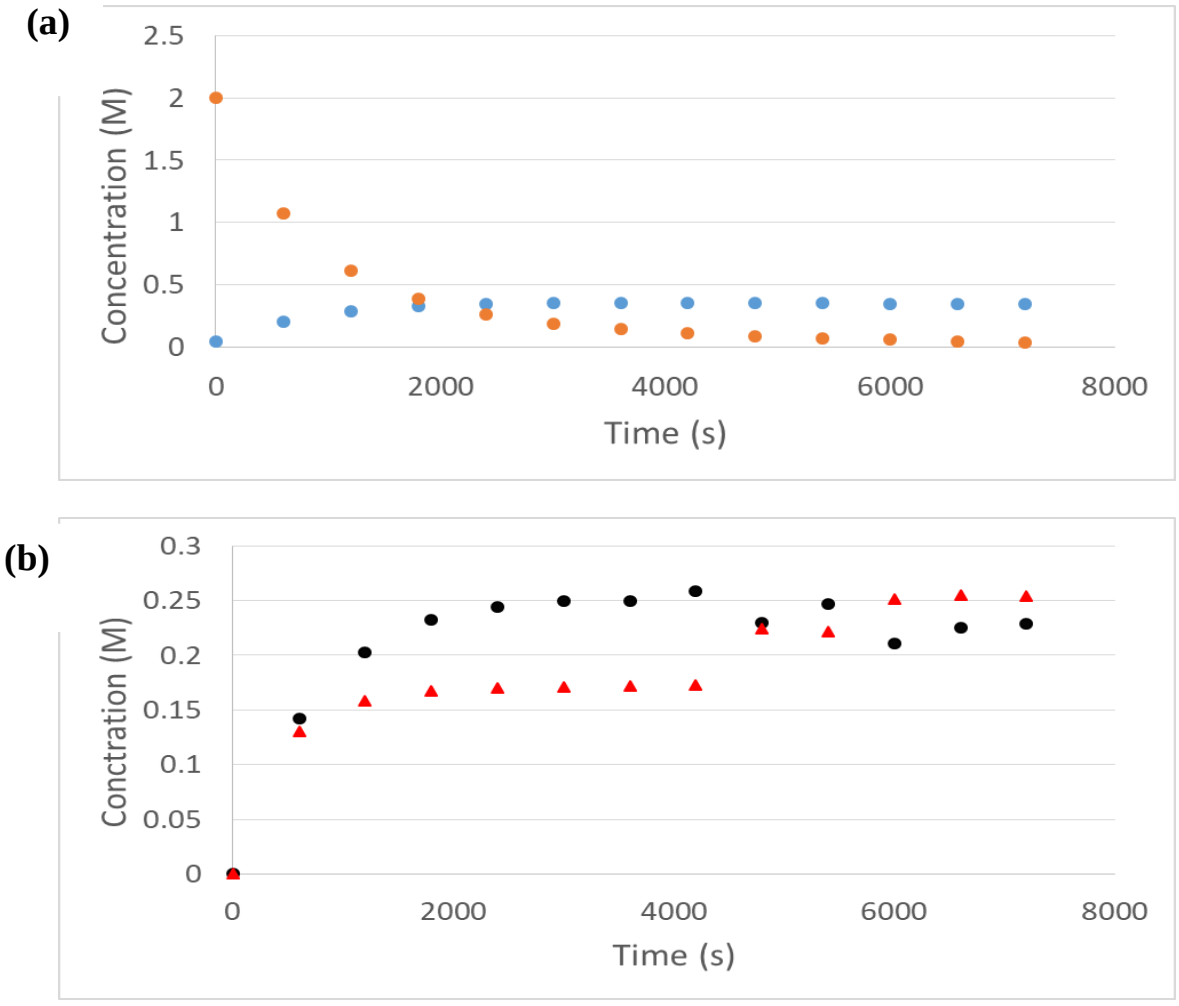

Figure 4.10. Ethylene consumption and product formation time profile for ethylene oligomerization with catalyst **3** activated by d-MMAO-3A. (a) orange: ethylene consumption, blue: alkene formation, (b) black: 1-hexene, red: 1-octene, referenced. [catalyst] = 1.0 mM, 780 equiv of MMAO-3A, [ethylene] = 2.36 M, $P_{hydrogen}$ = 5 bar, temp = 70 °C, solvent = benzene-d_6

The described in-situ ^{1}H NMR experiments with high-pressure NMR cell resulted in reproducible and reliable ethylene consumption as well as 1-hexene/1-octene production, which was confirmed by GC. However, this is after the calibration with two assumptions: (1) the changes in CH_3 regions are sorely dependent on 1-hexene and 1-octene production and (2) there is no significant change in the CH_3 signals due to an unexpected reaction that makes impurities. Polyethylene formation, although it is in small quantity, is another area we have to address in the future. The 1-octene forming catalysts are shown to cause more polymerization[1, 8, 17-18], which could reduce the headspace inside of the tube. We envision that selecting tri/tetra-merization catalytic systems with minimal side reactions (no leaching or polyethylene formation, this described method of operando ^{1}H NMR technique with high-pressure NMR cell would produce very high-quality data for kinetic and mechanistic studies.

F. Batch Reaction with Auto-sampling

In addition to high-pressure NMR cell, we studied the kinetics of selective ethylene oligomerization by an auto-sampler (the Parr 4878 Automated Liquid Sampler) from Parr Instrument Company. Auto-sampler enabled us to collect multiple liquid samples from the pressured reactor under high temperature and pressure. The extracted samples were then analyzed by GC for the quantification of 1-hexene and 1-octene. Although we are limited to fewer data points compared to the NMR study, we no longer had to alter the MMAO, which reduced the reactivity by increasing polyethylene formation.

The pre-catalysts **3** – **4** were activated with MMAO-3A (700 equiv) for 2 hours, and it was charged with ethylene and hydrogen to produce 1-hexene and 1-octene selectively.

These catalysts under batch conditions with 50 bar of ethylene at 70 °C were reported to be highly active with productivity over 430,000 $g_{product}g_{Cr}^{-1}h^{-1}$ with less than 0.5 wt% polyethylene. Our initial studies of pre-catalyst **3** at 70 °C resulted in very poor catalytic activity and polyethylene formation (Figure 4.11 a). After careful investigation, we observed that the temperature in the reactor reached above 90 °C during the ramping in the Parr system. It was reported most of the current oligomerization catalysts, other than recently developed PNP-type catalysts by Dow, including the Cr- N-phosphinoamidine catalysts are not stable and lose their activity above 70 °C.[1] Repeating the same experiment at 60 °C instead resulted in a notable increase in activity with selectivity matched with the reported values (Figure 4.11 b). However, a significant amount of polyethylene, about 22 wt. % compared to the alkene products, were observed.

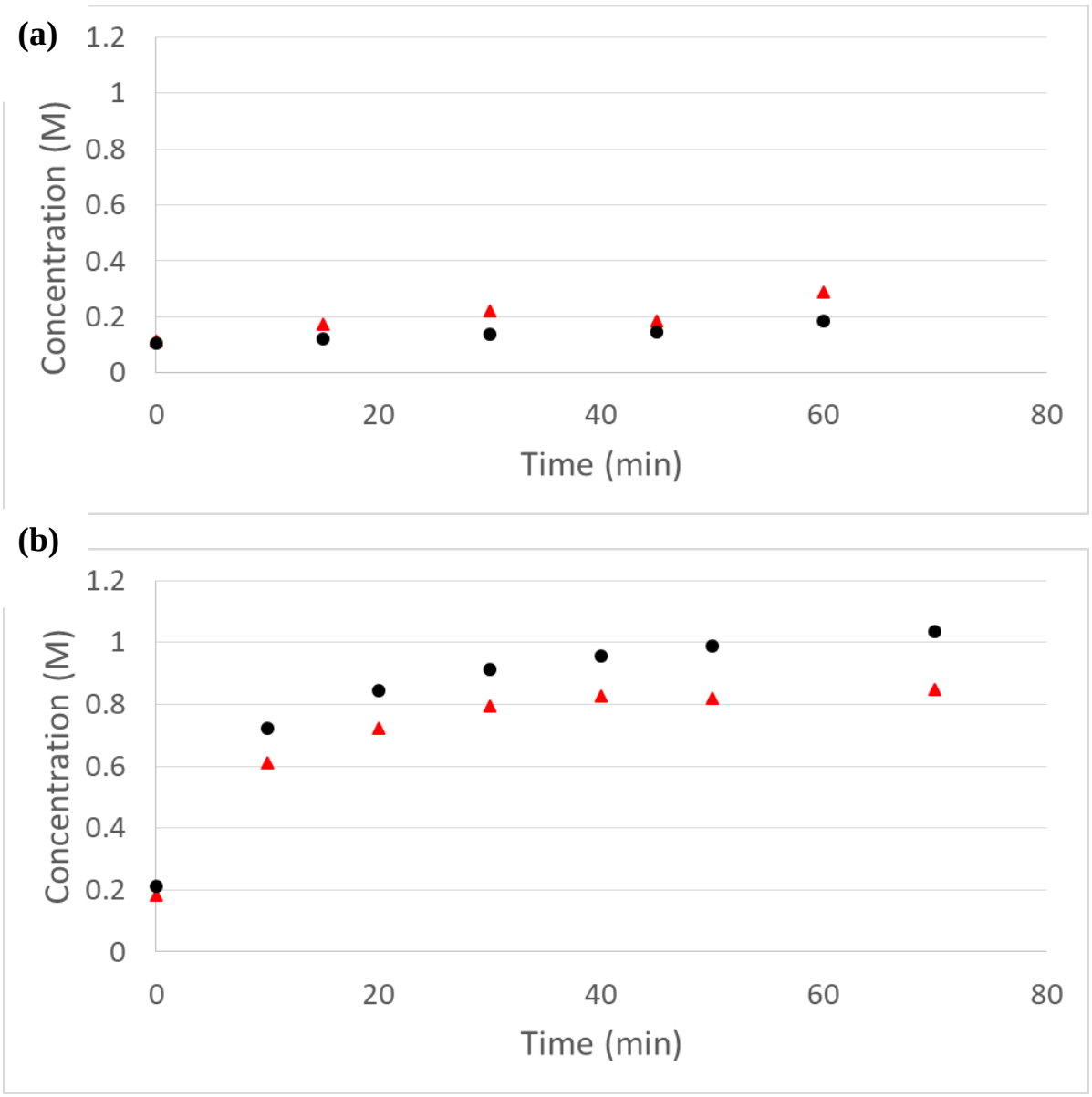

Figure 4.11. Product formation time profile for ethylene oligomerization with catalyst **3** activated by MMAO-3A at a different temperature: (a) at 70 °C and (b) 60 °C. black: 1-hexene, red: 1-octene. [catalyst] = 0.10 mM, 700 equiv of MMAO-3A, $P_{ethylene}$ = 50.0 bar, $P_{hydrogen}$ = 5 bar, solvent = cyclohexane and ethylbenzene.

With selective ethylene trimerization catalyst **4** (about 96% 1-hexene), the overall activity was much higher with low [1-octene] (Figure 4.12). The significantly lower polyethylene was collected (less than 1 wt. %), which is similar to the reported results.

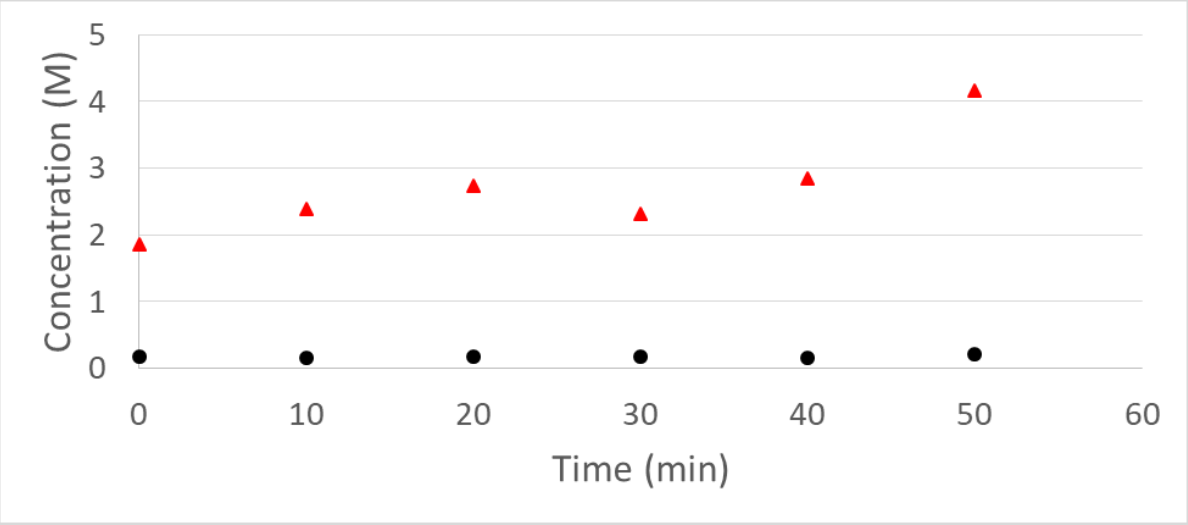

Figure 4.12. Product formation time profile for ethylene oligomerization with catalyst **4** activated by MMAO-3A. black: 1-hexene, red: 1-octene. [catalyst] = 0.10 mM, 700 equiv of MMAO-3A, $P_{ethylene}$ = 52.0 bar, $P_{hydrogen}$ = 5 bar, temp = 60 °C, solvent = cyclohexane and ethylbenzene

The fact that the catalyst **4** did not undergo ethylene polymerization is good evidence that this batch reactor with auto-sampling could be a viable way to study ethylene tri/tetramerization. In the literature, the polymerization of ethylene is known to be caused by a lack of heat transfer that results in hot spot buildup.[1] The degradation or change in active-sites is detrimental to the oligomerization of ethylene. If we address the overheating issues of the reactor and carefully optimize the conditions, this method could be practicable for kinetic study.

G. Conclusion

We described two methods to obtain kinetic data of ethylene tri-/tetramerization catalyzed by industrially impactful chromium/MMAO system: (1) operando ^{1}H NMR spectroscopy using high-pressure NMR tube cell and (2) pressured reactor connected to an auto-sampler. We demonstrated that these methods have great potential to monitor both ethylene consumption and product formation with high sensitivity. In the NMR studies of ethylene tetramerization, leaching unknown impurities during the reactions hindered us from obtaining reliable kinetic data. In both methods of NMR and batch studies, the degradation of catalytic sites into polymerization sites resulted in significant polyethylene byproducts. With a better selection of the catalyst and activator, the methods described in this thesis will enable us to study the kinetics and mechanism of ethylene tri-/tetramerization.

H. Supporting Information

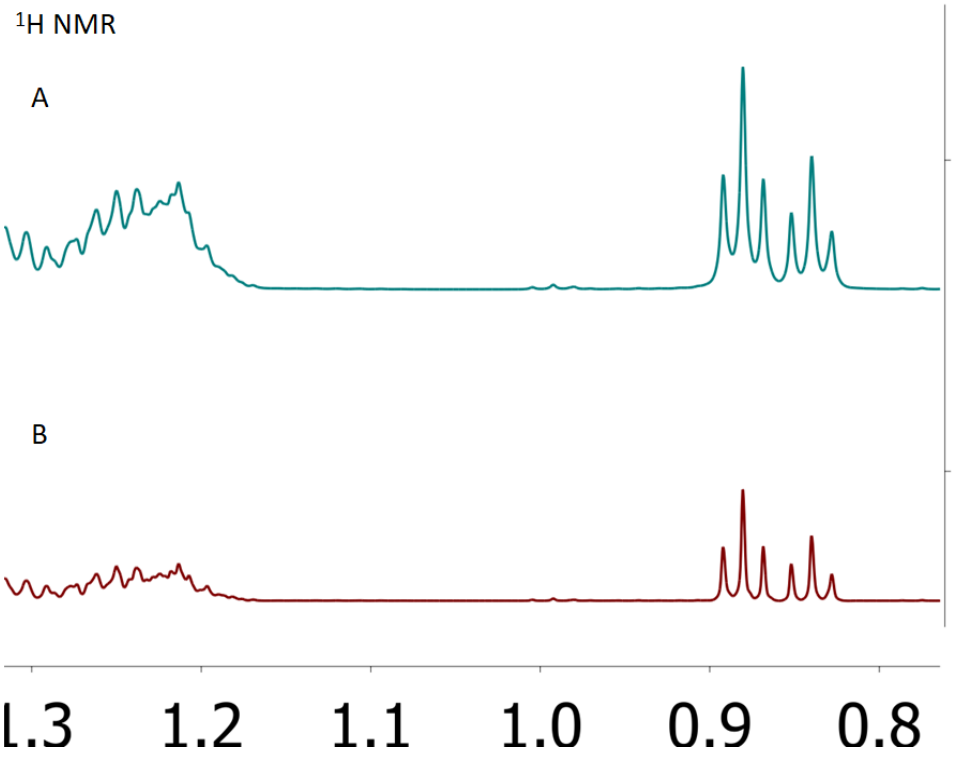

Figure SI 4.1. ^{1}H NMR of 1-hexene/1-octene mixture in benzene-d_6. (a) after Lorentzian apodization at 0.20 Hz; (b) after bell apodization at 15°.

Using aromatic solvents (benzene-d_6 and toluene-d_8), instead of cyclohexane-d_{12}, made the CH_3 of 1-hexene and 1-octene distinguishable with a slight overlap in ^{1}H NMR. When a typical FID processing method of Lorentzian apodization at 0.20 Hz was used, the CH_3 signals were slightly overlapped (**SI 4.1 A**). By using sine bell apodization at ~15°, we could resolute the signals with good separation (**SI 4.1 B**). With sine bell apodization, the overall gain was reduced but the integrations of two signals were not affected.

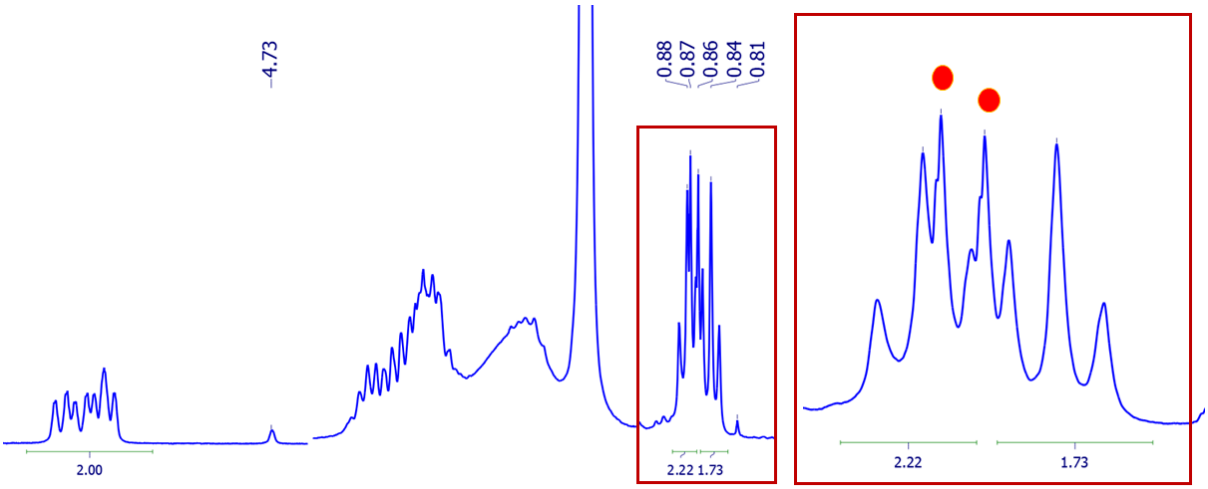

Figure SI 4.2. ^{1}H NMR of 1-hexene/1-octene mixture with activated catalyst **2** by 600 equiv of d-MMAO-3A in benzene-d_6.

Catalyst **2** was activated by 600 equiv of d-MMAO-3A (dried for 10 min) for 2 hours and mixed with 1-hexene/1-octene. Figure SI 4.2 shows that additional signals (labeled in red) are present in the CH_3 regions. The additional signals were not observed with MMAO-3A. We suspect that the structure of MMAO is altered during the drying process and unknown compounds like alkylaluminum are leached.

(a)

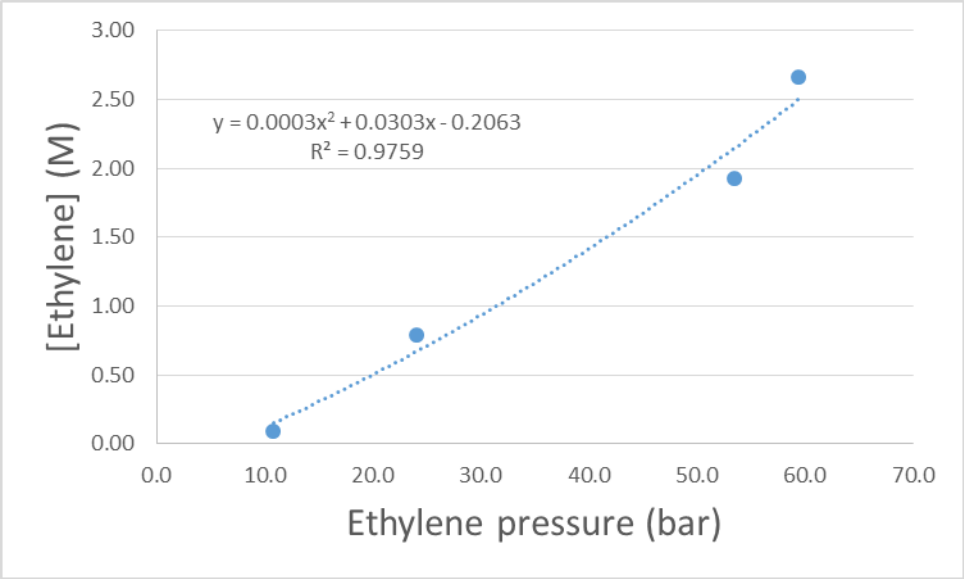

(b)

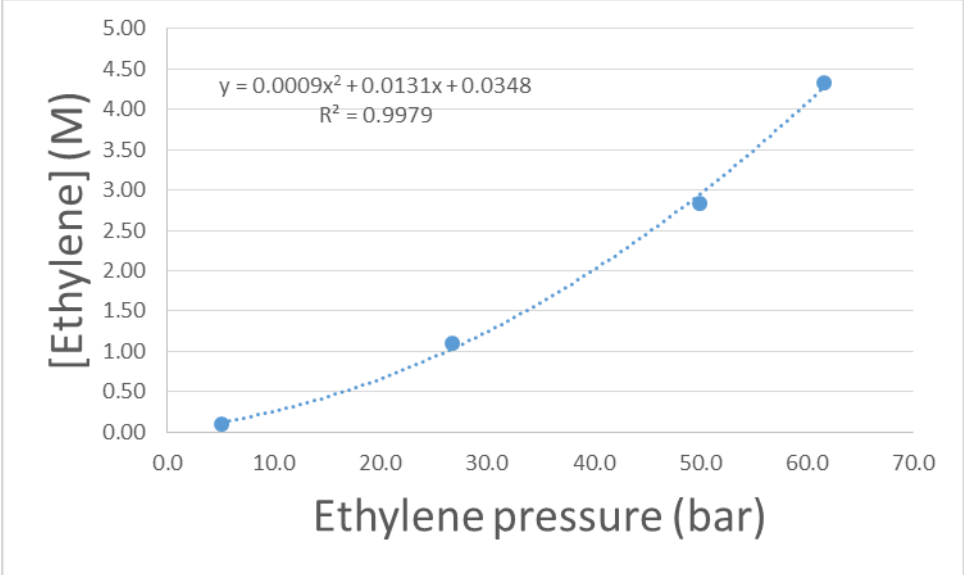

Figure SI 4.3. Ethylene calibration in different solvent; hydrogen pressure = ca. 5 bar. (a) solvent = benzene-d_6; (b) solvent = cyclohexane-d_{12}.

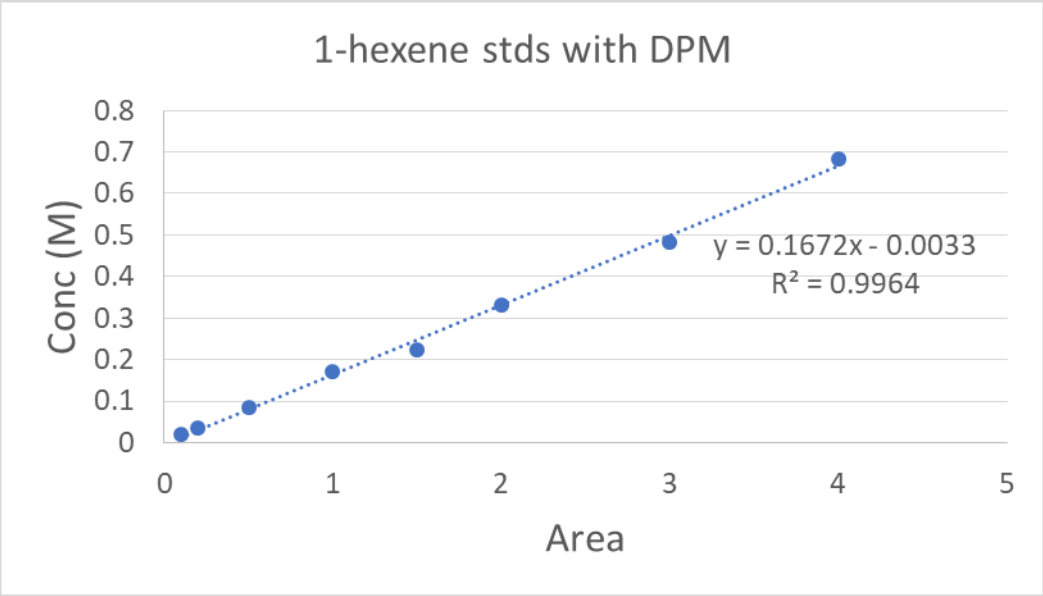

Figure SI 4.4. Calibration plot for 1-hexene for GC analysis (NMR scale), IS = diphenylmethane

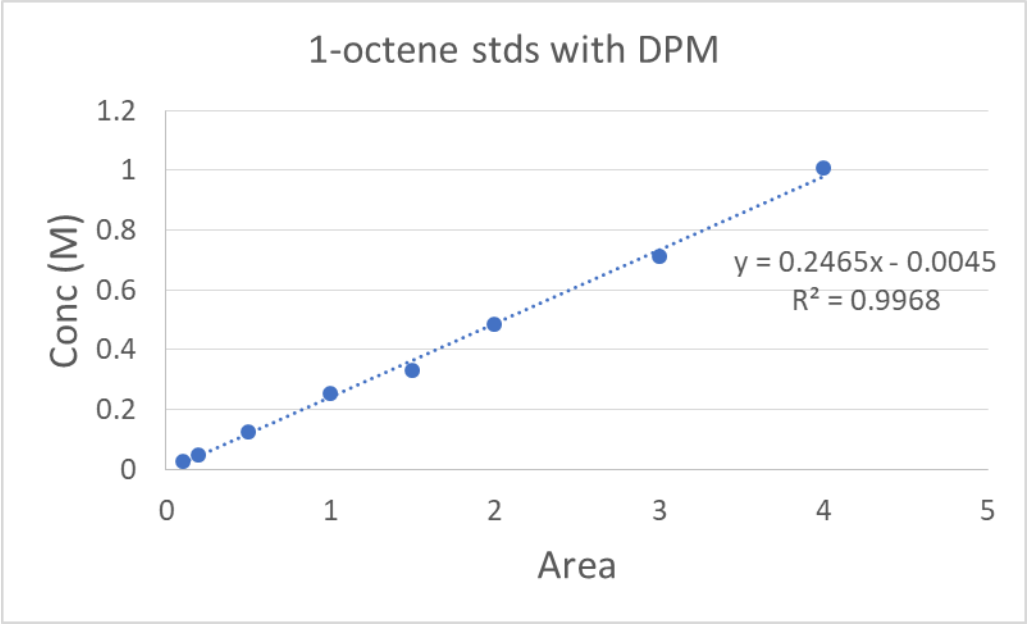

Figure SI 4.5. Calibration plot for 1-octene for GC analysis (NMR scale), IS = diphenylmethane

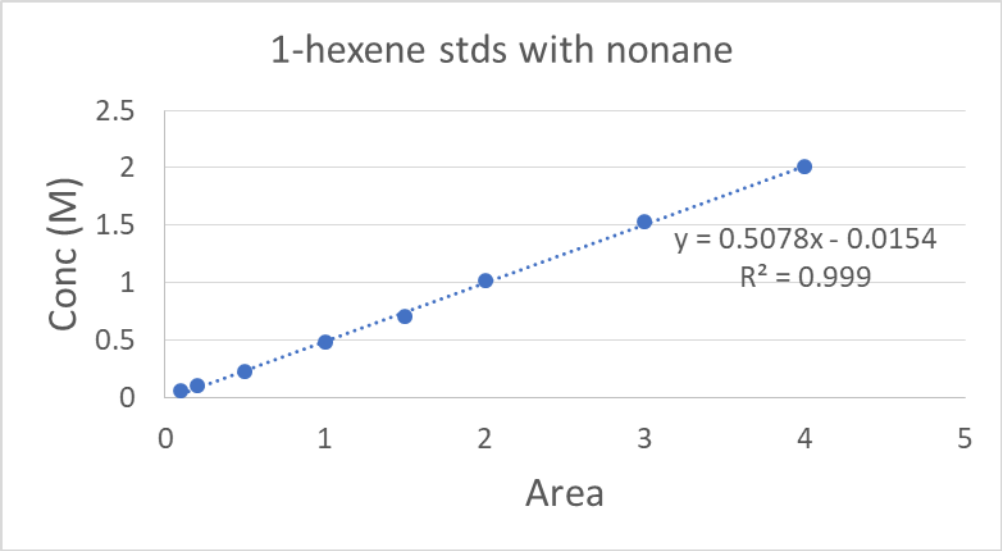

Figure SI 4.6. Calibration plot for 1-hexene for GC analysis (Batch scale), IS = nonane

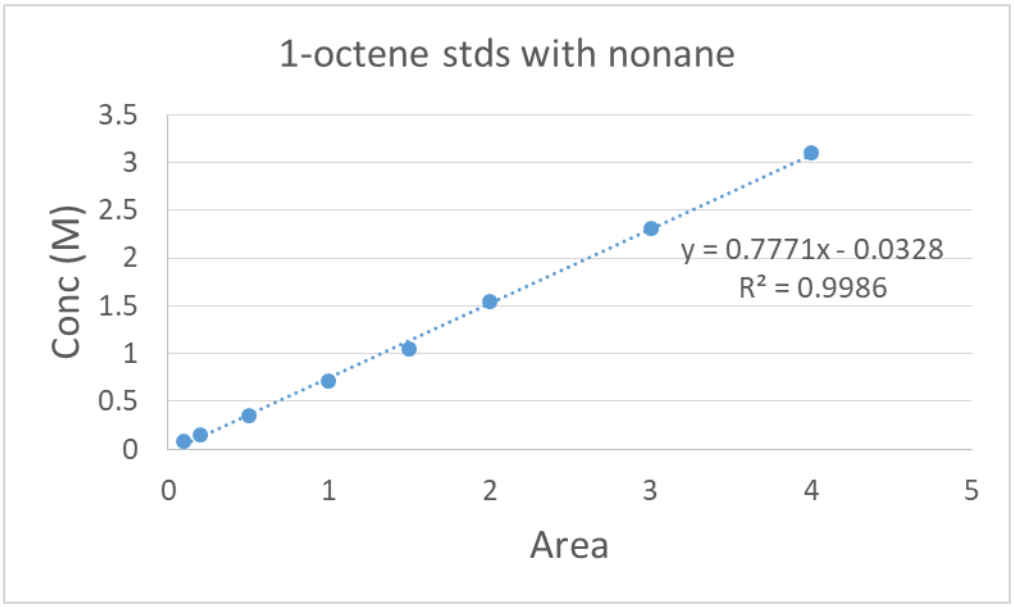

Figure SI 4.7. Calibration plot for 1-octene for GC analysis (Batch scale), IS = nonane

I. Experimental Procedure

1. General Consideration

All reactions were performed in an argon-filled glove box or using standard Schlenk techniques under argon unless otherwise specified. Ethylene (99.999%), purchased from Praxair, was filtered through Oxiclear purifier (RGP-R1-500) for oligomerization. Solvents were degassed, purified with a solvent purification system (Pure Process Technology INC), and stored over activated molecular sieves prior to use. Benzene-d_6, cyclohexane-d_{12}, and toluene-d_8 were dried with CaH_2 and stored over activated molecular sieves. MMAO-3A in heptane (7% Al) was purchased from Akzo Nobel Polymer Chemicals and used as received. Diphenylmethane was purchased from Aldrich and stored over molecular sieves before use. All other reagents were purchased from commercial vendors (Fischer Scientific and Sigma) and used without further purification. Precatalysts were prepared and provided by our collaborator (Dr. Orson Sydora from Chevron Phillips Chemical). The high-pressure NMR cell with a zirconia tube (the NMR cell 13/105) and its manifold were purchased from Daedalus Innovations. Gases were added to the NMR tube using an in-house-built gas line. The pressure-reactor and Automated Liquid Sampler (4878) were purchased from Parr Instrument Company. All ^1H and array NMR experiments were done on a Varian Unity Inova AS600 600MHz with Varian triple resonance $^1H/^{13}C/^{15}N$ probe with PFG, 5mm at 25 °C unless otherwise specified. The 1-hexene/1-octene mixture from NMR and batch studies were analyzed by gas chromatography/flame ionization detection (GC-FID) (Model 7890A, Agilent Technologies, Santa Clara, CA) using response factors relative to the internal standard of heptane or diphenylmethane.

2. *In-situ* ^{1}H NMR Experiments Using High-pressure NMR Cell

The procedure for NMR scale copolymerization was adopted and modified from literature.[12] In a typical experiment with catalyst **1**, catalyst (0.0038 g, 5 μmol), MMAO-3A (1.1783 g, 600 equiv), and diphenylmethane (1.6823 g, 10 mmol) were mixed and diluted to 10.0 mL in a volumetric flask with benzene-d_6. A 0.25 mL fraction of this solution and an additional 0.25 mL of benzene-d_6 were mixed and placed in the zirconia NMR tube. The sealed NMR tube cell was taken out of the glovebox and connected to the gas line. After the line was purged under vacuum, hydrogen gas (5 bar) was added to the NMR cell followed by the addition of ethylene gas (50 bar). As long as the NMR cell was not physically disturbed, gases were not dissolved in the solution. The NMR cell was carefully placed in the spectrometer, and the temperature of the spectrometer was set to the desired temperature (25 – 80 °C) and set all parameters. After the temperature equilibrated, the tube was taken out and the reaction was started by shaking the NMR cell for 30 seconds. Then the cell was transferred into the spectrometer, and the reactions were monitored by array ^{1}H NMR.

3. Batch Reaction with Auto-sampling

The procedure for NMR scale copolymerization was adopted and modified from literature.[5] A 75 mL stainless steel reactor from Parr Instrument Company was dried under vacuum for over 24 hours. In a typical experiment with catalyst **3**, catalyst (0.0022 g, 0.1 mM), MMAO-3A (0.962 g, 600 equiv), ethylbenzene (1.0 g), and cyclohexane (ca. 10 mL) were added to a 20-mL vial containing a stir bar. The solution was stirred for 0.5 – 2 hours before diluted to 25 mL with the addition of nonane as an internal standard (0.254 g, 1.981 mmol). The reactor was transferred out of the glovebox and connected to the gas lines and

the auto-sampler. The reactor was then heated to 5 °C below the reaction temperature, charged with hydrogen and ethylene and increased the temperature to the desired temperature. At every 10 min, the auto-sampler collected ca. 0.75 mL of the reaction solution, which was quickly sealed and cooled in an ice-bath. Once cooled, the solution was diluted with cyclohexane (ca. 1 mL) and filtered through a plug of silica to remove catalyst/activator and prepared as a GC sample. Each sample was analyzed by GC-FID. At the end of the reaction, the reaction was cooled in an ice-bath. When the reactor temperature reached below 25 °C, the unreacted ethylene and hydrogen gas were vented. The reactor solids were collected by filtering the reaction and cleaning the reactor walls. The solids were dried under vacuum and mild heat and weighted.

J. References

1. Sydora, O. L., Selective Ethylene Oligomerization. *Organometallics* **2019,** *38* (5), 997-1010.

2. Kissin, Y. V., Polyethylene, Linear Low Density. *Kirk-Othmer Encyclopedia of Chemical Technology* **2015**, 1-33.

3. Smith, M. B., Monomer-dimer equilibria of liquid aluminum alkyls. I. Triethylaluminum. *The Journal of Physical Chemistry* **1967,** *71* (2), 364-370.

4. Keim, W., Oligomerization of ethylene to alpha-olefins: discovery and development of the shell higher olefin process (SHOP). *Angew Chem Int Ed Engl* **2013,** *52* (48), 12492-6.

5. Sydora, O. L.; Jones, T. C.; Small, B. L.; Nett, A. J.; Fischer, A. A.; Carney, M. J., Selective Ethylene Tri-/Tetramerization Catalysts. *Acs Catalysis* **2012,** *2* (12), 2452-2455.

6. Bollmann, A.; Blann, K.; Dixon, J. T.; Hess, F. M.; Killian, E.; Maumela, H.; McGuinness, D. S.; Morgan, D. H.; Neveling, A.; Otto, S.; Overett, M.; Slawin, A. M.; Wasserscheid, P.; Kuhlmann, S., Ethylene tetramerization: a new route to produce 1-octene in exceptionally high selectivities. *J Am Chem Soc* **2004,** *126* (45), 14712-3.

7. Overett, M. J.; Blann, K.; Bollmann, A.; Dixon, J. T.; Haasbroek, D.; Killian, E.; Maumela, H.; McGuinness, D. S.; Morgan, D. H., Mechanistic investigations of the ethylene tetramerisation reaction. *J Am Chem Soc* **2005,** *127* (30), 10723-30.

8. Overett, M. J.; Blann, K.; Bollmann, A.; de Villiers, R.; Dixon, J. T.; Killian, E.; Maumela, M. C.; Maumela, H.; McGuinness, D. S.; Morgan, D. H.; Rucklidge, A.; Slawin, A. M. Z., Carbon-bridged diphosphine ligands for chromium-catalysed ethylene tetramerisation and trimerisation reactions. *Journal of Molecular Catalysis a-Chemical* **2008,** *283* (1-2), 114-119.

9. Walsh, R.; Morgan, D. H.; Bollmann, A.; Dixon, J. T., Reaction kinetics of an ethylene tetramerisation catalyst. *Applied Catalysis A: General* **2006,** *306*, 184-191.

10. Tang, S.; Liu, Z.; Yan, X.; Li, N.; Cheng, R.; He, X.; Liu, B., Kinetic studies on the pyrrole–Cr-based Chevron-Phillips ethylene trimerization catalyst system. *Applied Catalysis A: General* **2014,** *481*, 39-48.

11. Qi, Y.; Dong, Q.; Zhong, L.; Liu, Z.; Qiu, P. Y.; Cheng, R. H.; He, X. L.; Vanderbilt, J.; Liu, B. P., Role of 1,2-Dimethoxyethane in the Transformation from Ethylene Polymerization to Trimerization Using Chromium Tris(2-ethylhexanoate)-Based Catalyst System: A DFT Study. *Organometallics* **2010,** *29* (7), 1588-1602.

12. Gunasekara, T.; Kim, J.; Preston, A.; Steelman, D. K.; Medvedev, G. A.; Delgass, W. N.; Sydora, O. L.; Caruthers, J. M.; Abu-Omar, M. M., Mechanistic Insights into Chromium-Catalyzed Ethylene Trimerization. *Acs Catalysis* **2018,** *8* (8), 6810-6819.

13. Kulangara, S. V.; Haveman, D.; Vidjayacoumar, B.; Korobkov, I.; Gambarotta, S.; Duchateau, R., Effect of Cocatalysts and Solvent on Selective Ethylene Oligomerization. *Organometallics* **2015,** *34* (7), 1203-1210.

14. Köhn, R. D.; Haufe, M.; Kociok-Köhn, G.; Grimm, S.; Wasserscheid, P.; Keim, W., Selective Trimerization ofα-Olefins with Triazacyclohexane Complexes of Chromium as Catalysts. *Angewandte Chemie* **2000,** *39* (23), 4337-4339.

15. Shaikh, Y.; Albahily, K.; Sutcliffe, M.; Fomitcheva, V.; Gambarotta, S.; Korobkov, I.; Duchateau, R., A highly selective ethylene tetramerization catalyst. *Angew Chem Int Ed Engl* **2012,** *51* (6), 1366-9.

16. Hagen, H.; Kretschmer, W. P.; van Buren, F. R.; Hessen, B.; van Oeffelen, D. A., Selective ethylene trimerization: A study into the mechanism and the reduction of PE formation. *Journal of Molecular Catalysis A: Chemical* **2006,** *248* (1-2), 237-247.

17. Agapie, T.; Labinger, J. A.; Bercaw, J. E., Mechanistic studies of olefin and alkyne trimerization with chromium catalysts: deuterium labeling and studies of regiochemistry using a model chromacyclopentane complex. *J Am Chem Soc* **2007,** *129* (46), 14281-95.

18. Agapie, T., Selective ethylene oligomerization: Recent advances in chromium catalysis and mechanistic investigations. *Coordination Chemistry Reviews* **2011,** *255* (7-8), 861-880.